

INVESTIGATION OF TUFF QUARRIES AROUND THE
TEMPLE OF APOLLON SMINTHEUS (ÇANAKKALE, TURKEY)

A THESIS SUBMITTED TO
THE GRADUATE SCHOOL OF NATURAL AND APPLIED SCIENCES
OF
MIDDLE EAST TECHNICAL UNIVERSITY

BY

DUYGU ERGENÇ

IN PARTIAL FULFILLMENT OF THE REQUIREMENTS
FOR
THE DEGREE OF MASTER OF SCIENCE
IN
RESTORATION IN ARCHITECTURE

SEPTEMBER 2011

Approval of the thesis:

**INVESTIGATION OF TUFF QUARRIES AROUND THE
TEMPLE OF APOLLON SMINTHEUS (ÇANAKKALE, TURKEY)**

submitted by **DUYGU ERGENÇ** in partial fulfillment of the requirements for the degree of **Master of Science in Restoration, Middle East Technical University** by,

Prof. Dr. Canan Özgen
Dean, Graduate School of **Natural and Applied Sciences**

Assoc. Prof. Dr. Güven Arif Sargın
Head of Department, **Architecture**

Prof. Dr. Emine N. Caner Saltık
Supervisor, **Architecture Dept., METU**

Prof. Dr. Tamer Topal
Co-Supervisor, **Geological Engineering Dept., METU**

Examining Committee Members:

Prof. Dr. Asuman Türkmenoğlu
Geological Engineering Dept., METU

Prof. Dr. Emine N. Caner Saltık
Architecture Dept., METU

Prof. Dr. Ömür Bakırer
Architecture Dept., METU

Assoc. Prof. Dr. Neriman Şahin Güçhan
Architecture Dept., METU

Inst. Dr. Fuat Gökçe
Architecture Dept., METU

Date:

16.09.2011

I hereby declare that all information in this document has been obtained and presented in accordance with academic rules and ethical conduct. I also declare that, as required by these rules and conduct, I have fully cited and referenced all material and results that are not original to this work.

Name, Last name : Duygu Ergenç

Signature :

ABSTRACT

INVESTIGATION OF TUFF QUARRIES AROUND THE TEMPLE OF APOLLON SMINTHEUS (ÇANAKKALE, TURKEY)

Ergenç, Duygu

M.Sc. in Restoration, Department of Architecture

Supervisor : Prof.Dr. Emine N. Caner Saltık

Co-Supervisor : Prof.Dr. Tamer Topal

September 2011, 167 pages

Studies to determine the location of antique quarries, from where building stones were obtained, are done by comparison of the properties of antique stones and the possible quarry sources around them. In the case when no stonemason marks exists, geologic formations that may be used as building stone should be investigated and properties of antique building stones and geologic formations should be correlated. The aim of this study was the investigation of tuff quarries that could be the source of tuffs used in the construction of Apollon Smintheus Temple.

For this purpose, the studies were carried out about the geology of the region, and possible three quarries selected around Smintheion.

Durability properties of stones in Temple and quarries were determined with the analyses of physical, physico-mechanical properties and artificial weathering tests of wetting-drying, salt crystallization; Effective porosity, bulk density, water absorption capacity, dry and saturated unit weight, salt content, ultrasonic pulse velocity, modulus of elasticity, uniaxial compressive strength, pore size distribution, capillary absorption and moisture absorption capacities were determined for Temple tuffs and possible quarry tuffs in fresh and artificial weathering cycles. Microstructural investigations were done by mineralogical, petrographical and chemical analyses

which were optical microscopy, stereomicroscopy, XRD, SEM, FTIR, MBA and XRF.

The results indicated that Temple tuffs and two of the three quarries (Fatma Gerdan and Kızılkeçili) had similar engineering geological and micrstructural properties. Therefore, they could be used as building stone during the construction of Temple.

Keywords: Ancient Quarry, Apollon Smintheus Temple, tuff, durability.

ÖZ

APOLLON SMINTHEUS TAPINAĞI ÇEVRESİNDEKİ TÜF TAŞ OCAKLARININ ARAŞTIRILMASI (ÇANAKKALE, TÜRKİYE)

Ergenç, Duygu

Yüksek Lisans, Restorasyon, Mimarlık Bölümü

Tez Yöneticisi : Prof.Dr. Emine N. Caner Saltık

Eş Tez Yöneticisi : Prof.Dr. Tamer Topal

Eylül 2011, 167 sayfa

Jeolojik formasyonun yapıtaşı olarak dayanıklılık özelliğinin yeterli olması geçmişte taş ocağı olarak kullanıldığı savını arttırır. Taşçı işaretlerinin kaybolmuş olduğu durumlarda çevrede yapıtaşı olarak kullanılacak jeolojik formasyonları araştırmak ve bu formasyonların özellikleriyle anıt taşlarının özelliklerini karşılaştırmak gerekmektedir. Bu çalışmanın amacı Apollon Smintheus Tapınağı'ndaki tüf yapıtaşlarının kaynağı olabilecek taş ocaklarını araştırmaktır.

Bu amaçla, bölge jeolojisi araştırılmıştır ve Tapınak çevresindeki üç taş ocağı incelenmiştir.

Tapınağın ve taş ocaklarının tüflerinin dayanıklılık özellikleri fiziksel, fizikomekanik özelliklerin analizleri ve yapay yaşlandırma olarak tuz kristallendirme ve ıslanma-kuruma döngüleriyle belirlenmiştir. Tüflerinin ilk hallerinin ve yapay yaşlandırma döngüleriyle yıpratılmış hallerinin gözeneklilik, birim hacim ağırlığı, su emme kapasitesi, kuru ve doymuş birim ağırlığı, tuz içeriği, ultrasonik hız, esneklik modülü, tek eksenli basınç dayanımı, gözenek boyu dağılımı, kılcal su emme ve nem emme kapasitesi belirlenmiştir. Tüflerin mineralojik ve petrografik özellikleri optik mikroskop, stereo mikroskop, XRD, SEM, FTIR, MBA, XRF gibi analizlerle incelenmiştir.

Sonular Tapınak tf ve  ocaktan ikisinin tflerinin (Fatma Gerdan ve Kızılkeili) benzer mhendislik jeolojisi ve mikroyapısal zellikler gstermektedir. Bu iki ta ocađının anıtın yapımında kullanılan tflerin kaynađı olma olasılıđı vardır.

Anahtar kelimeler: Antik Ta Ocađı, Apollon Smintheus Tapınađı, tf, dayanıklılık.

To my grandma and Bulut...

ACKNOWLEDGEMENTS

Firstly, I would like to express my gratitude to my supervisor Prof. Dr. Emine N. Caner Saltık and my co-supervisor Prof. Dr. Tamer Topal for their guidance and patience. I also thank to the jury members, Inst. Dr. Fuat Gökçe, Prof. Dr. Ömür Bakırer, Assoc. Prof. Dr. Neriman Şahin Güçhan and Prof. Dr. Asuman Türkmenoğlu for their constructive criticism and suggestions.

I am indebted to Prof. Dr. Coşkun Özgünel for giving the permission to work on the stone samples taken from the temple. I want to express my appreciations to Dr. Davut Kaplan for his sharing information and help in the field work. I have furthermore to thank to Dr. Fuat Gökçe for sharing his knowledge about the site and giving permission to use the necessary data from his PhD dissertation.

I am deeply indebted to K. Göze Akoğlu for her help and guidance in every step of thesis. I especially thank to Talia Yaşar for sharing her immense knowledge in optical microscopy. I would like to thank A. Şenay Dincer, O. Mete Işıkoğlu, Filiz Diri, Uğur Akyıldız, Oytun Ortaylı and Işıl Ertosun for their tolerance, support and invaluable friendship. I also thank to my colleagues in Material Conservation Laboratory.

I would especially like to thank beloved Doğa Arıkan for accompanying in the life.

Most importantly, I would like to thank my parents İclal Ergenç, Özer Ergenç, and my sister Ceren Ergenç for firing me with enthusiasm for research and for believing in me even if I do not believe myself.

TABLE OF CONTENTS

ABSTRACT	iv
ÖZ.....	vi
ACKNOWLEDGEMENTS	ix
TABLE OF CONTENTS	x
LIST OF TABLES	xiv
LIST OF FIGURES	xvi
CHAPTERS	
1. INTRODUCTION..	1
1.1 AIM OF THE STUDY	2
1.2 LOCATION OF THE STUDY AREA	3
1.3 THE TEMPLE OF APOLLON SMINTHEUS	4
1.3.1 HISTORY OF THE EXCAVATIONS	5
1.3.2 MATERIALS USED IN THE CONSTRUCTION OF TEMPLE.....	9
1.3.3 REGIONAL GEOLOGY OF TEMPLE	14
1.4 TUFF	19
1.5 PREVIOUS STUDIES ON TUFFS	21
2. MATERIALS AND METHODS.....	27
2.1 METHODOLOGY OF THE STUDY.....	27
2.2 FIELD.....	28
2.2.1 BABAKALE YOLU	28
2.2.2 FATMA GERDAN (DFG)	30
2.2.3 KIZILKEÇİLİ (DKK).....	34

2.2.4	TEMPLE	36
2.3	DESCRIPTION OF SAMPLES	40
2.4	DETERMINATION OF ENGINEERING GEOLOGICAL PROPERTIES OF SAMPLES	43
2.4.1	ARTIFICIAL WEATHERING TESTS	43
2.4.2	EFFECTIVE POROSITY AND UNIT WEIGHT	44
2.4.3	WATER ABSORPTION UNDER ATMOSPHERIC PRESSURE.....	45
2.4.4	COLOR SPECTROMETER MEASUREMENTS	46
2.4.5	QUALITATIVE ANALYSIS OF THE SOLUBLE SALTS BY SPOT TESTS.....	46
2.4.6	ULTRASONIC PULSE VELOCITY	47
2.4.7	CAPILLARY ABSORPTION	48
2.4.8	MOISTURE CAPILLARY ABSORPTION.....	48
2.4.9	UNIAXIAL COMPRESSIVE STRENGTH.....	49
2.4.10	PORE SIZE DISTRIBUTION	49
2.5	MINERALOGICAL AND PETROGRAPHICAL PROPERTIES OF SAMPLES	50
2.5.1	THIN SECTION ANALYSIS	50
2.5.2	CROSS SECTION ANALYSIS	51
2.5.3	X-RAY DIFFRACTION (XRD) ANALYSIS.....	51
2.5.4	X-RAY FLUORESCENCE (XRF) ANALYSIS.....	52
2.5.5	SCANNING ELECTRON MICROSCOPY (SEM) – ENERGY DISPERSIVE ANALYZER (EDX)	53
2.5.6	FOURIER TRANSFORM INFRARED SPECTROSCOPIC ANALYSIS (FTIR)	53
2.5.7	METHYLENE BLUE ADSORPTION TEST.....	54
3.	EXPERIMENTAL RESULTS	56

3.1	DETERMINATION OF ENGINEERING GEOLOGICAL PROPERTIES OF SAMPLES	56
3.1.1	DENSITY & POROSITY (EFFECTIVE POROSITY AND UNIT WEIGHT) AND WATER ABSORPTION CAPACITY	56
3.1.2	COLOR SPECTROMETER MEASUREMENTS	68
3.1.3	QUALITATIVE ANALYSIS OF THE SOLUBLE SALTS BY SPOT TESTS.....	71
3.1.4	ULTRASONIC PULSE VELOCITY and MODULUS OF ELASTICITY	71
3.1.5	CAPILLARY ABSORPTION	74
3.1.6	MOISTURE ABSORPTION	77
3.1.7	UNIAXIAL COMPRESSIVE STRENGTH.....	78
3.1.8	PORE SIZE DISTRIBUTION	84
3.2	MINERALOGICAL AND PETROGRAPHICAL WORKS	89
3.2.1	THIN SECTION ANALYSIS	89
3.2.2	X-RAY DIFFRACTION ANALYSIS	103
3.2.3	CROSS SECTION ANALYSIS	111
3.2.4	X-RAY FLOURESCENCE ANALYSIS (XRF).....	116
3.2.5	SCANNING ELECTRON MICROSCOPY (SEM) – ENERGY DISPERSIVE ANALYZER (EDX)	121
3.2.6	FOURIER TRANSFORM INFRARED SPECTROSCOPIC ANALYSIS (FTIR)	125
3.2.7	METHYLENE BLUE ADSORPTION TEST (MBA)	127
3.3	DURABILITY ASSESSMENT OF SAMPLES	128
3.3.1	AVERAGE PORE DIAMETER.....	129
3.3.2	SATURATION COEFFICIENT.....	129
3.3.3	WET TO DRY STRENGTH RATIO	130

4. DISCUSSION	132
5. CONCLUSION	141
REFERENCES.....	144
APPENDICES	
A. DENSITY – POROSITY- WATER ABSORPTION CAPACITY	152
B. ULTRASONIC PULSE VELOCITY	157
C. COLOR EXPERIMENT RESULTS	159
D. ORIENTED AND UNORIENTED X RAY DIFFRACTION	161
E. PLAN OF APOLLON SMINTHEUS TEMPLE	166

LIST OF TABLES

TABLES

Table 1. Tuff dimensions in the temple (Gökçe, 2000)	13
Table 2. Basic physical and physicochemical test values	57
Table 3. Basic physical and physicochemical test values of DBY after salt crystallization cycle.....	58
Table 4. Basic physical and physicochemical test values of DFG after salt crystallization cycle.....	58
Table 5. Basic physical and physicochemical test values of DKK after salt crystallization cycle.....	59
Table 6. Basic physical and physicochemical test values of DBY after wetting drying cycle.....	63
Table 7. Basic physical and physicochemical test values of DFG after wetting drying cycle.....	64
Table 8. Basic physical and physicochemical test values of DKK after wetting drying cycle.....	64
Table 9. “L, a, b” values of samples	69
Table 10. Qualitative analysis of soluble salts	71
Table 11. UV and Emod values of dry and saturated samples.....	72
Table 12. Capillary coefficient values of samples	75
Table 13. Capillary coefficient values of samples after salt crystallization cycle	76
Table 14. Moisture absorption coefficient values of samples.....	77
Table 15. UCS values of dry and saturated samples.....	78
Table 16. UCS values of samples after salt crystallization cycle	80
Table 17. UCS values of samples after wetting drying cycle	82
Table 18. Major element percentages of samples	116
Table 19. Minor element percentages of samples.....	117
Table 20. MBA and CEC values of samples.....	128

Table 21. Physical properties of samples at the beginning	152
Table 22. Physical properties of samples after 2 nd cycle of salt crystallization.....	152
Table 23. Physical properties of samples after 3 rd cycle of salt crystallization	152
Table 24. Physical properties of samples after 4 th cycle of salt crystallization	153
Table 25. Physical properties of samples after 6 th cycle of salt crystallization	153
Table 26. Physical properties of samples at the beginning	153
Table 27. Physical properties of samples after 3 rd cycle of wetting drying	153
Table 28. Physical properties of samples after 4 th cycle of wetting drying	153
Table 29. Physical properties of samples after 6 th cycle of wetting drying	154
Table 30. Physical properties of samples after 8 th cycle of wetting drying	154
Table 31. Physical properties of samples after 10 th cycle of wetting drying	154
Table 32. Physical properties of samples after 12 th cycle of wetting drying	154
Table 33. Physical properties of samples after 14 th cycle of wetting drying	154
Table 34. Physical properties of samples after 16 th cycle of wetting drying	155
Table 35. Physical properties of samples after 18 th cycle of wetting drying	155
Table 36. Physical properties of samples after 20 th cycle of wetting drying	155
Table 37. Physical properties of samples after 22 nd cycle of wetting drying.....	155
Table 38. Physical properties of samples after 24 th cycle of wetting drying	155
Table 39. Physical properties of samples after 26 th cycle of wetting drying	155
Table 40. Physical properties of samples after 28 th cycle of wetting drying	156
Table 41. UPV change after salt crystallization cycle	157
Table 42. UPV change after salt crystallization cycle	157
Table 43. UPV change after wetting drying cycle	158
Table 44. UPV change after wetting drying cycle	158
Table 45. UPV change after wetting drying cycle	158
Table 46. L, a, b values of DBY after salt crystalization cycle.....	159
Table 47. L, a, b values of DFG after salt crystalization cycle	159
Table 48. L, a, b values of DKK after salt crystalization cycle	159
Table 49. L, a, b values of DBY after wetting drying cycle	160
Table 50. L, a, b values of DFG after wetting drying cycle.....	160
Table 51. L, a, b values of DKK after wetting drying cycle	160
Table 52. “d values” of samples in XRD spectras	161

LIST OF FIGURES

FIGURES

Figure 1. Location map of the study area.....	4
Figure 2. Timeline of history of Apollon Smintheus Temple Excavation.....	8
Figure 3. Material mapping on the facade of temple (after Gökçe, 2000).....	10
Figure 4. Material mapping on cross section of temple (after Gökçe, 2000).....	11
Figure 5. Correlation of geological units in the region (after Ilgar et.al., 2008).....	15
Figure 6. Geological map of study area (after Ilgar et.al., 2008).....	16
Figure 7. Babakale Yolu Quarry	28
Figure 8. Babakale Yolu Quarry	29
Figure 9. Sample taken from Babakale Yolu Quarry.....	29
Figure 10. Babakale Yolu Quarry	30
Figure 11. Fatma Gerdan Quarry	31
Figure 12. Fatma Gerdan Quarry	31
Figure 13. Fatma Gerdan Quarry	32
Figure 14. Fatma Gerdan Quarry	32
Figure 15. Fatma Gerdan Quarry	33
Figure 16. Fatma gerdan Quarry	33
Figure 17. Fatma Gerdan Quarry	34
Figure 18. Kızılkeçili Quarry	34
Figure 19. Kızılkeçili Quarry	35
Figure 20. Kızılkeçili Quarry	35
Figure 21. Kızılkeçili Quarry (by Kaplan, 2009).....	36
Figure 22. Apollon Smintheus Temple tuff foundations (from excavation archive). 36	
Figure 23. Apollon Smintheus temple northeast façade	37
Figure 24. Apollon Smintheus Temple tuff foundations (by Kaplan, 2009)	37
Figure 25. Apollon Smintheus Temple sample taken	38
Figure 26. Apollon Smintheus Temple	38

Figure 27. Apollon Smintheus Temple	39
Figure 28. Apollon Smintheus Temple	39
Figure 29. Apollon Smintheion Roman Bath külhan tuff	40
Figure 30. Kızılkeçili tuff.....	40
Figure 31. Babakale Yolu tuff.....	41
Figure 32. Fatma Gerdan tuff.....	41
Figure 33. Temple stone 1.....	41
Figure 34. Temple stone 2.....	42
Figure 35. Roman Bath stone.....	42
Figure 36. Temple stone 4.....	42
Figure 37. Graph of absorbance vs conservation at 632 nm	55
Figure 38. Water absorption Capacity change of samples in salt crystallization cycles	59
Figure 39. Saturated Unit Weight change of samples in salt crystallization cycles ..	60
Figure 40. Porosity change of samples in salt crystallization cycles	60
Figure 41. Dry unit Weight change of samples in salt crystallization cycles	61
Figure 42. Saturation Coefficient change of samples in salt crystallization cycles ...	61
Figure 43. Bulk density change of samples in salt crystallization cycles	62
Figure 44. Porosity change of samples in wetting drying cycles.....	65
Figure 45. Saturated unit weight change of samples in wetting drying cycles	65
Figure 46. Water absorption capacity change of samples in wetting drying cycles ..	66
Figure 47. Dry unit weight change of samples in wetting drying cycles.....	66
Figure 48. Saturation coefficient change of samples in wetting drying cycles.....	67
Figure 49. Bulk density change of samples in wetting drying cycles.....	67
Figure 50. Clor values of Temple stones and fresh stones from quarries	68
Figure 51. Color change of samples after salt crystallization cycle.....	69
Figure 52. Color change of samples after wetting drying cycle	70
Figure 53. UPV change of samples after salt crystallization cycle.....	73
Figure 54. UPV change of samples after salt crystallization cycle.....	74
Figure 55. Capillary absorption rate of samples	75
Figure 56. Capillary absorption rate of samples after salt crystallization cycle	76
Figure 57. Moisture absorption graph of samples.....	77

Figure 58. Uniaxial Compressive Strength graph of samples.....	79
Figure 59. E_{mod} vs UCS graph of samples	80
Figure 60. UCS change of samples after salt crystallization cycle	81
Figure 61. E_{mod} vs UCS graph of samples after salt crystallization cycle	82
Figure 62. UCS change of samples after wetting drying cycle.....	83
Figure 63. E_{mod} vs UCS graph of samples after wetting drying cycle	83
Figure 64. Pore size distribution of DTS1	84
Figure 65. Pore size distribution of DTS4	85
Figure 66. Pore size distribution of DBY	85
Figure 67. Pore size distribution of DFG.....	86
Figure 68. Pore size distribution of DKK	86
Figure 69. Pore size distribution of DBY after 3rd salt crystallization cycle	87
Figure 70. Pore size distribution of DFG after 3rd salt crystallization cycle.....	88
Figure 71. Pore size distribution of DKK after 3rd salt crystallization cycle	88
Figure 72. Photomicrograph of DTS1, single nicol, 2,5x , Plg: plagioclase, VG: Volcanic glass	90
Figure 73. Photomicrograph of DTS1, cross nicol, 10x , Plg: plagioclase, Bi: Biotite	90
Figure 74. Photomicrograph of DTS1, cross nicol, 10x , Bi: Biotite.....	91
Figure 75. Photomicrograph of DTS1, cross nicol, 10x , weathered plagioclases	91
Figure 76. Photomicrograph of DTS2, cross nicol, 5x , Bi: Biotite.....	92
Figure 77. Photomicrograph of DTS2, cross nicol, 5x , plagioclase	93
Figure 78. Photomicrograph of DTS3, single nicol, 5x , hematite coatings are seen.	94
Figure 79. Photomicrograph of DTS2, cross nicol, 10x , Biotite.....	94
Figure 80. Photomicrograph of DTS4, single nicol, 5x	95
Figure 81. Photomicrograph of DTS4, cross nicol, 10x	96
Figure 82. Photomicrograph of DTS4, cross nicol, 10x	96
Figure 83. Photomicrograph of DBY, cross nicol, 5x, S: sanidine, Plg: plagioclase	97
Figure 84. Photomicrograph of DBY, cross nicol, 5x, S: sanidine, Plg: plagioclase	98
Figure 85. Photomicrograph of DBY, single nicol, 5x	98
Figure 86. Photomicrograph of DBY, cross nicol, 5x.....	99
Figure 87. Photomicrograph of DBY, single nicol, 5x	99

Figure 88. Photomicrograph of DFG, single nicol, 10x, biotite	100
Figure 89. Photomicrograph of DFG, single nicol, 20x, hematite corrosion.....	101
Figure 90. Thin section image of DKK, single nicol, 5x	102
Figure 91. Thin section image of DKK, single nicol, 10x	102
Figure 92. Thin section image of DKK, cross nicol, 10x	103
Figure 93. X-Ray Diffraction of DTS4	104
Figure 94. Unoriented X-Ray Diffraction graph of samples. Sm: smectite, Ab: albite, An: anorthite, Q: quartz, Bi: biotite, Sa: sanidine, Hem: hematite	105
Figure 95. X-Ray Diffraction of DTS1 as unoriented, air-dried, ethylene glycolated and heated. S: smectite,.....	106
Figure 96. X-Ray Diffraction of DTS2 as unoriented, air-dried, ethylene glycolated and heated. S: smectite, F: feldspar, Q: quartz.....	107
Figure 97. X-Ray Diffraction of DBY as unoriented, air-dried, ethylene glycolated and heated. S: smectite, F: feldspar, Bi: biotite, Sa: sanidine, Hem: hematite, Ch: chlorite, I: illite.....	108
Figure 98. X-Ray Diffraction of DFG as unoriented, air-dried, ethylene glycolated and heated. S: smectite, F: feldspar, Q: quartz.....	109
Figure 99. X-Ray Diffraction of DKK as unoriented, air-dried, ethylene glycolated and heated. S: smectite, F: feldspar, Q: quartz.....	110
Figure 100. Cross section image of DTS1	111
Figure 101. Cross section image of DTS2	112
Figure 102. Cross section image of DTS3	113
Figure 103. Cross section image of DTS4	113
Figure 104. Cross section image of DFG.....	114
Figure 105. Cross section image of DBY	115
Figure 106. Cross Section of DKK	115
Figure 107. SiO ₂ vs Al ₂ O ₃ graph	118
Figure 108. Fe ₂ O ₃ vs Al ₂ O ₃ graph.....	118
Figure 109. SiO ₂ vs Fe ₂ O ₃ graph	119
Figure 110. CaO vs Na ₂ O graph	119
Figure 111. K ₂ O vs Pb graph	120
Figure 112. Ba vs Zr graph	120

Figure 113. Al/(Al+Fe) vs Al/(Al+Mg) graph	121
Figure 114. SEM image of DFG with honeycomb morphology of smectite	122
Figure 115. SEM image of DFG	122
Figure 116. SEM image of DKK showing quartz etch and feldspar fragments	123
Figure 117. SEM image of DKK honeycomb type smectite in feldspar and quartz grains	123
Figure 118. SEM image of DKK	124
Figure 119. SEM image of DKK	124
Figure 120. FTIR spectra of DTS1 peaks between 4000-3000 cm ⁻¹ : 3623,3606 ...	126
Figure 121. FTIR spectra of DBY peaks between 4000-3000 cm ⁻¹ : 3618,3546.....	126
Figure 122. FTIR spectra of DFG peaks between 4000-3000 cm ⁻¹ : 3608, 3546.....	127
Figure 123. FTIR spectra of DKK peaks between 4000-3000 cm ⁻¹ : 3619, 3564 ...	127
Figure 124. C.E.C. values of samples	128
Figure 125. Wet to dry strength ratio of samples	130
Figure 126. Oriented and unoriented smectite peaks of DTS1 (red; air dried 12, 13, 15 Å, blue; glycolated 16, 17Å, gren; heated 9,10 Å)	162
Figure 127. Oriented and unoriented smectite peaks of DFG (red; air dried 13 Å, blue; glycolated 16 Å, gren; heated 10 Å)	163
Figure 128. Oriented and unoriented smectite peaks of DKK (red; air dried 15 Å, blue; glycolated 17 Å, gren; heated 10 Å)	164
Figure 129. Oriented and unoriented illite peaks of DBY (red; air dried 10 Å, blue; glycolated 10 Å, gren; heated 10 Å)	165
Figure 130. Plan of Apollon Smintheus Temple.....	166
Figure 131. General plan of Smintheion	167

CHAPTER 1

INTRODUCTION

A detailed analysis of a work of art must include an esteem and understanding of the materials used (Brandi, 1977). During the conservation and preventive care of historical sites, geological background and research have inevitable significance. Conservation interventions cannot be defined without a considerable analysis of the material used in their construction (Herz, Garrison, 1998).

Conservation and presentation of historic quarries should be considered together with the relevant archaeological site. The research on the determination of antique quarries provides useful information to conservation science as well as to archaeology and geology of the region. Tuffs that have low unit weight, high porosity and good durability properties attract attention in antique structures as well as in Seljuk-Ottoman period monuments that have come to our times.

Since the prehistoric times, igneous, metamorphic and sedimentary rocks have been quarried and transported to serve as building stone. After the metal tools were invented, quarrying techniques were developed for removing blocks of stone from geological formations. Blocks of rocks were quarried using hallows cut in the rock and then removing them from below by the help of wooden wedges. “To quarry large blocks of stone, the rock must be free of closely spaced joints, cracks or other planes of weakness. However, some well-spaced bedding and joint planes are necessary to permit breaking into blocks with flat surfaces.” (Rapp, 2000).

Most of the time, only high-status stone blocks were transported from longer distances whereas local quarries were used for larger constructions (Torok,

2007,2010). Since local stones do not require high transportation costs they can be extracted whenever suitable (Bell, 1990).

The correct identification of building stone also has many implications for interpretation of a site's cultural, technological and commercial history. Because the majority of ancient societies chose building materials that were already available, the structural or aesthetic limitations of the material were the secondary considerations to ease of procurement. The adaptations made by ancient builders to the limitations of these materials reflect technological advances and cultural aspects (Rapp, 2000).

It is significant to concern a set of techniques which cover the whole characteristics of the rock, such as chemical, mineralogical and petrographical fingerprints (Ramseyer et.al., 2006). Mineralogical and petrographical analyses better reveal the microstructural properties. Comparison of mineralogical and petrographical properties of antique building stones and geologic formations is beneficial in provenance studies. Correlation of major elements, minor elements and trace elements is also beneficial, in case sufficient database about the subject is present.

1.1 AIM OF THE STUDY

Studies to determine the location of antique quarries, from where building stones were obtained, are done by comparison of the properties of antique stones and the possible quarry sources around them. In the case when no stonemason marks exists, geologic formations that may be used as building stone should be investigated and properties of antique building stones and geologic formations should be correlated.

This present study was done for the purpose to designate the quarries of the tuffs used in the Hellenistic period architecture at the Temple of Apollon Smintheus in Gülpınar, Çanakkale. The reason for the selection of tuff was the fact that tuff has constituted the foundation and majority of the stones used in the construction of the temple in current situation and tuff is the most deteriorated stone of temple. The reason for the selection of that region was the fact that besides the importance of the

Temple, it has appropriate working conditions and some quarries and the geologic formations were located around that site.

In this study, samples taken from the temple and samples taken from three regions that have the possibility of being quarry used were compared by analyses. Fundamental properties that were used in comparisons were diversified. The comparative studies of surface deteriorations of monument's stone and deteriorations of open air surfaces of geologic formations are important. Besides, their durability properties were necessary to be compared. If the durability of stone in a geologic formation is satisfactory to be building stone, that would increase the possibility of its use as quarry in the past. Durability properties were determined with the analyses of physical, physico-mechanical properties and artificial weathering tests such as wetting-drying, salt crystallization and freezing-thawing cycles. Microstructural investigation should be done by different methods in a correlation study. Comparison of mineralogical and petrographical properties of antique building stones and geologic formations was beneficial in provenance.

1.2 LOCATION OF THE STUDY AREA

Troas is the historical name of the Biga peninsula in the northwestern part of Anatolia (Figure 1). This region now is part of Çanakkale Province bounded by the Dardanelles to the northwest, by the Aegean Sea to the west and separated from the rest of Anatolia by the massif that forms Mount Ida. Troas is drained by two main rivers, which join at the area having the ruins of Troy. *Grenikos*, *Kebren*, *Simoeis*, *Rhesos*, *Rhodos*, *Heptaporos* and *Aisepos* were seven rivers of the Troas and the names of the river gods that inhabited each river (Özgünel, 2001). Biga Peninsula was selected as the case study area of this thesis because of its rich geological information background.



Figure 1. Location map of the study area

1.3 THE TEMPLE OF APOLLON SMINTHEUS

Apollo Smintheus Temple, where the first episode of the Iliad epic emerged, is situated on the south-west corner of Biga Peninsula. It is within the boundaries of the city of Çanakkale and in the municipality of Gülpınar which was called "Külahlı" until 1920's. The temple is currently located in a garden of the town which is nourished by spring waters. This could be the reason why the temple was erected on this site where plenty of water existed. The people of Alexandria Troas had come to consult the oracle of Apollo and the god needed water for prophecy. It was constructed during the second century B.C.

The temple was first discovered by the traveler Jean Baptista Le Chevalier in 1785 as he was traveling from Lecton (Babakale) to Alexandria Troas, and it was identified

as Ionic in style. Later, in 1853, the English admiral R.N. Spratt visited the temple and described it as an Ionic pseudo-dipteral Temple of Apollo. In 1866, R. Pullan excavated the temple for two months. In 1966, Hans Weber illustrated some of the fragments and the frieze of the building in an article. The Archaeological Museum of Çanakkale made surveys in 1971-73 in this region. Since 1980, formal excavations and restoration in and around the temple have been carried out by archaeologists under the directorship of Prof. Dr. Özgünel from University of Ankara.

The temple is dated to the second half of the second century BC. With its reliefs, whose stories are coming from the Iliad of Homer, Temple of Apollo Smintheus is the unique example of the Ionic style of the Troas region of Turkey. In this temple the pseudo-dipteral plan was used. The temple had 8 columns on its front and back and 14 on each of its long sides. Its stylobate measured 23.20m x 41.65m rising up on an eleven stepped krepidoma (Özgünel, 2001).

1.3.1 HISTORY OF THE EXCAVATIONS

J.M. Cook states that European travellers have discovered the Holy place but Jean Baptiste Lechevailier is the one that executed the first modern archaeological investigations in 1785 and 1786 (Lechevailier, 1799). On the way to Alexandria Troas, he had seen the remains (Cook, 1973). In 1853, while coming with the aim of mapping the Troas region, admiral R.N. Spratt had discovered the Ionic style temple and introduced it to the archaeological world. He determined that the temple pertains to the cult of Apollon Smintheius by the two tablets in the temple and the village (Spratt, 1856). In 1866, Richard Popplewell Pullan had excavated the area and the plan was drawn. One tablet was sent to England to be cleaned. C.T. Newton had commented on the tablet and proved it to be the Apollon Smintheus Temple (Newton, 1887). After a long gap, during the factory construction on the hieron¹, some destruction happened in 1964 and in 1966 Hans Weber reminded and localized

¹ A consecrated place (Hasol, 2005)

² An enclosed, sacred precinct or marked-off plot of land in ancient Greek which have temples stoas,

the temple to the archaeological community by publishing the frieze blocks and architectural elements (Weber, 1966). Between the years 1971 and 1973 Çanakkale Archaeology Museum had drilling-explorations in the temple and its surroundings. In 1980, archeological excavations had started and it has continued until today.

Excavations by Prof. Dr. Coşkun Özgünel and his team had started in 1980. After 1989, some works related with restoration- conservation were done by the leadership of Fuat Gökçe, as restoration architect, together with the excavation activities.

In 1989 the drainage system was done in front of the krepis (stairs) on south façade of Temple, thus the problem of rising damp was solved. Deteriorations seen on the stairs were tried to be stopped by cleaning from allochthonous materials. Then a mortar mixture of tuff dust, small grain sand, lime, oxidized soil, dye and water were mixed and applied on tuff surfaces. The aim was to constitute a protective layer on the tuffs that could increase the strength of tuffs. Pilot experiments at the site showed that mixture had similar color, fragility and water penetration properties with authentic material and seemed to be compatible and increased the strength of stone. Andesite-basalt and marble blocks were carried into the free space in the temenos² and exhibited.

Places in tatters (loss of original volume and plan properties) were decided to be restored by consolidation of the authentic part and the reconstruction of missing parts with new material. Artificial andesites were prepared by spraying ochre up to Stylobate level. Artificial marble (white cement, large marble grains) and andesite steps were put above the concrete base. Steps were prepared by Portland cement mortars, stone grains, red ochre and mortar including small and large grained sand. They were poured into timber moulds with anchor sticks and were kept unsaturated and were left drying in time. In 1990, artificial andesite and tuffs were made. The consolidation of tuffs by spraying was begun. In 1991 repair and anastylosis were applied at the southwest of the temple. Andesite bases were almost finished in the krepis. More than 90 step block were casted up to 10th stair. 11th stair row was

² An enclosed, sacred precinct or marked-off plot of land in ancient Greek which have temples stoas, altars, holy trees etc. (Hasol, 2005)

prepared and kept for following year applications. In 1992 “Underwater Explorations” were done by METU Underwater Club. Landscaping was applied in 1992. In 1994, infrastructure was constituted in south west corner by making six artificial marbles of 140*140 cm. In addition, drainage system was designed for the depot in the museum. In 1995, anastylosis of columns were done. Computer aided designs showed that 3 columns contain 6 drums each. Decays in the drums which were because of ageing and olive oil factory, did not enable their anastylosis successively. In 1997 anastylosis and reconstruction continued (Figure 2).

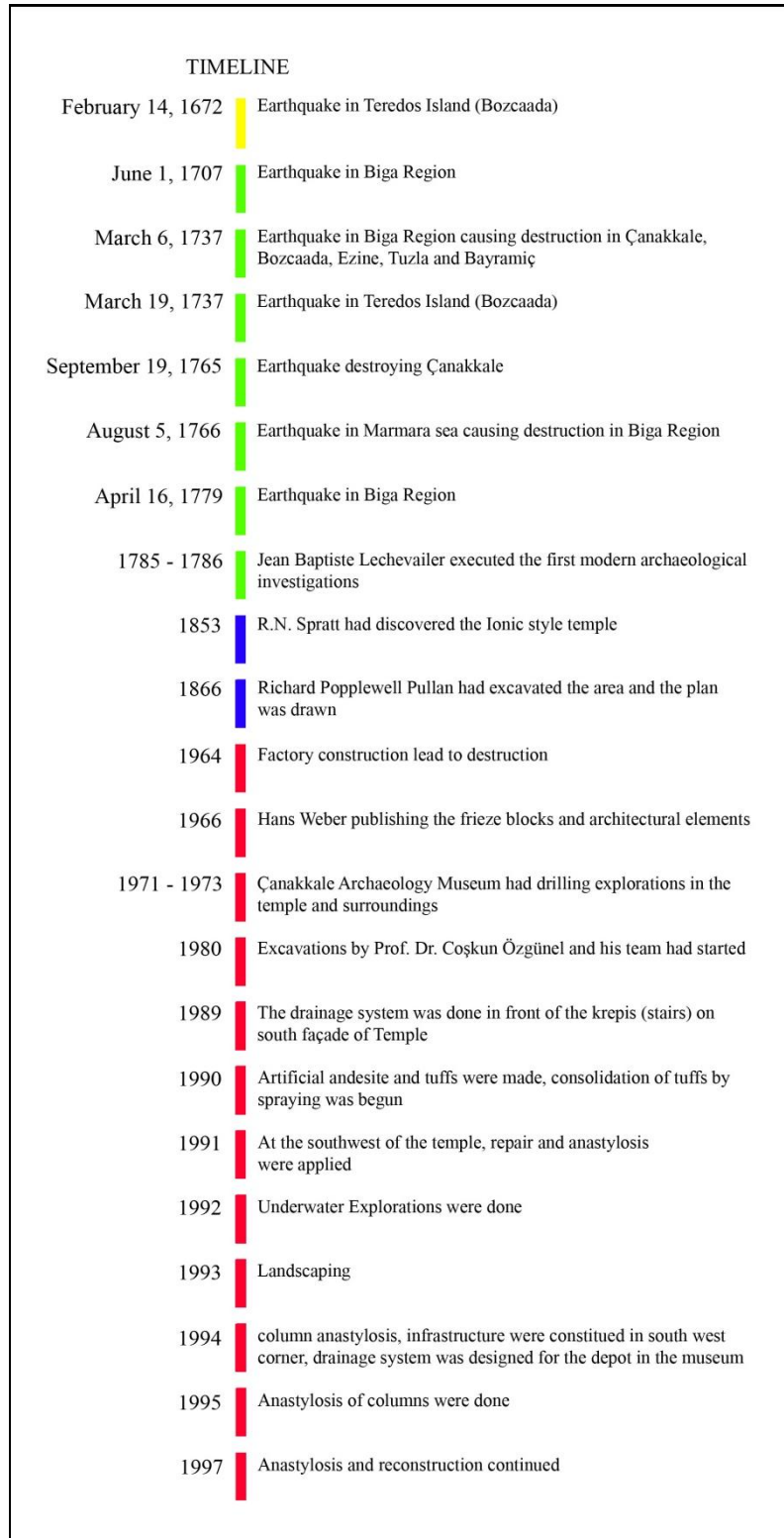


Figure 2. Timeline of history of Apollon Smintheus Temple Excavation

1.3.2 MATERIALS USED IN THE CONSTRUCTION OF TEMPLE

The temple was thought to be constructed over a soft basin (Tekkaya, 1982,; Özgünel, 2001), however, in the 2007 Smintheion Excavation Report it was written that the main rock was schist and the temple was constructed over it. Andesite-basalt came over tuff and the upper parts and columns were marble (Figure 3). According to the archaeologists, the reason for the preference of tuff was not because the temple was on a soft basin or swamp like area as it was in some other Apollon Temples. The use of tuff as a buffer zone to protect the upper parts of the Temple must have been thought.

The 1980 excavations showed and the 2007 excavations have proved that the temple had slopes on the north and northwest (Figure 4). Gökçe (2000) claimed that for the purpose of eliminating the rise between west long side and east long side, 40- 50 cm high rubble stones were used on the west side below the first row tuff blocks.

Tuff blocks were observed in 4-5 rows. Only on the pedestal of the columns andesites were used as plint and tuffs were not preferred. Tuffs were bonded each other with wooden clamps of 3,5-4,20 cm.

In Smintheion, tuff was used as a foundation stone and as well as for filling. Gökçe (2000) mentioned in his dissertation that while immediate surroundings are investigated, neither today nor in the past, tuff was not used in any other construction other than Smintheion, however, in the 2008 excavation findings in a Roman period bath, it was found that tuff blocks were used in arch of *Külhan* entrance of Roman period Bath. The same period edifices the Bergama Zeus Altar and the Apollon Smintheus Temple resemble each other in construction of their foundations and the use of tuff.

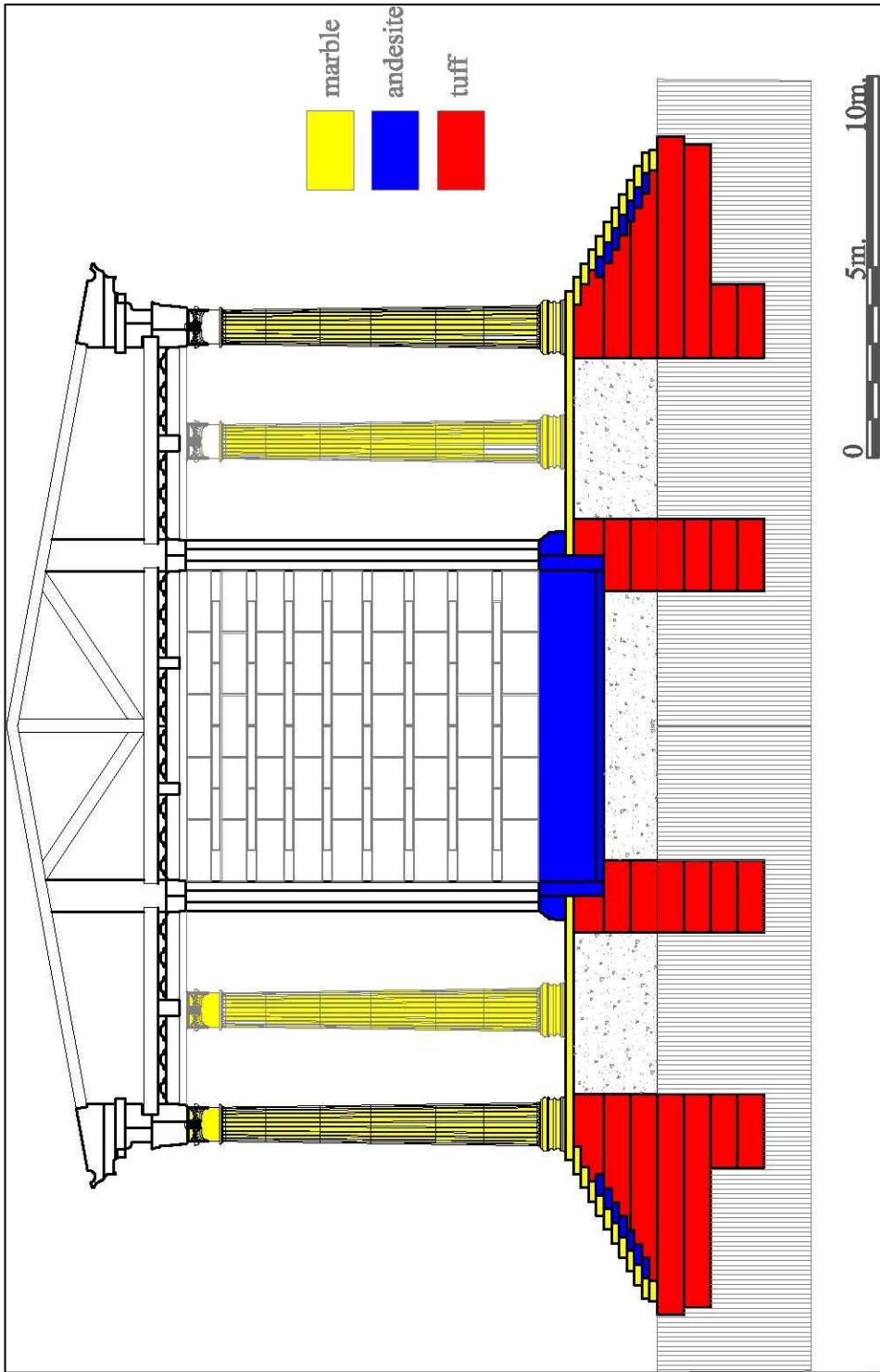


Figure 3. Material mapping on the facade of temple (after Gökçe, 2000)

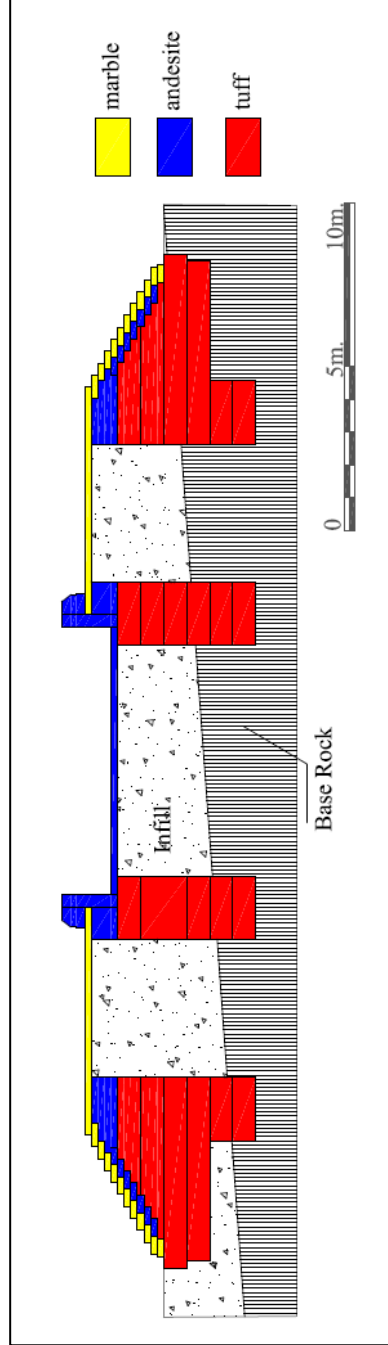


Figure 4. Material mapping on cross section of temple (after Gökçe, 2000)

Tuff is a very porous, light and soft material. Those features imply the convenience of extraction from the quarry, working the stone blocks and transportation. Indeed, in open air conditions some tuffs are affected by weathering and easily fall apart. Vitruvius (2005) states that tuff is highly durable at interiors, but easily affected by frost. However; under heavy stones it can be durable so that it would not be affected by weathering conditions.

The best conserved part of the temple is its foundations. Two rows of western edge of tuff foundations forming *kreipdoma*³, third line of other parts, five lines of *cella*⁴ foundation and three lines of filling foundation wall at *pteroma*⁵ are totally preserved. Two blocks at the fourth line of filling foundation wall were conserved in situ. Late period water well cross section which is done by carving a part of northwest of temple out showed that the main rock is schist (Gülpınar Excavation report, 2007).

Drilling made in the foundation of the *cella* showed that a part of the first row was placed on the main rock. Foundation at the southeast edge starts just over the main rock, though, the foundation on the northwestern part have rock infill. It is important that in the construction times, though it was easier, foundation was not preferred in lower elevation, an infill (rubble stone) was used to raise the elevation of Temple (Gökçe, 2000).

Tuff was used in the ground floor and they were not well-proportioned rectangular prisms of 69-71 cm height with variable width and length (Table 1). The altar in front of the temple (30 m) was made of tuff.

³ A treads platform that the temple sits on (Hasol, 283) .

⁴ Collonaded main place in the middle (Hasol, 336).

⁵ In a temple, the area between the *cella* or cell walls and the colonnade.

Table 1. Tuff dimensions in the temple (Gökçe, 2000)

Stair foundation		Cella foundation		Lintel walls	
Width (cm)	Length (cm)	Width (cm)	Length (cm)	Width (cm)	Length (cm)
74	115	85	165	85	75
75	85	85	175	85	110
76	185	85	180	85	125
84	140	85	185	86	75
80	120	85	188	87	145
85	140	85	195	87	130
85	155	90	255	89	170
85	158	95	175		
85	165	145	190		
86	156				

Generally tuff blocks measure 85 cm in width and 75-255 cm in length (Table 1). Gökçe (2000) reminds that tuffs would not be seen after the construction was completed. That's why the heights and thickness of the stones should be the same with other stones used in the upper parts.

Dimensions of tuff blocks at the foundation side walls were quite irregular. The lengths of the stones were variable, being around 85 cm, the stones might be extracted from quarry nearly at those dimension. Tuffs may be used in irregular dimensions which they were extracted because shaping tuff may cause much more loss. Highly porous tuffs were used in the lower parts which needed much material by that time, labor and money had been saved (Gökçe, 2000).

Gökçe (2000) stated that the use of tuff at the foundations (as a buffer) increased earthquake resistance of the temple and controlled the rising damp in the temple walls.

Andesite as a tough material constituted a healthy layer between tuff and marble and corrected the irregularities off tuff and provided an even elevation. Besides, marble could ruggedly be clamped.

Andesite was used inside the marble covering and under the columns. The last substratum layer of kreipdoma, cella and column pillars were of andesite. In-situ found andesites were; southeast edge- most of first row blocks (40,4 m), a few second, third, fourth step rows, southwest corner, northwest and northeast edges- a few first step rows. Fourteen pillars at the southeast edge, three blocks at the southwest and the northeast corner are totally preserved. There was no conserved andesite column ground in northwest edge (Gökçe, 2000).

1.3.3 REGIONAL GEOLOGY OF TEMPLE

The Apollon Smintheus Temple is located in Gülpınar town, in the southwestern part of Biga Peninsula, between the Aegean Sea and Edremit Bay. The study area is surrounded by geological formations belonging to Tertiary period where the broad region has rocks from Permian to Quaternary.

In MTA report (İlgar et.al. 2008), it was stated that on pre-Tertiary rocks, there are lithological units including sedimentary and volcanic rocks (Figure 5), formed in Eocene-Quaternary time interval.

AGE	LITHOLOGY	EXPLANATION
Quaternary	Qual	Alluvion
Pliocene	Tplb	Conglomerate Sandstone
Pliocene - Late Miocene	Tmplg	Siltstone
Middle Miocene	Tmbb Tmc Tmay	Andesitic Dacite Ignimbrite Basalt
Early Miocene	Tmb Tmba Tma	Andesite Pyroclastic Rocks

Figure 5. Correlation of geological units in the region (after Ilgar et.al., 2008)

Temple is located in the border of sedimentary and volcanic units. The area from Hamaxitos (Beşiktepe) to the sea is formed of marl and limestone (Kayan, 1994). Western part of the temple is sedimentary- alluvial whereas its east and south sides are of Miocene volcanic lithologic units.

A few kilometer south of the temple is Araplar Volcanic (Tma) (Figure 5) including grayish green colored andesitic rocks that are exposed in a very limited area (Öngür, 1973). Unit is thought be efficient in early Miocene. Beneath the farthest west point of Turkey, Babakale Volcanic (Tmba) that, Rock assemblage including various basaltic lava flows and derived breccias⁶ and intersecting andesitic dykes⁷ occur. The thickness of the unit is 200m (Öngür, 1973). Petrographical surveys proved that rocks are defined as basalt. The age of the unit is thought to be Early Miocene when regional stratigraphical situation is considered. In the southeastern part *Bademli Volcanic (Tmb)*; rock assemblage including various biotite rich basaltic lava flows is seen. The basin consists of coal, marl and limestone (Öngür, 1973). Paleological surveys proved that the age of the rocks is Early Miocene. Over these, *Ayvacık Volcanic (Tmay)* comes where Gülpınar town is located. At the lower parts the unit begins with white, pumice and ignimbritic tuffs and continues with basaltic andesites and andesitic pyroclastics. In microscopic investigations basaltic andesite and andesites are porphyritic and hypocrstalline porphyritic textured. The unit had been efficient in Middle Miocene.

Çamkabalak Ignimbrite (Tmç) is the largest unit in the area that three quarry/ bedrock is chosen for the study (Figure 5). Gray, red, brown ignimbritic rocks are designated as Çamkabalak Ignimbrite (Dönmez et.al.,2005). At the bottom, tile red welded volcanic rocks are observed and they are overlaid by white and gray big pumice fragments. Upper part of the unit includes gray, 15 cm fiamme⁸ form, good welded and covering, high temperature flow phase products. Thin section analyses explain the rocks as lithic tuff and ignimbrite. Ignimbrites around Behramkale had

⁶ a rock type comprised of often large angular fragments of pre-existing rock and set within a finer-grained rock matrix or cement (Williams et.al., 1954).

⁷ thin vertical veins of igneous rock that form when magma enters and cools in fractures found within the crust (Williams et.al., 1954).

⁸ Lens shaped, mm to cm volcanoclastic form (Williams et.al., 1954).

come from Behram caldera, most of which are swallowed under sea today (Öngür, 1973). The geochronologic age of the unit is Early Miocene, however, regional stratigraphic location pointed out that ignimbritic volcanism were active in Middle Miocene. Different rock fragments in the ignimbrite may cause the older age. The most important tuff quarries are in the east of the hieron. Except the west direction hills containing Upper Miocene conglomerate layers, the ridges on which Gülpınar City lies, have tuff layers (Kaplan, 2009).

Kızılkeçili, Kocaköy (Fatma Gerdan) and Babakale road are in *Tmç* lines. The source of Fatma Gerdan fountain that provides the drinking water for Gülpınar, is rich in tuff. Tuff can be observed in everywhere from Tuzla border, Kızılkeçili Village to Babakale Village field. Along the both sides of the spring ancient quarries of tuff is detected. It is possible to see the traces of cut tuff blocks at the site. Another similar quarry is on the old way of Babakale and small valley under Değirmentepe. Old Babakale Road (to Khrysa) was used in the ancient period that is confirmed from the spring sided parapet blocks belonging to the Roman Bridge (Kaplan, 2009).

Tuff Member (Tmçt): Inside the Çamkabalak Ignimbrite, ignimbritic debris tuffs having plenty of pumice and rock fragments and obsidian, transitive with Middle Miocene aged lacustrine deposits are named as Tuff Member (Öngür, 1973). West of temple includes *Gülpınar formation (Tmplg):* Formation is located in the west of Biga Peninsula, along the shoreline between Gülpınar and Geyikli. It consists of yellow-beige color clayish limestone, limestone and fossiliferous limestone and siltstone, sandstone and pebble stone. The thickness range is between 3 and 40 cm. The formation overlies the Behram ignimbrites with unconformity. Pebble stone and sandstones were deposited in the beach-coast area whereas limestones were deposited in lacustrine or lagoon environment inside the coastline. MTA reports describe the age of the formation as Late Miocene- Early Pliocene (Duru et.al.,2007; Ilgar et.al., 2008).

The temple nearly stands on the *Bayramiç formation (Tplb)*. Plio-Quaternary age fluvial deposits in Biga and Gelibolu Peninsulas are named as Bayramiç formation in regard of the stream. It consists of scarlet-brown conglomerates, sandstone and mudstones. The formation includes alluvial fan, braided and meandering channels.

Bayramiç Formation overlies all former unconformable units. It has a wide area in Ezine, northern Biga, Gönen and Manyas. The thickness of the unit is 200-300 m on land, 1500 m in Edremit Bay. The western part of Gülpınar (volcanic basin) was formed with the tectonic evolution terminating the Upper Miocene Sedimentation (Kayan, 1994). *Alluvium (Qal)*: Pebble, sand and mud deposits that formed on plains in coastal areas, depression areas and riverbeds are alluvium. They are quaternary in age.

1.4 TUFF

Fragmented products of volcanoes are called pyroclastics because of the clastic⁹ nature of the constituents. The term pyroclastic refers to rocks resulting from volcanism. The most common pyroclastic rock of interest is called tuff, which is well-indurated ash of minerals, glass, and small rock fragments. To be classed as tuff, the material must be solidified. Tuffs have a grain size generally finer than 4 mm (Rapp, 2002). Lapilli and volcanic ash accumulation formed rocks are called tuffs. Three types of tuff are distinguished according to the type of pyroclastic element dominant in its composition; vitric tuffs, lithic tuffs and crystal tuffs. For petrographical purposes, tuff is generally classified in relation to the nature of the volcanic rock of which it consists (Çoğulu,1973). The detailed explanation is as given below.

1- Vitric tuffs are mainly composed of volcanic glass fragments. Most of them are rhyolite in composition. **Ryholitic tuffs** contain pumiceous, glassy fragments and small scoriae with quartz, alkali feldspar, biotite and hornblende. Volcanic glass fragments occur as finer than 4 mm, angular, concave, convex, needle form, flat, etc. Colors differ between light and dark brown. They include crystal pieces.

⁹ Pertaining to a rock composed of particles derived from preexisting rocks and transported some distance from their origin (Rapp, 2002).

Ignimbrites are tuffs formed by welded volcanic glass fragments. *Palagonitic tuffs* are formed by hydrated basic glass fragments (palagonites) during undersea volcanism. *Syderomelan* is called volcanic glass with basalt composition. The term ignimbrite refers to deposits from very hot pyroclastic flows sometimes also called ash flow tuff or welded tuff. Most have a rhyolitic or dacitic composition, and contain feldspar, quartz and biotite, along with glass.

Welded tuff is a pyroclastic rock, of any origin, that was adequately hot at the time of deposition to weld together. As in the case of ignimbrites, welded tuffs can be deposited from pyroclastic density currents. Throughout welding, the glass shards and pumice fragments stick together.

2- Lithic tuffs

Mainly formed by lava particles <4mm. These particles may have come from old lava flows or separated from adjacent rock units. For instance, besides basalt, andesite, obsidian, various sedimentary and metamorphic rock fragments can be seen.

3- Crystal tuffs are mainly composed of crystal pieces. Generally, they are broken, eroded and angular grained.

Dacitic tuffs have hornblende, pyroxene, Na-plagioclase and quartz. *Andesitic tuffs* do not contain quartz. *Trachyte tuffs* contain little or no quartz but much sanidine or anorthoclase and sometimes feldspar, with rare biotite, augite and hornblende. *Basaltic tuffs* are black, dark green or red in colour; vary greatly in coarseness and have olivine, augite, labradorite and magnetite crystals. *Ultramafic tuffs* are extremely rare; their characteristic is the abundance of olivine or serpentine and the scarcity or absence of feldspar and quartz (Çoğulu,1973).

Heiken (2006) stand out that tuffs make excellent building materials either block itself or pozzolana. “When used for building stone, ignimbrite is sawn or broken away from a quarry face along natural cooling joints and then fashioned into blocks by hand or with power saws. These blocks, with enough strength for multiple-storey buildings, stone walls, and other structures, are resistant to weathering, are

lightweight, and have good insulating properties—better than most other natural building stones” (Heiken, 2006).

Volcanic tuffs have been used as building stones in many countries and represent a major component of the building mass of ancient monuments in Europe. Tuff, well known by the Romans as a building raw material, was appreciated because of its availability, lightness and durability against physical weathering. In particular, they were used as a necessary constructional material in churches especially popular for the arches and piers of a vault. Besides, tuff stone was used as an additive to improve mortar or cement, known as the pozzolana trass (Geisweid, J., Schaaff, H., 2011).

In Anatolia, tuff has been used as building stone for years. Tuff was used in Hellenistic, Roman, Byzantine period temples, castles, fortification walls, Ahlat tombstones, caravanserais of Seljuk, palaces of Ottoman and houses.

1.5 PREVIOUS STUDIES ON TUFFS

Some studies on tuffs dealing with their engineering properties to be used as building stones, conservation and source studies about tuff were summarized.

Topal and Doyuran (1997) determined material and mass properties of the Cappadocian tuff. The average pore diameter, saturation coefficient, wet-to-dry strength ratio, static rock durability index, index of rock durability, and slake-durability index of the tuff were used for the durability assessment of the rock, and of the fairy chimneys. The mercury porosimeter was used to study the pore size distribution and to find the average pore diameter of the Cappadocian tuff. A value of 0.11 μm was obtained from the test results (Topal, 1995), which suggested that the Cappadocian tuff was susceptible to frost damage. A saturation coefficient greater than 0.8 indicated low durability (susceptible to frost activity) (Hirschwald, 1912; TSE, 1977). However, many stones had saturation coefficients in the range of 0.66-0.77. In that range, the saturation coefficient gives an unreliable guide (Anon, 1975; BRE, 1983). The saturation coefficient of the Cappadocian tuff was 0.78. Cappadocian tuff might be considered to be frost susceptible based on the saturation

coefficient even though it was very close to the boundary. The wet-to-dry strength ratio of the tuff was determined as 33% in vertical and 19% in the horizontal directions. Those ratios have shown that the Cappadocian tuff had very poor durability. The sodium sulphate soundness test performed on the tuff indicated complete disintegration of the tuff after four cycles (Topal and Doyuran, 1996). The index of rock durability was found to be 0,13 in the vertical direction and 0,10 in the horizontal direction considering the compressive strength, effective porosity, and linear strain of the Cappadocian tuff. Those values revealed that the Cappadocian tuff had low durability.

Caner-Saltık et.al. (1993) discussed the surface deterioration of Göreme tuffs in the open air museum area by examination of their mineralogy and petrography, durability, physical and mechanical properties as well as microclimatic conditions. The investigations were done through optical and electron microscopy; XRD, spectrophotometric methods, pH, conductivity, temperature and humidity measurements. Durability was calculated by the help of salt crystallization, wetting drying and freezing thawing cycles. The surface alterations (color change, biodeterioration, crust, scales and granular disintegration) were examined up to about ten cm depth from the surface. Plagioclase feldspars were used as indicator for the depth of alteration. Analyses of thin sections and analytical methods showed that majority of feldspars were unaltered at that depth.

In the study of Vacchiano et. al (2008) a number of commercial polymeric resins, with different chemical composition were used, as protective coatings to prevent water from entering into the porous material. The protectiveness of the treatments was evaluated performing capillary absorption and total immersion tests and salts crystallization cycles, both on untreated and treated samples. To estimate the over time effectiveness of the treatments, colorimetric measurements and UV weathering tests were also done. The pore-size distribution was measured via a mercury porosimeter. Specimens used for this test had a cubic shape of 4 cm. SEM, XRD as micro analyses and Rock Durability Index were carried out. Silicon resins in water solution gave the best result in eco-compatibility, reduction of absorbed water, coloring and weathering resistance after UV weathering.

Torok and Prikryl (2010) gathered and summarized the techniques that could be used in understanding the behavior and diagnosis of deterioration used in historical monuments.

Bianchetti et. al (1982) studied on tuff blocks to determine their degradation process. Mineralogical petrographical analysis, XRD, SEM, mercury porosimetry and chemical analysis were done beside soluble salt content, porosity, bulk density, water absorption determination and laboratory ageing. Conservation treatments were tried to reduce porosity by modification of the mechanical characteristics of the stone. Silicon based consolidation substances were used and the experiments were repeated on treated samples. Chemical agents did not change the porosity so much but conservation treatments were aimed to decrease the water absorption to prevent soluble salt movement.

While studying on the durability of macroporous monumental stones used in historical town of Campania, according to standard procedures, Langella et. al. (2000) carried out the wet-dry and salt crystallization tests on Neopolitan Yellow Tuffs, Campanian and Piperno Ignimbrites. Open porosity, water absorption by total immersion; ultrasonic velocities (direct measurement), uniaxial compressive strength were measured. In order to evaluate the physico-mechanical and mineralogical features of the stones, those parameters were measured at regular intervals. SEM observations gave the opportunity to follow the changes of intergranular relationships.

Zedef et. al. (2007) studied on seven samples from fresh rocks and five samples from weathered rocks in order to compare their chemical compositions and loss on ignition (LOI) values while studying on the effects of salt crystallization on stones of historical buildings and monuments. Chemical, physical and mineralogical properties of rocks were investigated. Tuff samples had the highest LOI values due to the presence of perlitic texture in those rocks studied. The tuffs of Kiziloren caravanserai were completely disintegrated after salt crystallization cycles that tuffs were the weakest stone against salt crystallization.

D'Arienzo et al. (2008) conducted thermogravimetric analysis (TGA), water absorption tests, colorimetric measurements, water absorption by capillarity, water vapour permeability, uniaxial compression tests, abrasion resistance, SEM, XRD and petrographic analyses in the study of nanocomposite system based on polymers for strengthening tuff stone. Analyses were carried out on untreated and treated tuff samples.

In order to investigate the technical properties and geological aspects of the building stone of Naples, Calcaterra et.al. (2000) have conducted the tests with different dimensions of samples of Piperno tuffs. Such as; pycnometer tests, capillary absorption tests; water absorption by total immersion, water vapor permeability; ultrasonic velocity and uniaxial compressive tests, point load tests were done as well as mineralogical and petrographical analyses. Reaction to weathering agents and basic parameters of Piperno stone were determined that was to be defined as moderately strong rock.

Steindlberger (2004) studied weathering behavior of tuffs in Hesse-Germany with cubic samples. Density, bulk density, capillary water absorption, water absorption by immersion and under vacuum, saturation coefficient, hygric dilatation, compressive strength, open porosity and pore sizes were determined. Tuff stones were highly porous and less dense.

Topal and Sözmen (2003) investigated the depths and characteristics of weathering zones developed in white and pink tuffs of Midas monument by optical microscopy, XRD, chemical analyses, SEM and by determining some index parameters. Ageing tests were also performed. It is found that, thin section analyses, LOI (Loss on Ignition) and WPI (Weathering potential Index) are good indicators to determine weathering depth of tuffs. Wet to dry strength ratio gives better stone durability assessment.

Dessandier, Bromblet and Mertz (2000) worked with five tuff samples, poor to good durability, for a comparative study. After mineralogical and petrophysical characterization salt crystallization and wetting-drying ageing tests were conducted. Optical microscopy, XRD, FTIR, methylene blue adsorption were used and total

porosity, water absorption coefficient, capillary coefficient, compressive strength and specific surface area were determined. Important remarks were that the richer the rock in clastic elements, the poorer its cementation. Among the accessory minerals, however, the tuff samples contained particularly swelling clays like smectite.

The study of Paterno and Charola (2000) which was about the consolidation tests carried out on samples both treated and untreated tuff samples were artificially aged by wet-dry cycles. The outcomes of microscopy, IR analysis, water absorption and mechanical tests, showed that the cycle produced considerable deterioration for both treated and untreated specimens. Excluding the increase in porosity, partial leaching of iron ions decreasing the color of the stone to a depth of two mm and a surface deposition of amorphous silica were observed in the untreated specimens. Some flaking of the consolidant was observed and all samples showed the presence of a faint white efflorescence of amorphous silica in SEM analysis.

Topal et.al. (1993) studied deterioration mechanisms of Göreme tuffs. It was investigated through petrographical and geochemical methods. Analyses used in that study were thin section studies, X-ray powder diffraction, major and trace element analyses to determine the degree and depth of weathering and unit weight, porosity, water absorption were determined in order to understand the physical effect of deterioration. The chemical deterioration was mainly found to depth of two cm and discoloration due to biotite and alteration of rock fragments were up to seventeen cm depth. Feldspar weathering was seen up to eight cm depth. Although trace elements were important in determination of depth of weathering but the major element analyses should be regarded in tuff deterioration mechanisms.

Vacchiano (2006) studied decay analysis and materials compatibility due to renovation purposes. The work was focused on the study of the decay phenomena of tuff stones, widely used as building material in the historic centre of Salerno, and on suitable treatments for their repair and preservation. Their mineralogical, chemical, physical and mechanical characterizations were carried out. Non-weathered tuff stones collected in quarry were also characterized and their properties were compared with those shown by the tuff-stone in buildings. Treatments were applied and tests were repeated. Siliconic resins in water showed a good compromise

between the reduction of the absorbed water, the yellowing of the original material and the loss of performances due to the UV exposure.

Graue et.al., (2011) studied on quality assessment of replacement stones for the Cologne Cathedral by their mineralogical and petrophysical necessities. Besides optical properties, petrophysical criterias are also defined as well as strength values. Results showed that capillary water absorption, water saturation, drying processes and moisture dilatation could resulted in the deterioration.

Dreesen and Dusar (2004) studied historical building stones focusing on the role of petrography in provenance and durability assessment. Thirty-five stones including tuff were studied mineralogically and comparative study was done successively. Finally, recommendations were made for replacement stones, whose intrinsic characteristics often differed from those of the original stones.

Johnson et.al (2007) has used XRF and isotope analyses for provenance study. This project presents instrumental neutron activation analysis (INAA) characterization of 120 geologic samples from 4 fine grained basalt quarries on the Samoan Island of Tutuilan. Statistical methods, both canonical discriminant analysis (CDA) and principal component analysis (PCA) were applied to the INAA data. The quarries could be differentiated after INAA data and CDA gave better results than PCA. In the end, multiple Tutuilan quarries were clearly differentiated by INAA. Church said that “While artifact-centered studies attempt to source artifacts to their geological origin, material centered studies focus on geologic source material and are designed toward gathering baseline information” (Church, 1994).

CHAPTER 2

MATERIALS AND METHODS

2.1 METHODOLOGY OF THE STUDY

The study has three main stages. In the first stage, documents such as maps, photographs, reports, articles and books were collected. 1:100.000 scale geological maps were obtained from MTA and redrawn by software Freehand 10. After a review of the related literature and the geology of the region, and after the help of the archaeologists of the excavation, the locations of the possible quarries that were to be studied in the thesis work were determined.

The second stage was the field work and sample collection. Volcanic formations, their characteristics, uniformity, petrography were examined during this stage. Discontinuities, cooling joints were tried to be measured. Dimensions of temple stones and geologic formation stones were measured. Photographs were taken for the documentation. Sampling was done as block samples collection (70*100*80 cm). Quarries were selected and sampled to be compared with the tuffs of temple.

The work in the laboratory constitutes the third stage. Blocks were brought from three different locations. They were examined for their physical and physicommechanical properties (engineering geological properties) as well as microstructural properties and compared with the tuff samples taken from the monument. The blocks were cut into 4*4*4 cm cubes. The prepared cubes were used in cycle tests. Thin sections were prepared by MTA (General Directorate of Mineral Research and Exploration). Cross sections were prepared. Grinding was done for

XRD and salt concentration tests. XRF and Mercury Porosimetry analyses were done by METU Central Laboratory.

2.2 FIELD

The most important quarries that were probably used in antiquity were thought to be located in the slope of the stream running through the Gülpınar town, Çamkabalak formation. It was possible to come across with the empty places indicating cutting traces of the tuff blocks. Three locations were selected to be examined as ancient quarries: Babakale Road, Fatma Gerdan and Kızılkeçili.

2.2.1 BABAKALE YOLU

The quarry is on the old way of Babakale southwest of temple. It had traces that were thought to be an antique quarry thought because it was as well used as quarry today (Figure 10).

In the field it was observed that stones were some kind of tuff tougher than vitric tuff although they had similarity in color (Figure 7, Figure 8). Due to the convenience of transportation, the largest block sample was taken from there (Figure 9).



Figure 7. Babakale Yolu Quarry

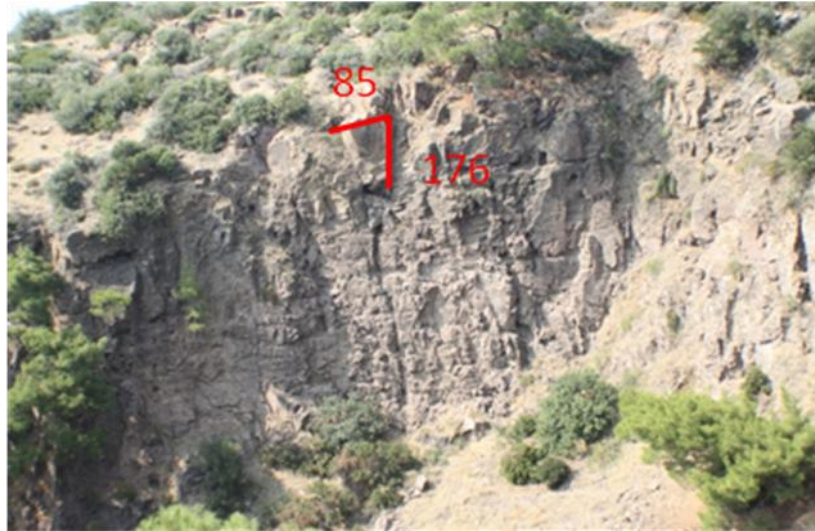


Figure 8. Babakale Yolu Quarry



Figure 9. Sample taken from Babakale Yolu Quarry



Figure 10. Babakale Yolu Quarry

2.2.2 FATMA GERDAN (DFG)

Fatma Gerdan region was on the south of temple. In the bedrock vitric tuff formations similar to the ones in Göreme were in abundance. Gülpınar town still used the drinking water coming from Fatma Gerdan with tuff channels (Figure 11).

It was observed that gray-brownish color tuff stone was similar with the temple tuff in color, fabric and texture. Large block dimensions similar with the temple tuff blocks supported the idea of it being an antique quarry, although stone surfaces were smoothed, corner and edges were rounded due to physical weathering (Figure 12-16).



Figure 11. Fatma Gerdan Quarry



Figure 12. Fatma Gerdan Quarry



Figure 13. Fatma Gerdan Quarry



Figure 14. Fatma Gerdan Quarry



Figure 15. Fatma Gerdan Quarry



Figure 16. Fatma gerdan Quarry

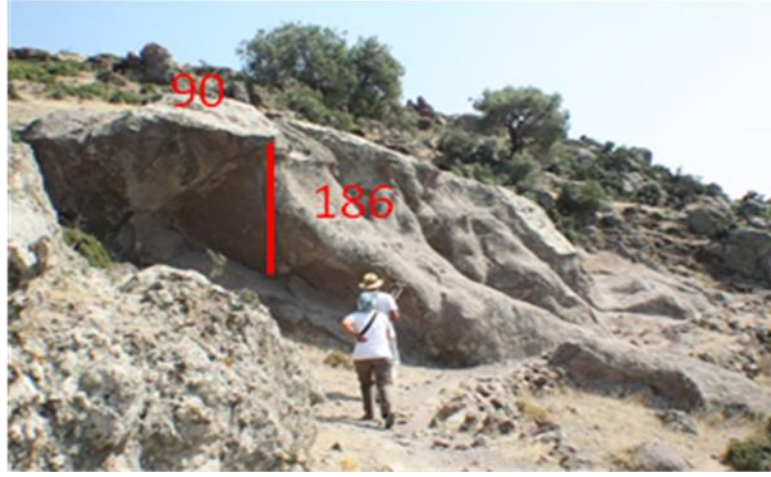


Figure 17. Fatma Gerdan Quarry

2.2.3 KIZILKEÇİLİ (DKK)

It was located in the east of Apollon Smintheion. It was in the steep valley (Figure 18). Gray color large tuff blocks same with the temple tuffs were the first observation in the field (Figure 19-21). Vitric tuff features similar with Apollon Smintheus Temple tuffs were noted.

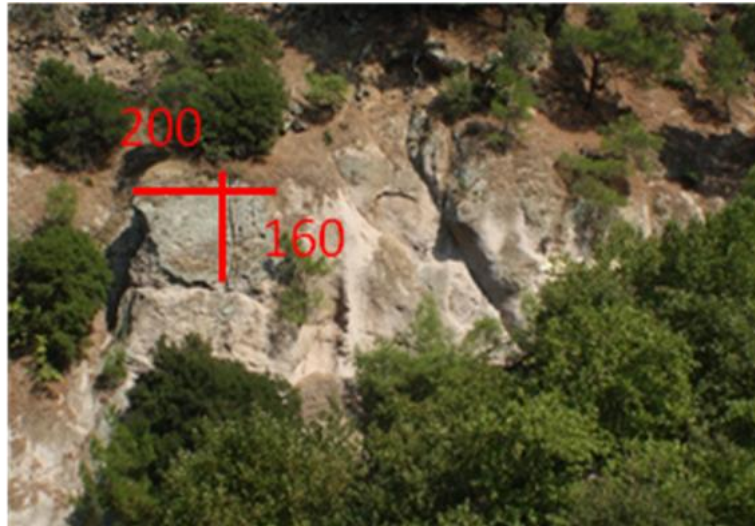


Figure 18. Kızılkeçili Quarry

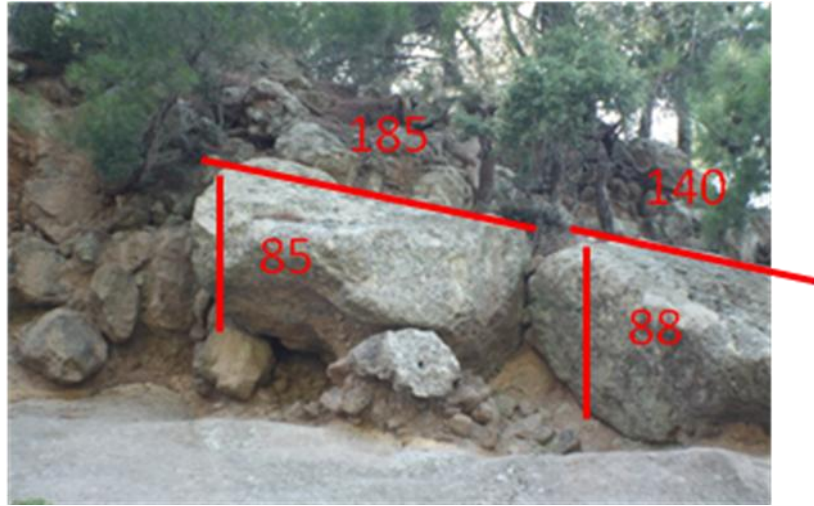


Figure 19. Kızılkeçili Quarry



Figure 20. Kızılkeçili Quarry



Figure 21. Kızılkeçili Quarry (by Kaplan, 2009)

2.2.4 TEMPLE

Tuffs in the temple were gray colored, weathered and had vitric tuff appearance (Figure 22, Figure 23, Figure 24). Samples were taken from tuff steps on northeast and northwest facades (Figure 25).



Figure 22. Apollon Smintheus Temple tuff foundations (from excavation archive)



Figure 23. Apollon Smintheus temple northeast façade



Figure 24. Apollon Smintheus Temple tuff foundations (by Kaplan, 2009)



Figure 25. Apollon Smintheus Temple sample taken

Vegetation was observed near tuffs (Figure 26-28). In the Roman Bath of holy place pinky tuffs were observed in the arch of külhan (Figure 29).



Figure 26. Apollon Smintheus Temple



Figure 27. Apollon Smintheus Temple



Figure 28. Apollon Smintheus Temple



Figure 29. Apollon Smintheion Roman Bath külhan tuff

2.3 DESCRIPTION OF SAMPLES

Description of samples with code, dimensions and explanations are shown below (Figure 30-36);

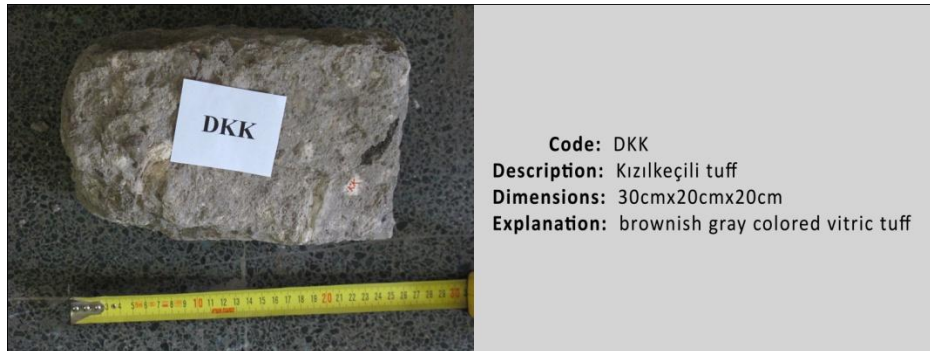


Figure 30. Kızılkeçili tuff



Figure 31. Babakale Yolu tuff

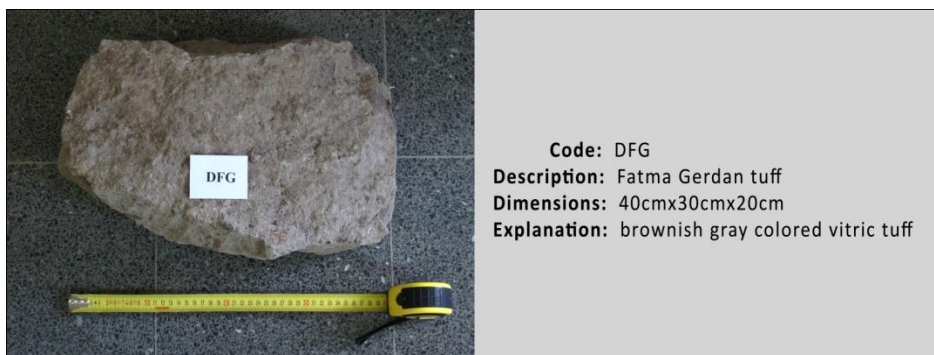


Figure 32. Fatma Gerdan tuff

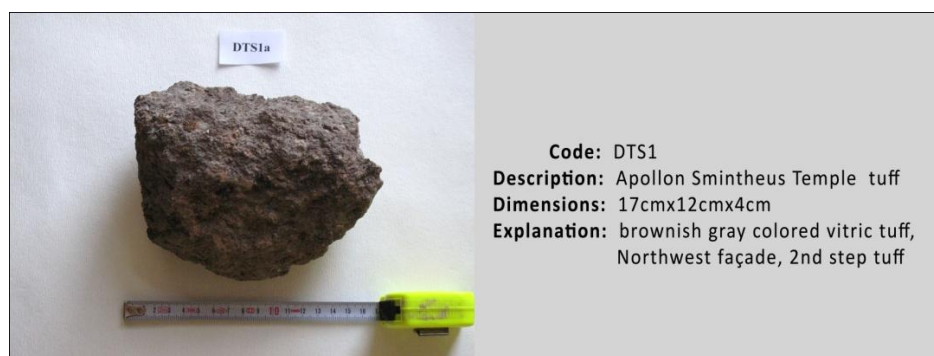


Figure 33. Temple stone 1

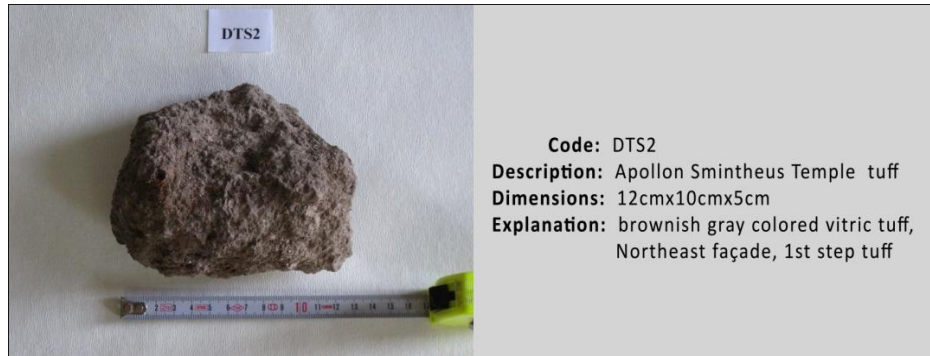


Figure 34. Temple stone 2

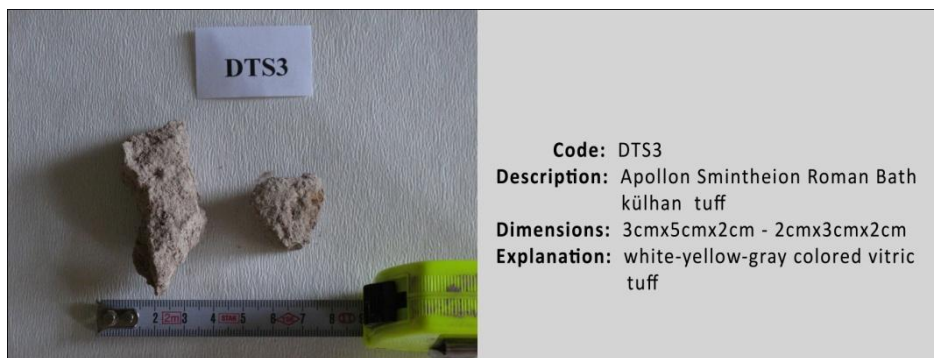


Figure 35. Roman Bath stone

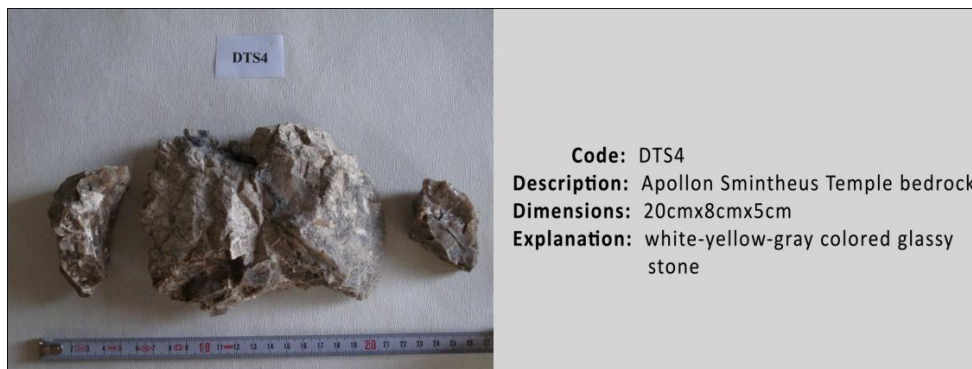


Figure 36. Temple stone 4

2.4 DETERMINATION OF ENGINEERING GEOLOGICAL PROPERTIES OF SAMPLES

The tests were performed on 2 cubic tuff samples from temple (DTS), 155 cubic tuff samples of first quarry (DBY), 52 cubic tuff samples of second quarry (DFG), 26 cubic tuff samples of third quarry (DKK). They were artificial weathering tests of salt crystallization and wetting drying and effective porosity, dry and saturated unit weight, water absorption capacity, bulk density, ultrasonic pulse velocity, capillary and moisture absorption, uniaxial compressive strength and pore size distribution.

2.4.1 ARTIFICIAL WEATHERING TESTS

The tests were performed in order to examine the deterioration factors that have major roles in deterioration of tuffs. Natural weathering behavior of stone could be better understood via correlation of those test results. According to the environmental conditions of the region two weathering tests; salt crystallization and wetting drying were applied.

2.4.1.1 SALT CRYSTALLIZATION TESTS

The test was performed on 26 cubic tuff samples of first quarry (DBY), 26 cubic tuff samples of second quarry (DFG), 13 cubic tuff samples of third quarry (DKK). Samples were immersed in $\text{Na}_2\text{SO}_4 \cdot 10\text{H}_2\text{O}$ solution for 1 hr. Then they were dried in 60 °C oven for 24 hours. After that, they were cooled to room temperature. The test was repeated 4 times. Later, samples were washed for 1.5 months every day to clean up the salt. Evaluations were done by measuring weight loss, effective porosity, water absorption capacity, ultrasonic velocity and uniaxial compressive strength of the samples. DKK and DFG samples were disintegrated after 3rd cycle of salt crystallization; DBY samples were more durable to the salt crystallization. Unless

disintegration happened 10% of weight loss was considered to end the cycle and 6 cycles were applied to DBY samples.

2.4.1.2 WETTING-DRYING TESTS

This ageing test was intended for the evaluation of the wetting and drying resistance of tuffs. It was aimed to determine the material loss produced by repeated wetting and drying of specimens.

The test was performed on 26 cubic tuff samples of first quarry (DBY), 26 cubic tuff samples of second quarry (DFG), 13 cubic tuff samples of third quarry (DKK). For the wetting-drying tests, the samples were immersed for 24 hours in distilled water at 15-20°C. The samples were dried in an oven at 60 °C. They were then cooled to room temperature. This procedure was repeated 32 times. Evaluations were done by measuring weight loss, porosity, water absorption capacity, ultrasonic velocity and uniaxial compressive strength of the samples. DKK samples were disintegrated after 8th cycle of wetting drying, DFG samples endured until 28th cycle and again DBY samples were more durable to wetting drying. Unless disintegration happened 10% of weight loss was considered to end the cycle and 28 cycles were applied to DBY samples.

2.4.2 EFFECTIVE POROSITY AND UNIT WEIGHT

Effective porosity and unit weight are important index properties of a rock. The increase in the pores in the fabric of a rock material decreases its strength, and increases its deformability. The pores also affect the unit weight which means the weight per unit volume of a material. They can be determined by the same test.

The samples were oven dried at around 100°C until constant mass and then weighed (M1-dry weight). Then, they were placed in a tray and covered with distilled water at

room temperature of about 20°C and left immersed for 24 hours. They were left under vacuum for about 20 minutes in order to let water into all pores.

Each sample was taken out of the tray and weighed immersed in water (M2-Archimedes' weight). Then the sample was wiped with a wet paper and weighed again (M3-saturated weight).

Real density was the mass per real volume and calculated as $(M1 / (M1-M2)) \times 100$.

On the other hand bulk density was the mass per apparent volume so that the calculation differs as $(M1 / (M3-M2)) \times 100$.

Unit weight is the density x gravity.

Since porosity is the voids in the solid mass as percent it is calculated as $(1 - (\text{Bulk density} / \text{Real density})) \times 100$.

The test was performed on 2 cubic tuff samples from temple (DTS), 155 cubic tuff samples of the first quarry (DBY), 52 cubic tuff samples of second quarry (DFG), 26 cubic tuff samples of third quarry (DKK).

2.4.3 WATER ABSORPTION UNDER ATMOSPHERIC PRESSURE

Water absorption capacity (WAC) is the maximum amount of water which a sample can absorb under the certain conditions.

That test was intended to measure the amount of water absorbed by a rock under atmospheric pressure and expressed in percentage and was calculated as $((M3-M1) / M1) \times 100$.

The test was performed on 2 cubic tuff samples from temple (DTS), 155 cubic tuff samples of first quarry (DBY), 52 cubic tuff samples of second quarry (DFG), 26 cubic tuff samples of third quarry (DKK).

2.4.4 COLOR SPECTROMETER MEASUREMENTS

Determination of color depended on different external factors as personal and environmental conditions. Different methods were used for the purpose of color for the scientific studies. Munsell Classification and CIELAB System were the main methods having different principles. In the experiment CIELAB System were used.

CIELAB system was widely used for the objective instrumental color measurement. In the method, color was described as three coordinates. CIE L* represented lightness which range from 0 to 100, CIE a* represented greenness and CIE (positive) b* represented yellowness (Wyszecki et al., 1982).

Spectrophotometer CM-2600d/2500d Konica Minolta was used as the device of color measurements.

2.4.5 QUALITATIVE ANALYSIS OF THE SOLUBLE SALTS BY SPOT TESTS

The amount of salt in the sample was determined by measurement of electrical conductivity as percent by weight. For that test, powdered stone samples were dried in an oven at 60°C for 24 hours. From each sample 1 g was taken and mixed with 50ml distilled water. The mixtures were left closed for settlement of suspended particles for 24 hours and then filtered. The amount of soluble salt in the samples was determined with the conductivity measurements of the salt extract solutions. Electrical conductivity measurements were done using a conductometer of Metrohm AG Herisau, Kondoktometer E382. Percent salt in the sample was calculated using the following equations (Black, 1965).

$$EC = [(0.0014 * R_{std}) / (R_{ext})] \text{ (mhos-cm}^{-1}\text{) where;}$$

EC: electrical conductivity

R_{std} : the cell resistance with standard solution (0.01 N KCl)

R_{ext} : the cell resistance with extract solution

% salt in the sample = $[A \cdot V_{\text{ext}} / 1000] \cdot [100 / W_s]$ where;

A: salt concentration (mg/l) = $640 \cdot \text{EC}$ (mmhos cm⁻¹)

V_{ext} : volume of the extract solution (ml)

W_s : Weight of sample (mg)

2.4.6 ULTRASONIC PULSE VELOCITY

In this experiment, it was intended to measure the velocity of transmission of elastic waves. The modulus of elasticity of stones was determined by ultrasonic pulse velocity measurements and bulk density of the samples (ASTM 2845-90; RILEM 1980).

The instrument used was a pulse generating test equipment, PUNDIT plus with its probes, transmitter and receiver of 220 kHz for all samples. Direct measurement was applied.

In the method, the impulse was imported to the specimen and the time required for the ultrasonic waves to pass the minimum cross section of test specimen was measured.

The velocity of the waves was calculated by using the following formula.

$$V : l/t$$

Where,

V : velocity (m/s)

l : the distance traversed by the wave (mm)

t : travel time (s)

The modulus of elasticity was then obtained through the bulk density of the sample and velocity of wave by the following equation (RILEM, 1980).

$$E_{\text{mod}} = D \cdot V^2 (1 + \nu_{\text{dyn}}) (1 - 2\nu_{\text{dyn}}) (1 - \nu_{\text{dyn}})$$

Where;

E_{mod} : modulus of elasticity (N/m²)

D : bulk density of the specimen (kg/m³)

v : wave velocity (m/sec)

ν_{dyn} : Poisson's ratio

In that equation, Poisson's ratio differed from 0.1 to 0.5. Considering the similarities between plaster, mortar and lightweight concrete, and other case studies for tuffs were investigated, $\nu_{\text{dyn}} = 0.20$ seemed to be a reasonable value for this case (Topal 1995).

2.4.7 CAPILLARY ABSORPTION

The capillary properties of rocks are important issue in regard of evaporation and suction of water due to the control mechanism of movement of water thus soluble salts.

The test was performed as weight difference measurement in time while the sample absorbed water by capillarity. Sample is suspended to the water and every five minutes until thirty minutes, and then every half an hour a measurement was taken. The difference between the initial weights gave the capillary absorption coefficient.

2.4.8 MOISTURE CAPILLARY ABSORPTION

The moisture capillary absorption test was intended to apply because water moved through fine pores to large pores because capillary suction was greater in finer pores than in large ones. Saturation degree affected the movement of water in the rock thus

moisture capillary absorption was needed to be measured under the saturation value (Schaffer, R.J., 1932).

Moisture absorption implied the finest pore ($<0.5 \mu$). Though it was a long procedure it can be repeated several times and gave an idea about pore size distribution (Caner-Saltık et al., 1998).

In order to get the 80% relative humidity environment, 10% CaCl_2 solution is put in a dessiccator (Large, 1967). A couple of days later, when the environment have 80% RH and 20°C the samples were placed in it and weight difference was measured periodically, until constant weight was achieved.

2.4.9 UNIAXIAL COMPRESSIVE STRENGTH

The point load test was developed by Broch and Franklin (1972) for classifying and characterizing rock material. The International Society of Rock Mechanics (ISRM) standardized and established it in 1985. In addition, the point load test can be performed on samples with different shapes, either core or irregular shaped samples. The point load strength index can be used to calculate other strength parameters since it correlates with uniaxial compressive strength (Broch and Franklin, 1972; ISRM, 1985).

The tests were performed on the samples of temple and quarry both in dry and saturated conditions. Specimens of weathering tests were measured in dry state.

2.4.10 PORE SIZE DISTRIBUTION

There are several methods to understand the pore size distribution. Optical microscopy, moisture capillary absorption, image analysis are examples of them. However pore size distribution can be gathered from mercury porosimetry. The measurements were done in METU Central Laboratory with the device Quantachrome Corporation, Porosimeter 60. DKK sample was measured in The Laboratoire de Recherche des Monuments Historique (LRMH).

The operation of Mercury Porosimeters depends on the physical principle that a non-reactive, non-wetting liquid would not penetrate fine pores until sufficient pressure is applied to force its entry. The relationship between the applied pressure and the pore diameter was given by the Washburn equation:

$$D = \sqrt{\frac{4 \times \cos\theta}{P}}$$

P=Applied Pressure

D=Pore Diameter

X=Surface Tension of mercury (480 dyne/cm)

Θ =Contact angle between mercury and pore wall

2.5 MINERALOGICAL AND PETROGRAPHICAL PROPERTIES OF SAMPLES

Petrography deals with the description of rocks, their mineralogy, structures and textures. Thin section and cross section analyses under optical microscope, X-Ray Diffraction analysis, X-Ray Fluorescence Analysis, Scanning Electron Microscopy, FTIR analysis, Methylene Blue Adsorption were used to understand the mineralogical and petrographical features of rock samples. The comparisons of the results were made to see the relationship between rocks.

2.5.1 THIN SECTION ANALYSIS

For this analysis samples were placed into plastic molding boxes of 1.5x3x1cm. They were saturated with the polyester (ESKIM- extra POLYESTER) mixed with accelerator and hardener under vacuum of 100 torr.

Following their hardening, the molded samples were removed from boxes and cut into 1mm slices to be fixed and reduced to 30 μ thickness on microscope slides. Thin sections of the samples were examined using polarizing microscopes of Nikon AFX-

2A and Carl Zeiss equipped with a photographic attachments. Mineralogical and morphological properties, such as shape, size, and distribution of particles in the matrix were examined. Samples were prepared in MTA (General Directorate of Mineral Research and Exploration).

2.5.2 CROSS SECTION ANALYSIS

Stones were covered with polyester resin in the plastic cases (~1,5x3x1cm). After solidifying, the samples were taken in the containers and cut with thin diamond blade by Buehler-Isomet Low Speed Saw. The cut surfaces were coated with Geofix resin. After drying, the coated surfaces were polished with re-sanding papers (Silicone Carbide 320 and 600). The photographs of the samples were taken with a computer program Leica Application Suite (LAS) with stereomicroscope. The investigation was done on photographs which had the information about the groundmass, rock fragments and pores.

2.5.3 X-RAY DIFFRACTION (XRD) ANALYSIS

The fact of the contact of any sort of wave with objects whose dimensions are similar with the wavelength is diffraction. In XRD analyses, aligned X Rays are supposed to drop on sample and a proportion will be diffracted at angles depending on the crystal structure of the sample (Herz, Garrison, 1998). Basically from a qualitative or semi-quantitative approach, X-ray diffraction techniques are generally used to discover crystalline materials. The sensitivity of the method is highly reliant on the character of the material and abundance more than 5-10% (Nicol, 1975).

Mineralogical compositions of the samples were examined by XRD. The analyses were carried out on powdered stone samples. Both oriented and unoriented samples were prepared. Oriented samples were prepared for the analyses of clay minerals. Before the analyses, tuff was grounded in an agate mortar.

For the separation of clay minerals and preparation of their oriented samples, a powder sample of 10 g passing #200 mesh was placed in 600ml beaker and filled with distilled water. The sample and distilled water were centrifuged for 5 minutes at 700 rpm, in 100 ml tubes. Then the suspension was taken and re-centrifuged for 25 minutes at 4000 rpm. The tubes were removed and the water was decanted leaving the clay pasted at the bottom of the tubes. This remaining paste was removed with spatula and was spread on three glass plates. One of them was X-rayed as air-dried. The second plate was placed on a ceramic plate in a desiccator filled with ethylene glycol and the desiccator was placed in an oven operated for one hour at 50°C. After one hour, the oven was turned off and the plate was allowed to solvate overnight. Then, the glycolated plate was X-rayed immediately after removing it from the desiccators. The last plate was placed on a kiln at a temperature of 300°C for one hour. The heated plate was removed and instantaneously X-rayed (Jackson, 1975).

The instrument used was a Bruker D8 Advance Diffractometer, Sol-X detector. Analysis was done using $\text{CuK}\alpha$ radiation with, adjusted to 40kV and 40mA. The XRD traces were recorded for the 2θ values from about 2 to 70. Mineral phases were identified in XRD traces.

2.5.4 X-RAY FLUORESCENCE (XRF) ANALYSIS

X-ray fluorescence (XRF) is the emission of characteristic secondary X-rays from a material that has been energized by blasting with high-energy X-rays or gamma rays. The method is widely used for elemental analysis and chemical analysis (Herz, Garrison, 1998).

Abundance of an element is important parameter beside the matrix effect (Ferretti, 1993). In order to regard these effects calibration must be done. If the sample is close enough to the standards measurement will be more correct.

Analyses were done by METU Central Laboratory. Major and minor elements were identified.

2.5.5 SCANNING ELECTRON MICROSCOPY (SEM) – ENERGY DISPERSIVE ANALYZER (EDX)

Electron microscopes have resolution between 2 to 20Å while optical microscopes have 2000Å which means that resolution problems due to radiation wavelength are eliminated (Ferretti, 1993).

Tescan Vega II XMU was used as device. Samples from temple and quarries were analyzed to understand the microstructure.

Since all of the samples were non-conductive samples, surfaces were coated with conducting gold layer with a gold coater instrument.

2.5.6 FOURIER TRANSFORM INFRARED SPECTROSCOPIC ANALYSIS (FTIR)

The Fourier-transform infrared (FTIR) technique has been used for both qualitative and quantitative determination in mineral species (McMillan et al., 1988). It has advantages such as easy preparation, high sensitivity, and rapid analysis.

In the study, FTIR techniques were used to distinguish between different types of clay minerals and to obtain information relating to their composition, structure and structural changes upon chemical variation (Madejová, 2003).

FTIR measurements were performed on the powdered samples of the clay parts which were already prepared for oriented XRD analyses. The instrument was a Bruker Alpha P FTIR unit with ATR attachment.

2.5.7 METHYLENE BLUE ADSORPTION TEST

The Methylene Blue Adsorption (MBA) test is used to gain information about the existence/amount of clay minerals and their cation exchange capacity properties.

Since the Methylene Blue (MB) is nonabsorbent of water and the normality of the MB solution is not included in the MBA value, the MBA is not used for the valuation of the results. Instead, Cation Exchange Capacity (C.E.C) of samples are used that already the normality of MB solution is included in the calculation of C.E.C values. It is important to correlate the test results with the common clay mineral C.E.C and MBA values.

The spectrophotometer was SP3000 Plus OPTIMA and 1 cm length silica cells are used.

The test procedure was;

2,5 ml/L, 5 ml/L, 10 ml/L, 15 ml/L, 20 ml/L, 25 ml/L MB solutions were prepared and standard curve is drawn in order to find the best wavelength to be used. Wavelength 665 nm was the maximum absorption peak of methylene blue monomers (Rabinovitch and Epstein, 1941; Ramasamy, Anandalakshmi, 2008). However in this study over 632 nm wavelength gave the highest reliable peak and 25 ml/L MB solution gave ill defined standard curve thus 20 ml/L MB solution was used (Figure 37).

Tuff samples were powdered in an agate mortar passing through 200# mesh. Then 100 mg sample powder were put in 150/200/500 ml MB solution. The solution was mixed by a magnetic stirrer for 2 hours then centrifuged for 5 minutes. MBA of that solution was measured in the spectrophotometer.

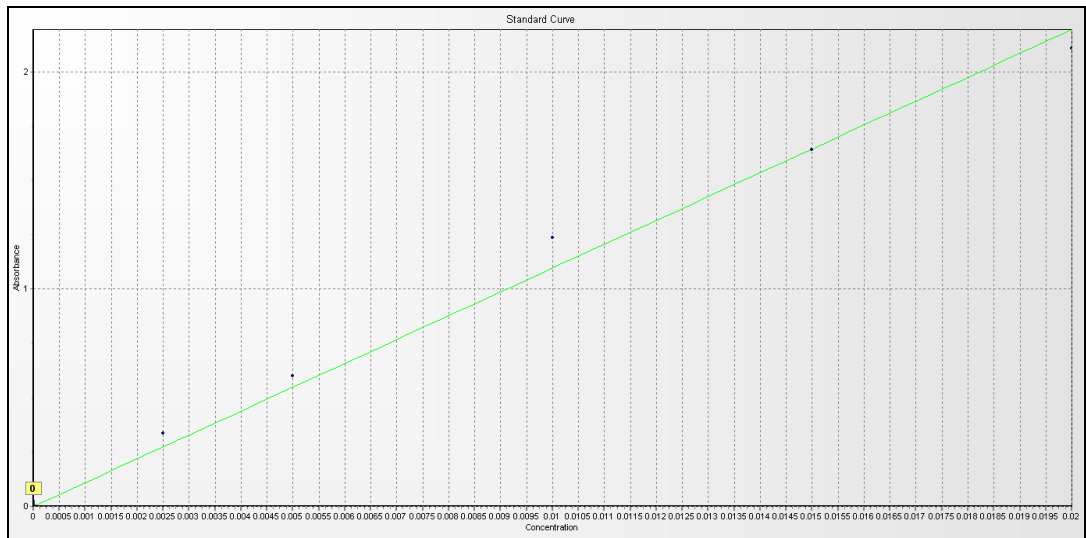


Figure 37. Graph of absorbance vs conservation at 632 nm

CHAPTER 3

EXPERIMENTAL RESULTS

In this chapter, experimental results were given in the order of engineering geological properties and petrographical properties analyses.

3.1 DETERMINATION OF ENGINEERING GEOLOGICAL PROPERTIES OF SAMPLES

In this section, results of engineering geological properties of samples are given.

3.1.1 DENSITY & POROSITY (EFFECTIVE POROSITY AND UNIT WEIGHT) AND WATER ABSORPTION CAPACITY

As mentioned above, experimental results are shown according to chronological order that results of basic physical and physicommechanical properties of firstly fresh samples from quarries and weathered samples from temple and then of after salt crystallization and wetting drying cycles.

3.1.1.1 FRESH SAMPLES FROM QUARRIES AND WEATHERED SAMPLES FROM TEMPLE

Temple stones had low unit weight ($12,76 \pm 1,19 \text{ N/m}^3$) and high porosity ($54 \pm 7,87$ %) values and high water absorption capacity value; $41,15 \pm 2,20$ % (Table 2).

The average effective porosity, dry and saturated unit weights of the tuff were $54 \pm 7,87$ % - $12,76 \pm 1,19 \text{ kN/m}^3$ - $18,02 \pm 1,96 \text{ kN/m}^3$; $16 \pm 2,15$ % - $24,24 \pm 1,62 \text{ kN/m}^3$ - $25,69 \pm 1,70 \text{ kN/m}^3$; $48 \pm 4,12$ % - $12,18 \pm 0,80 \text{ kN/m}^3$ - $16,72 \pm 1,09 \text{ kN/m}^3$; $45 \pm 5,31$ % - $13,78 \pm 1,36 \text{ kN/m}^3$ - $17,91 \pm 1,42 \text{ kN/m}^3$, respectively. Temple tuffs had the highest porosity and lowest bulk density, DFG and DKK followed it. DBY had the lowest porosity and the highest bulk density.

The average water absorption capacities of tuffs were $41,15 \pm 2,20$ % ; $6,48 \pm 0,85$ % ; $38,39 \pm 2,85$ % ; $32,39 \pm 5,36$ %, respectively (Table 2).

Table 2. Basic physical and physicomechanical test values

Tuff samples;	P(%)	D (g/cm³)	WAC (%)	Sat. Coef	Dry unit weight	Sat. Unit weight
DTS	$54 \pm 7,87$	$1,30 \pm 0,12$	$41,15 \pm 2,20$	$0,77 \pm 0,07$	$12,76 \pm 1,19$	$18,02 \pm 1,96$
DBY	$16 \pm 2,15$	$2,47 \pm 0,17$	$6,48 \pm 0,85$	$0,4 \pm 0,03$	$24,24 \pm 1,62$	$25,69 \pm 1,70$
DFG	$48 \pm 4,12$	$1,24 \pm 0,08$	$38,39 \pm 2,85$	$0,8 \pm 0,05$	$12,18 \pm 0,80$	$16,72 \pm 1,09$
DKK	$45 \pm 5,31$	$1,40 \pm 0,14$	$32,39 \pm 5,36$	$0,7 \pm 0,07$	$13,78 \pm 1,36$	$17,91 \pm 1,42$

3.1.1.2 SALT CRYSTALLIZATION CYCLE

Porosity values of DBY, DFG and DKK were slightly increased as 16% to 21%, 48% to 56% and 45% to 54%. That is to say, DBY porosity increased 31% (Table 3), DFG porosity increased 16% (Table 4) and DKK porosity increased 23% (Table 5).

Bulk density of DBY changed to $2,31 \text{ g/cm}^3$ from $2,47 \text{ g/cm}^3$, while bulk densities of DFG and DKK changed from $1,24$ to $1,21 \text{ g/cm}^3$ and from $1,40$ to $1,38 \text{ g/cm}^3$ respectively.

Water absorption capacity increased by salt crystallization (Figure 38), saturated unit weight slightly increased. Increase in WAC was considerable for DKK and DFG (Figure 39), effective porosity increased (Figure 40), dry unit weight was not affected by salt crystallization (Figure 41), saturation coefficient did not considerably change by salt crystallization (Figure 42), also bulk density decrease was slight (Figure 43). Salt crystallization which was very destructive test caused sudden or slight change in a very short time. That made observation difficult.

DBY

Table 3. Basic physical and physicommechanical test values of DBY after salt crystallization cycle

Test cycle	P(%)	D (g/cm ³)	WAC (%)	Real D	Sat. Coef	Dry unit weight	Sat. Unit weight
0	16,00	2,47	6,48	2,95	0,40	24,24	25,69
1	15,64	2,13	7,41	2,53	0,47	20,87	22,40
2	18,39	2,54	7,24	3,11	0,39	24,90	26,71
3	18,71	2,54	7,37	3,13	0,39	24,89	26,73
4	19,97	2,45	8,17	3,06	0,4	24,05	26,01
5	20,96	2,31	9,09	2,92	0,43	22,61	24,67

DFG

Table 4. Basic physical and physicommechanical test values of DFG after salt crystallization cycle

Test cycle	P(%)	D (g/cm ³)	WAC (%)	Real D	Sat. Coef	Dry unit weight	Sat. Unit weight
0	48,00	1,24	38,39	2,40	0,80	12,18	16,72
1	51,44	1,19	43,37	2,46	0,84	11,70	16,74
2	63,62	1,26	50,66	4,68	0,80	12,37	18,61
3	52,56	1,15	45,71	2,52	0,87	11,29	16,45
4	55,85	1,11	42,12	2,49	0,83	11,09	16,88

DKK

Table 5. Basic physical and physicochemical test values of DKK after salt crystallization cycle

Test cycle	P(%)	D (g/cm3)	WAC (%)	Real D	Sat. Coef	Dry unit weight	Sat. Unit weight
0	45,00	1,40	32,39	2,58	0,70	13,78	17,91
1	45,68	1,22	41,35	2,47	0,82	11,98	16,93
2	50,51	1,26	43,01	2,74	0,80	12,35	17,62
3	53,78	1,38	45,87	2,15	0,73	13,53	17,03

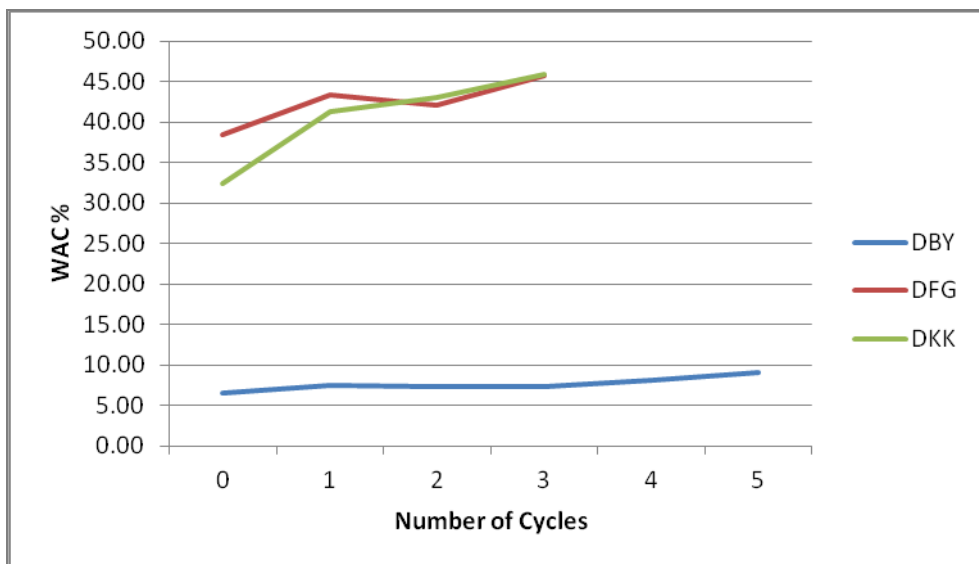


Figure 38. Water absorption Capacity change of samples in salt crystallization cycles

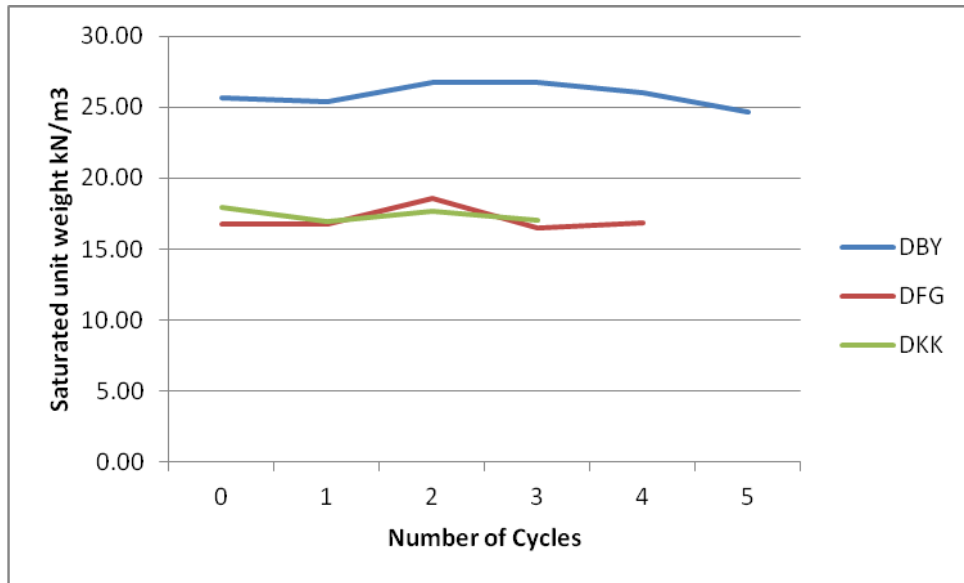


Figure 39. Saturated Unit Weight change of samples in salt crystallization cycles

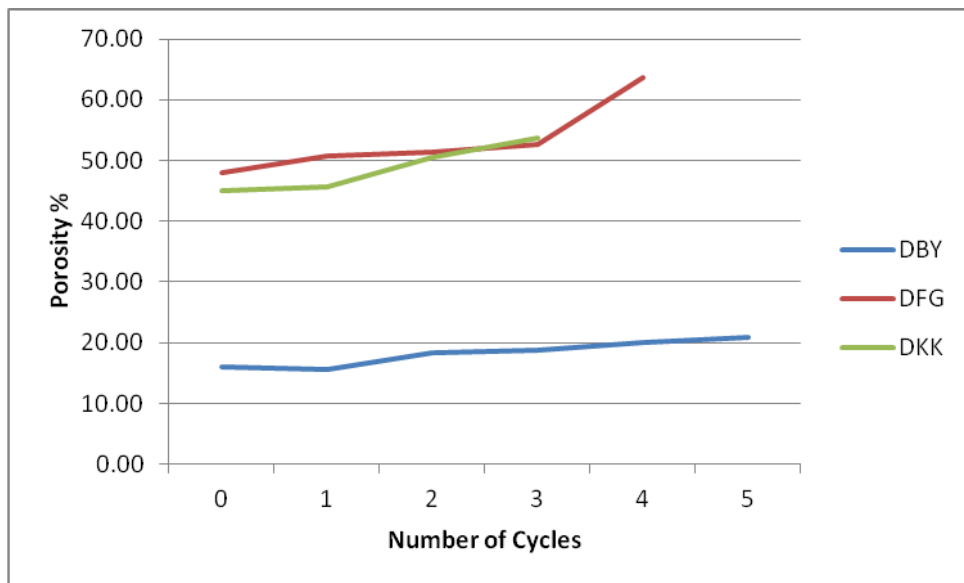


Figure 40. Porosity change of samples in salt crystallization cycles

Porosity increase in the rocks reduces the durability against weathering. Besides, increase in the porosity leads to have lower density and be effective on heat and sound conductivity (Goodman,1989; Korcanç, 2007).

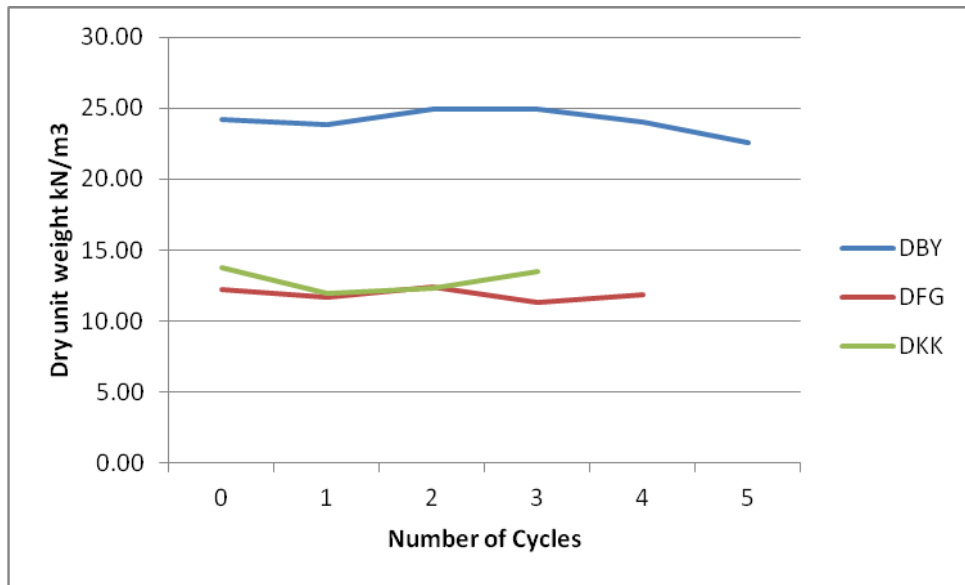


Figure 41. Dry unit Weight change of samples in salt crystallization cycles

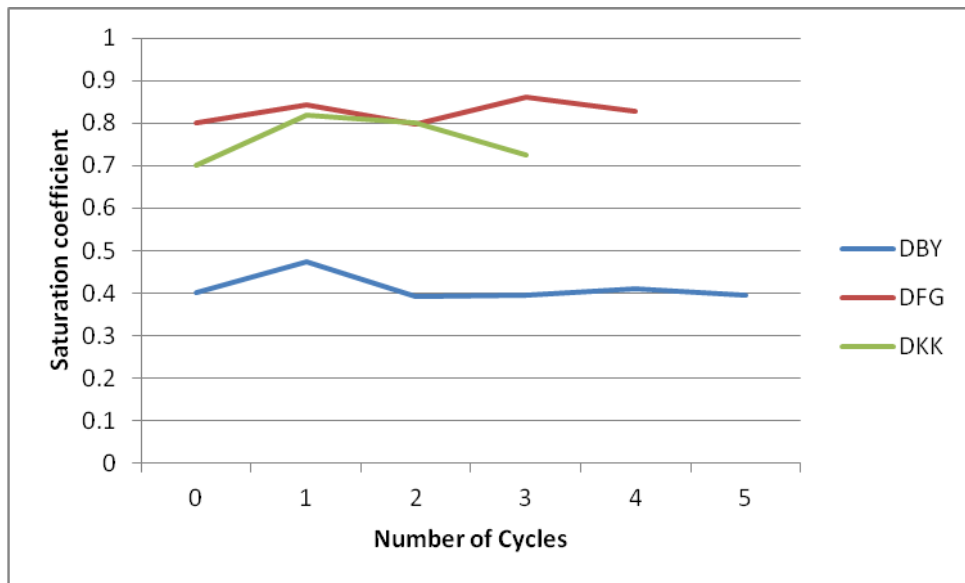


Figure 42. Saturation Coefficient change of samples in salt crystallization cycles

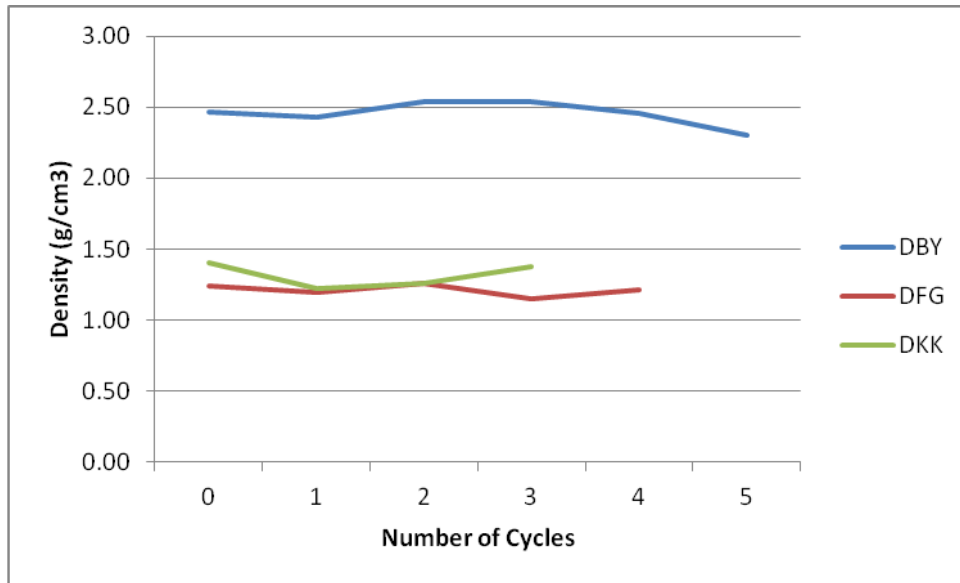


Figure 43. Bulk density change of samples in salt crystallization cycles

3.1.1.3 WETTING DRYING CYCLE

Although wetting drying cycle is less destructive than salt crystallization cycle, most of the samples were disintegrated during the experiment. This may be because of the resolution product clay minerals in the pores (Franklin and Chandra, 1972). Presence of clay minerals in the microstructure of the tuffs, their swelling and concentration during wetting-drying cycles might have caused the disintegration of tuff samples after eight and twenty eight cycles of wetting- drying.

Porosity values of DBY, DFG and DKK were slightly increased as 16% to 21%, 48% to 63% and 45% to 53%. That is to say, DBY porosity increased 31%, DFG porosity increased 31% and DKK porosity increased 17%. The reason of slight increase of DKK might be the less number of cycles.

Bulk density values of DBY, DFG and DKK are a little decreased as $2,47 \text{ g/cm}^3$ to $2,28 \text{ g/cm}^3$; $1,24 \text{ g/cm}^3$ to $1,22 \text{ g/cm}^3$ and $1,4 \text{ g/cm}^3$ to $1,31 \text{ g/cm}^3$ (Table 6, Table 7, Table 8).

Water absorption capacity of DFG and DKK considerably increased, increase of DBY was not noticeable (Figure 46), saturated unit weight of samples slightly increased (Figure 45), effective porosity increased (Figure 44), dry unit weight of samples fluctuated and slightly changed (Figure 47), there were no considerable change saturation coefficient (Figure 48), bulk density decrease of samples were slight (Figure 49).

DBY

Table 6. Basic physical and physicommechanical test values of DBY after wetting drying cycle

Test cycle	P(%)	D (g/cm ³)	WAC (%)	Real D	Sat. Coef	Dry unit weight	Sat. Unit weight
0	16,00	2,47	6,48	2,95	0,4	24,24	25,69
3	17,83	2,55	7,01	3,11	0,39	25,03	26,78
4	18,00	2,45	7,37	2,99	0,41	24,03	25,80
6	19,83	2,53	7,84	3,16	0,40	24,79	26,73
8	19,55	2,54	7,68	3,16	0,39	24,94	26,85
10	18,18	2,34	7,76	2,86	0,43	22,96	24,75
12	18,85	2,34	8,06	2,88	0,43	22,92	24,77
14	20,25	2,34	8,66	2,93	0,43	22,93	24,91
16	19,15	2,33	8,23	2,88	0,43	22,85	24,73
18	18,34	2,54	7,20	3,12	0,39	24,93	26,73
20	18,22	2,55	7,14	3,12	0,39	24,98	26,77
22	19,54	2,44	8,05	3,03	0,41	23,94	25,86
24	20,73	2,52	8,22	3,19	0,40	24,76	26,79
26	19,98	2,50	8,06	3,12	0,40	24,53	26,49
28	21,36	2,28	8,69	3,15	0,41	24,34	26,43

DFG

Table 7. Basic physical and physicochemical test values of DFG after wetting drying cycle

Test cycle	P(%)	D (g/cm ³)	WAC (%)	Real D	Sat. Coef	Dry unit weight	Sat. Unit weight
0	48,00	1,24	38,39	2,4	0,8	12,18	16,72
3	47,71	1,20	39,64	2,31	0,83	11,80	16,48
4	45,52	1,10	41,58	2,02	0,91	10,75	15,21
6	51,25	1,25	41,13	2,59	0,80	12,23	17,26
8	50,66	1,27	40,02	2,59	0,79	12,42	17,39
10	56,55	1,37	41,14	3,24	0,73	13,45	19,00
12	56,72	1,37	41,38	3,24	0,73	13,41	18,97
14	48,24	1,16	41,81	2,23	0,87	11,33	16,07
16	48,71	1,16	42,05	2,26	0,86	11,37	16,15
18	49,48	1,22	40,57	2,43	0,82	11,96	16,82
20	50,05	1,23	40,74	2,47	0,81	12,04	16,95
22	39,39	1,70	28,99	2,73	0,74	16,70	20,56
24	55,01	1,32	41,70	3,05	0,76	12,91	18,30
26	63,66	1,25	51,00	3,61	0,80	12,28	18,53
28	63,11	1,22	52,00	3,43	0,82	11,92	18,11

DKK

Table 8. Basic physical and physicochemical test values of DKK after wetting drying cycle

Test cycle	P(%)	D (g/cm ³)	WAC (%)	Real D	Sat. Coef	Dry unit weight	Sat. Unit weight
0	45,00	1,4	32,39	2,58	0,7	13,78	17,91
3	50,26	1,34	37,81	2,70	0,75	13,13	18,06
4	52,49	1,11	47,21	2,38	0,90	10,92	16,07
6	51,57	1,40	36,84	2,93	0,71	13,70	18,76
8	53,32	1,31	40,69	2,88	0,76	12,85	18,08

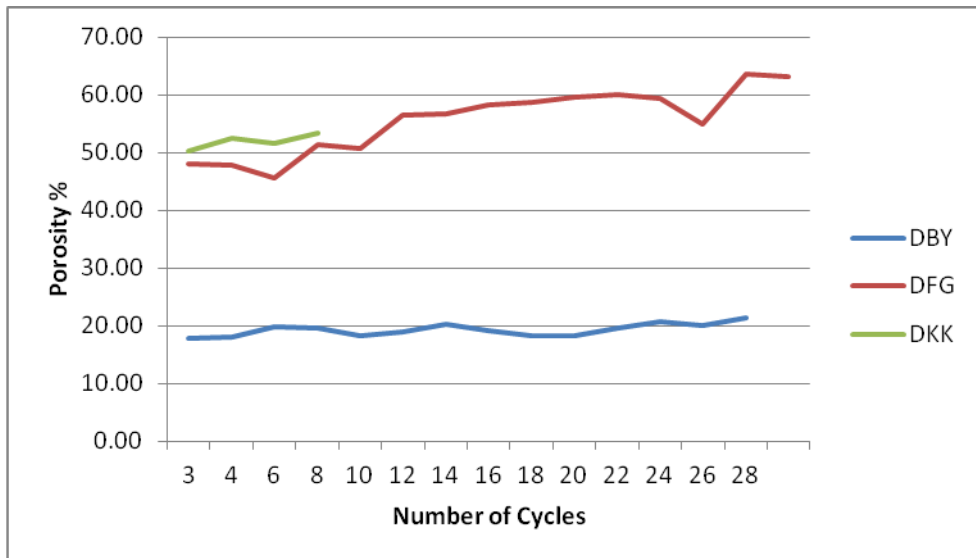


Figure 44. Porosity change of samples in wetting drying cycles

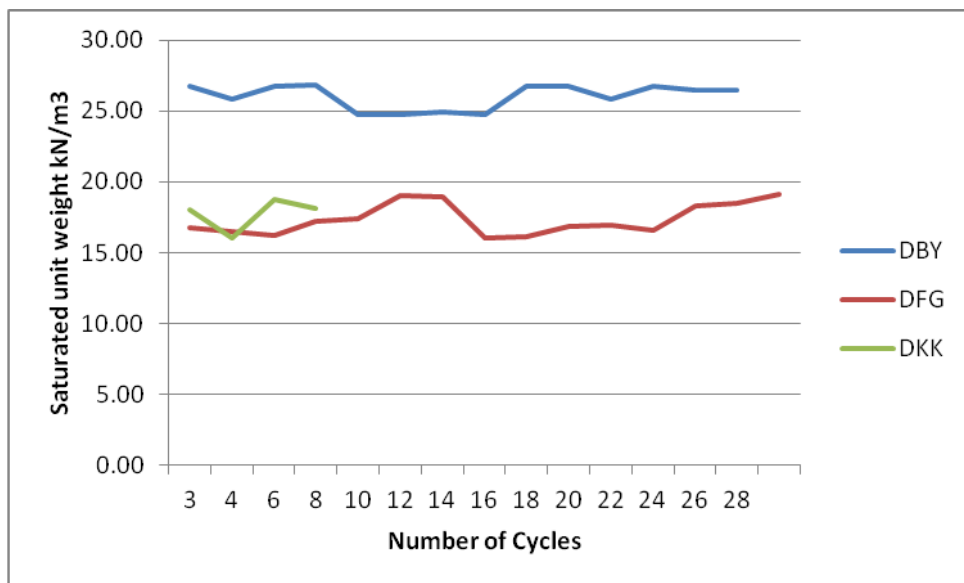


Figure 45. Saturated unit weight change of samples in wetting drying cycles

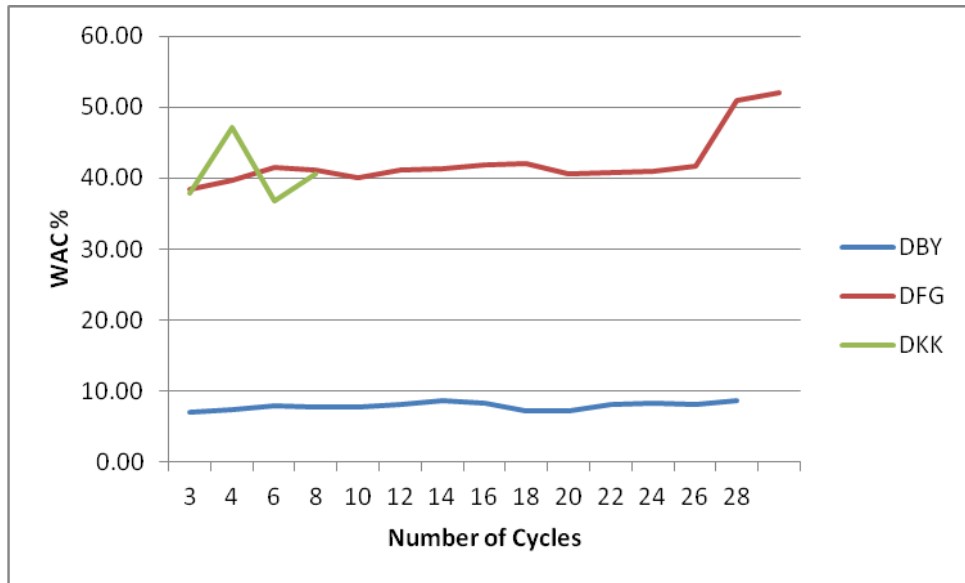


Figure 46. Water absorption capacity change of samples in wetting drying cycles

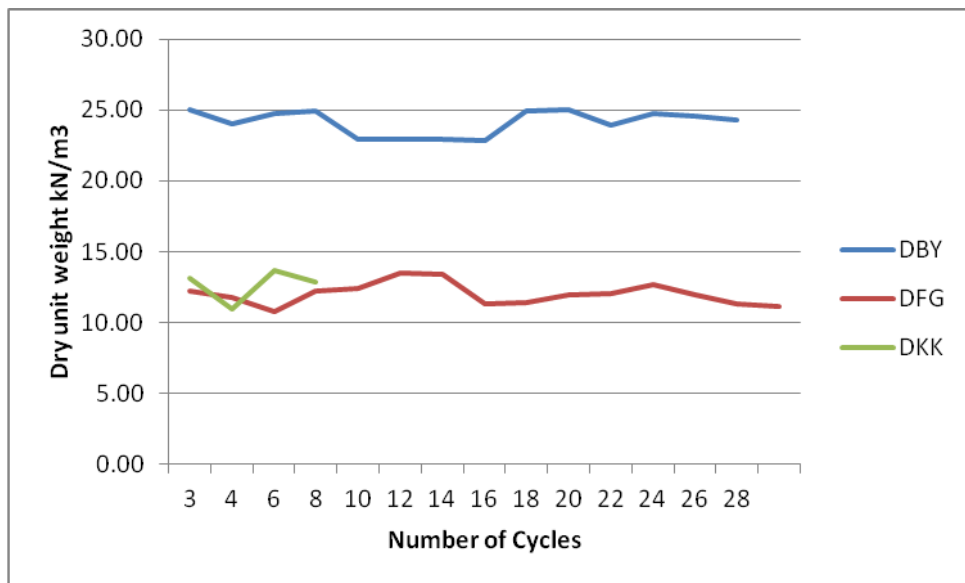


Figure 47. Dry unit weight change of samples in wetting drying cycles

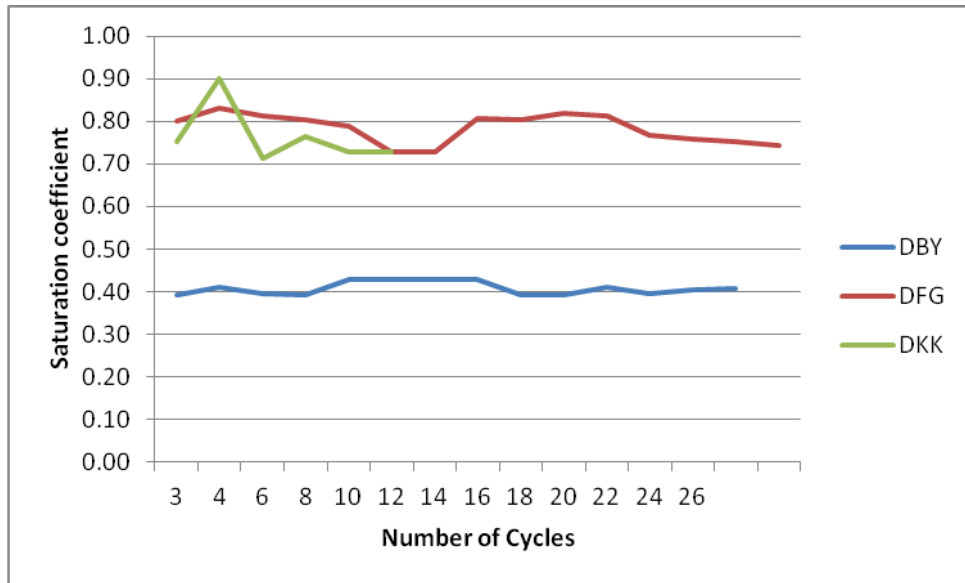


Figure 48. Saturation coefficient change of samples in wetting drying cycles

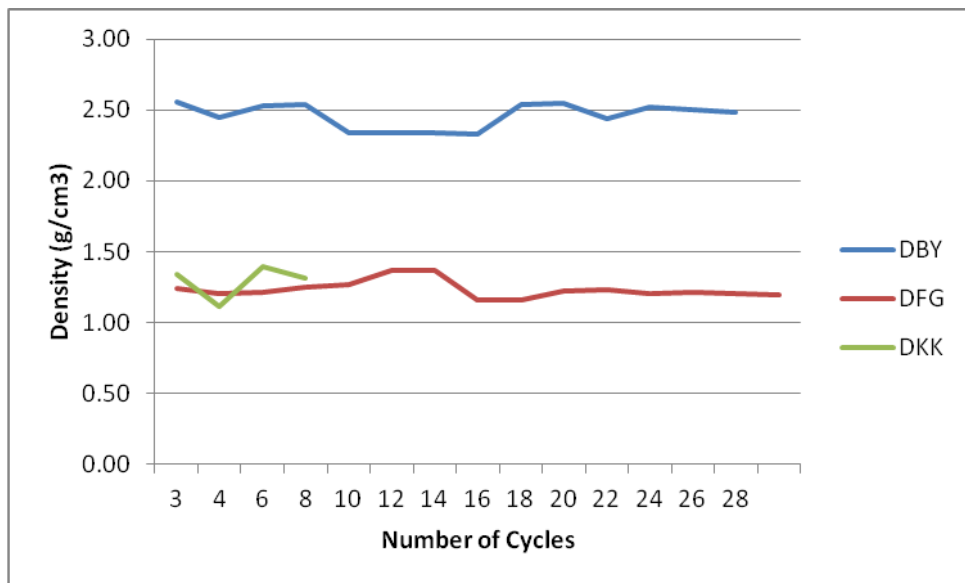


Figure 49. Bulk density change of samples in wetting drying cycles

3.1.2 COLOR SPECTROMETER MEASUREMENTS

Experimental results are shown according to chronological order that results of color properties of firstly fresh samples from quarries and weathered samples from temple and then of after salt crystallization and wetting drying cycles.

3.1.2.1 FRESH SAMPLES FROM QUARRIES AND WEATHERED SAMPLES FROM TEMPLE

‘L’ values of DTS1 and DBY, DFG and DKK are nearly same. ‘a’ values of DBY, DFG and DKK are close to each other and in the range of DTS1 and DTS2. ‘b’ values of DTS2 and DFG are same and close to DTS1 and DKK (Table 9).

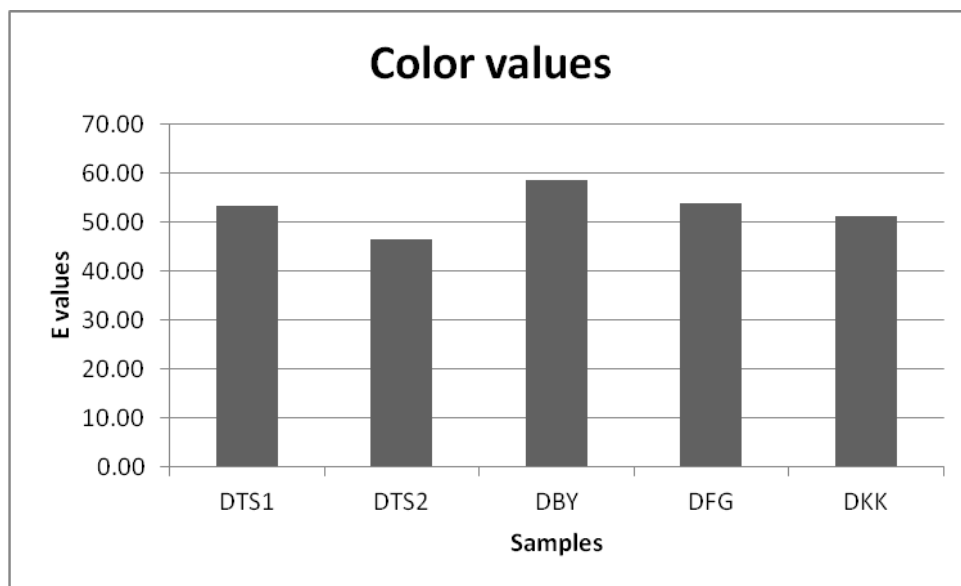


Figure 50. Clor values of Temple stones and fresh stones from quarries

Table 9. “L, a, b” values of samples

	L	a	b
DTS1	52,56±1,02	2,16±1,78	7,99±1,78
DTS2	45,35±6,85	4,99±1,19	8,74±0,74
DBY	58,39±1,21	3,60±0,25	4,26±0,73
DFG	52,92±1,66	3,76±0,26	8,78±0,24
DKK	50,74±6,85	3,49±0,84	6,93±1,24

3.1.2.2 SALT CRYSTALLIZATION CYCLE

L a b values of DBY change after salt crystallization cycle (Table 46) but altered values of DFG and DKK are closer to temple stone L a b values (Table 47, Table 48). The ΔE values higher than 3 can be detected by naked eye. The colors of the tuffs turned to more brownish with weathering. Color of DKK was more affected by weathering. DFG followed it.

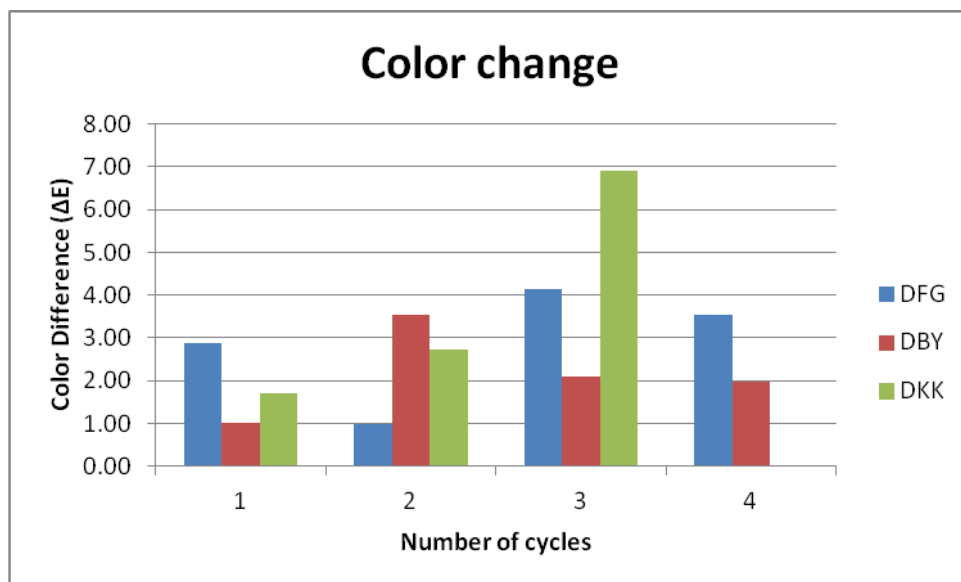


Figure 51. Color change of samples after salt crystallization cycle

3.1.2.3 WETTING DRYING CYCLE

Change L a b values of DBY after wetting drying cycle (

Table 49) show similar values with DTS1 and values of DFG and DKK are closer to DTS2 L a b values (

Table 51). The ΔE values higher than 3 can be detected by naked eye. The colors of the tuffs turned to more brownish with weathering. Color of DKK was more affected by weathering. DFG followed it.

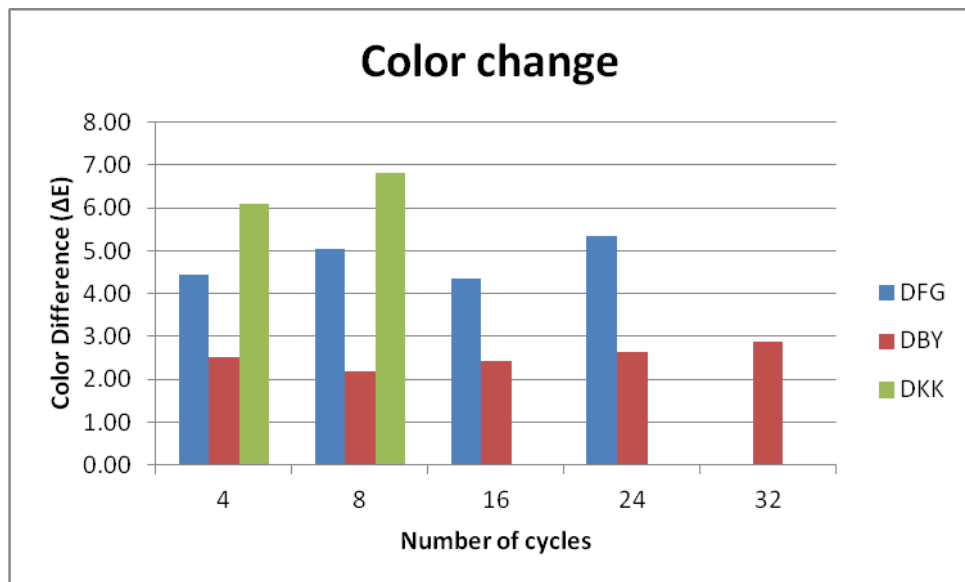


Figure 52. Color change of samples after wetting drying cycle

3.1.3 QUALITATIVE ANALYSIS OF THE SOLUBLE SALTS BY SPOT TESTS

Table 10. Qualitative analysis of soluble salts

sample	weight(g)	Rext	Rstd	EC	A	%salt
DTS1a	1,01	31	0,41	1,87E-05	0,011943	0,1
DTS1b	1	9	0,41	0,0000697	0,044608	0,2
DTS2	1,01	8,3	0,41	0,0000697	0,044608	0,2
DTS3	1,05	1,45	0,41	0,000399	0,255342	1,2
DTS4	1	15	0,41	3,86E-05	0,024683	0,1
DFG	1	38	0,41	1,52E-05	0,009743	0
DBY	1	15	0,41	3,86E-05	0,024683	0,1
DKK	1	16,6	0,41	3,49E-05	0,022304	0,1

DTS1, DTS2, DTS4, DFG, DBY and DKK have low salt concentrations such as 0.1, 0.2, 0.2, 0.1, 0, 0.1 and 0.1 % respectively (Table 10). The uppermost value which is 1.2% of DTS3 (Külhan tuff) is still in the low concentration side.

3.1.4 ULTRASONIC PULSE VELOCITY and MODULUS OF ELASTICITY

Experimental results are shown according to chronological order that results of basic ultrasonic pulse velocity and modulus of elasticity values of firstly fresh samples from quarries and weathered samples from temple and then of after salt crystallization and wetting drying cycles.

3.1.4.1 FRESH SAMPLES FROM QUARRIES AND WEATHERED SAMPLES FROM TEMPLE

Table 11. UV and Emod values of dry and saturated samples

	UV (m/s)	EMOD (GPa)	Saturated UV (m/s)	EMOD (GPa)
DTS1	1011,74	1,42	899,74	1,12
DTS2	1279,34	1,83	1106,54	1,49
DBY	1813,42±121	7,56±1,1	1140,16	3,39
DFG	1102,97±226	1,41±0,6	975,03	1,18
DKK	1021,37±250	1,41±0,7	914,19	1,1

Ultrasonic velocity values are close to each other except DBY which has 1813 m/s ultrasonic pulse velocity. UPV values of dry samples DTS1, DTS2, DFG and DKK are 1011,74 m/s, 1279,34 m/s, 1102, 97 ± 226 m/s and 1021,37 ± 250 m/s respectively (Table 11). Saturated Ultrasonic Pulse Velocity values decreased a bit but with the same ratio. The values are 899,74 m/s, 1106,54 m/s, 975, 03 m/s and 914,19 m/s respectively.

Modulus of Elasticity values are in the same trend as the ones of ultrasonic velocity. The values of samples in the same order are; 1,42 GPa, 1,83 GPa, 7,56 ± 1,1 GPa, 1,41 ± 0,6 GPa and 1,41 ± 0,7 GPa.

3.1.4.2 SALT CRYSTALLIZATION TESTS

Ultrasonic Pulse Velocity values of DBY, DFG and DKK decrease after 5th 4th and 3rd salt crystallization cycle were given respectively (Figure 53). The changes were; 1813 m/s to 1767 m/s, 1083 m/s to 988 m/s and 942 m/s to 908 m/s respectively (Table 41,

Table 42). Artificial weathering by Salt crystallization cycles resulted in sudden decrease in UPV values.

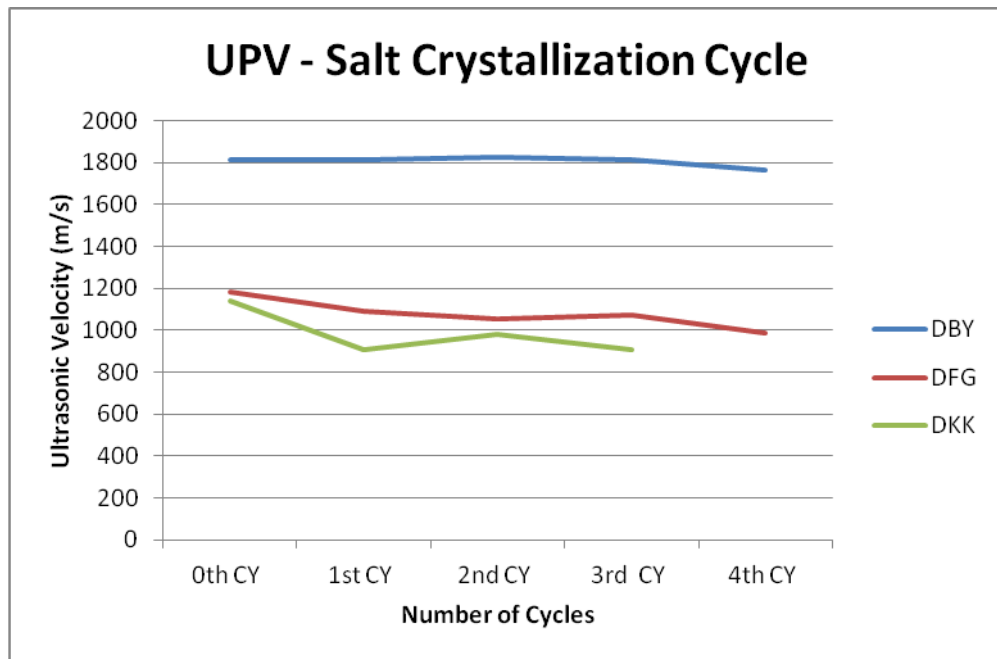


Figure 53. UPV change of samples after salt crystallization cycle

3.1.4.3 WETTING-DRYING TESTS

Velocity decreased after cycles of wetting drying cycle (Figure 54). DBY velocity decreased from 1815 m/s to 1642 m/s, DFG velocity decreased 1083 m/s to 924 m/s and velocity of DKK decreased 942 m/s to 917 m/s (Table 43, Table 44,

Table 45). Artificial weathering by wetting-drying cycles resulted in gradual decrease in UPV values.

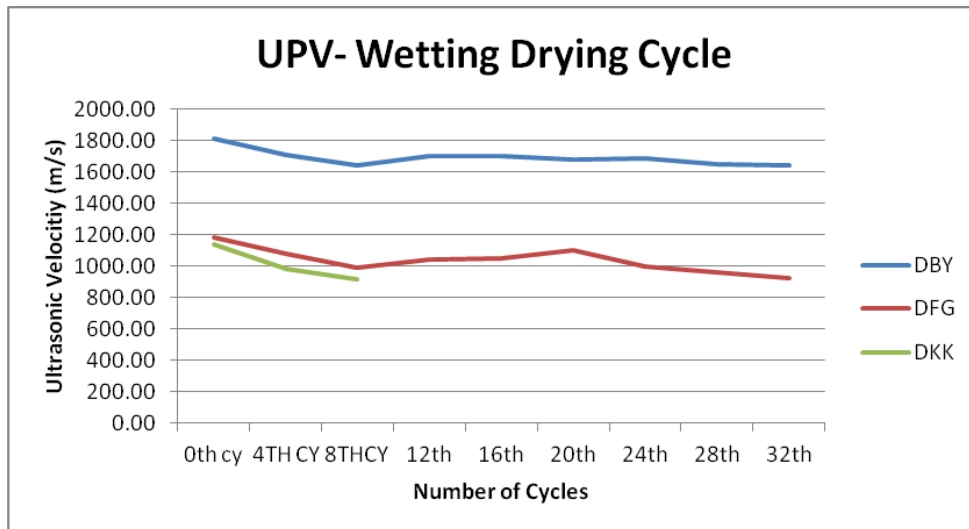


Figure 54. UPV change of samples after salt crystallization cycle

3.1.5 CAPILLARY ABSORPTION

As mentioned above, experimental results were given according to chronological order that results of capillary absorption properties of firstly fresh samples from quarries and weathered samples from temple and then of after salt crystallization cycle.

3.1.5.1 FRESH SAMPLES FROM QUARRIES AND WEATHERED SAMPLES FROM TEMPLE

Temple samples DTS1, DTS2 and DKK, DFG had high capillary coefficient values (Figure 55). Temple stones had the highest capillary coefficients, DFG and DKK followed them. DBY has the lowest capillary coefficients.

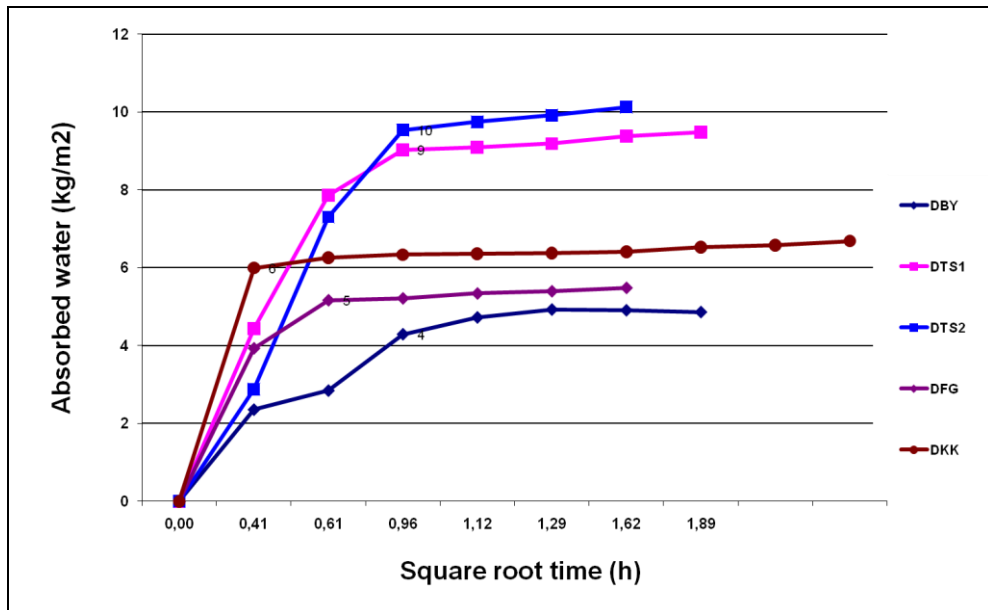


Figure 55. Capillary absorption rate of samples

DTS1 had $10,5 \text{ kg/m}^2/\text{s}^{1/2}$ and DTS2 has $12,3 \text{ kg/m}^2/\text{s}^{1/2}$, DBY, DFG and DKK's capillary coefficients are 4,6, 9,1 and 11,4 $\text{kg/m}^2/\text{s}^{1/2}$ respectively (Table 12).

Table 12. Capillary coefficient values of samples

SAMPLES	Capillary coefficient $\text{kg/m}^2/\text{s}^{1/2}$
DBY	$4,61 \pm 0,2$
DFG	$9,12 \pm 1,7$
DKK	$11,43 \pm 2,5$
DTS1	$10,50 \pm 0,1$
DTS2	$12,30 \pm 4,4$

3.1.5.2 SALT CRYSTALLIZATION TESTS

Capillary coefficients of DFG and DKK were increased by the salt crystallization cycles (Figure 56). The values came closer to temple stone capillary coefficients.

DBY has the lowest capillary coefficients. DBY, DFG and DKK's capillary coefficients were 3.33, 9,5 and 16 $\text{kg/m}^2/\text{s}^{1/2}$ respectively (Table 13).

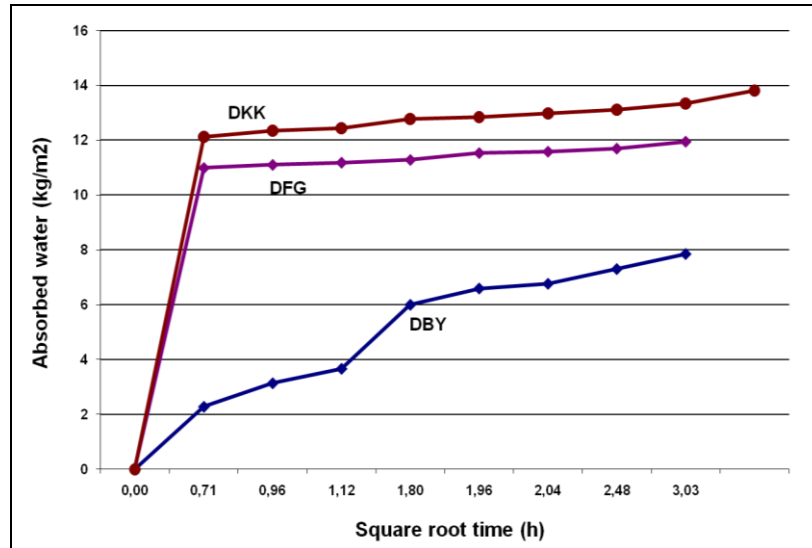


Figure 56. Capillary absorption rate of samples after salt crystallization cycle

Table 13. Capillary coefficient values of samples after salt crystallization cycle

SAMPLES	Capillary coefficient $\text{kg/m}^2/\text{s}^{1/2}$
DBY	$3,33 \pm 0,2$
DFG	$9,51 \pm 1,1$
DKK	$16 \pm 2,5$

3.1.6 MOISTURE ABSORPTION

Table 14. Moisture absorption coefficient values of samples

Samples	Moisture absorption coefficient $\text{kg/m}^2/\text{s}^{1/2}$
DBY	$1,32 \pm 1,23$
DFG	$2,04 \pm 2,05$
DKK	$2,32 \pm 1,67$
DTS1	$2,23 \pm 3,56$
DTS2	$1,68 \pm 2,68$

Temple samples DTS1, DTS2 and DKK, DFG had low moisture absorption values (Figure 57). DTS1 has 2,2 and DTS2 has 1,7 $\text{kg/m}^2/\text{s}^{1/2}$, DBY, DFG and DKK's moisture absorption coefficients are 1,3, 2,04 and 2,3 $\text{kg/m}^2/\text{s}^{1/2}$ respectively (Table 14). Results could be commented as number of small pore size of temple stones and DFG and DKK were similar.

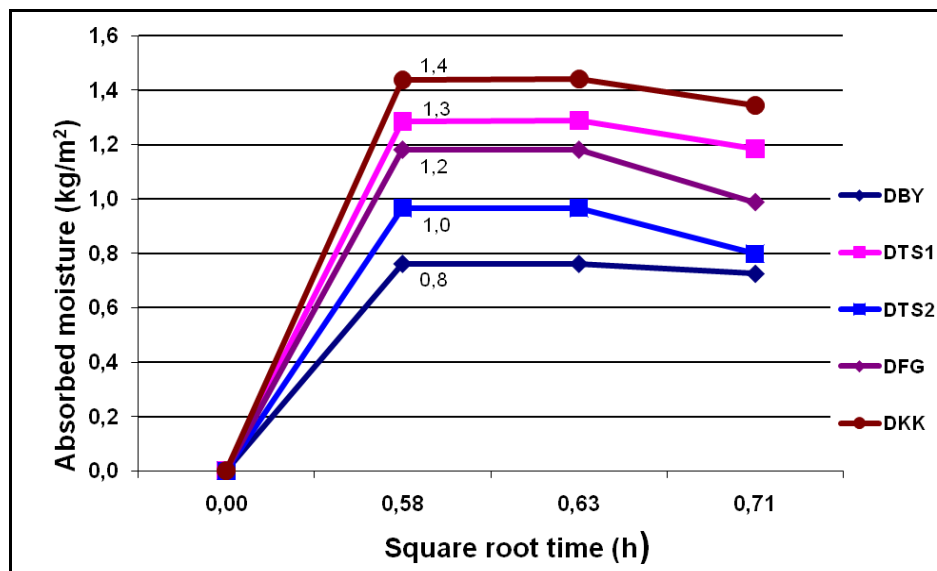


Figure 57. Moisture absorption graph of samples

3.1.7 UNIAXIAL COMPRESSIVE STRENGTH

As mentioned above, experimental results were shown according to chronological order that results of uniaxial compressive strength values of firstly fresh samples from quarries and weathered samples from temple and then of after salt crystallization cycle.

3.1.7.1 FRESH SAMPLES FROM QUARRIES AND WEATHERED SAMPLES FROM TEMPLE

Table 15. UCS values of dry and saturated samples

	Dry UCS (MPa)	Saturated UCS (MPa)
DTS1	3,80 ± 0,17	2,58 ± 0,05
DTS2	4,64 ± 0,23	2,83 ± 0,20
DTS4	18,01 ± 11,02	17,08 ± 6,07
DBY	24,70 ± 2,67	19,89 ± 0,91
DFG	5,78 ± 2,17	4,12 ± 1,24
DKK	4,94 ± 1,66	3,43 ± 0,14

DTS1, DTS2 and DKK, DFG had low uniaxial compressive strength values that close to each other (Figure 53). DTS1, DTS2, DBY, DFG and DKK's uniaxial compressive strength were 3.80, 4.64, 5.78 and 4.94 MPa respectively (Table 15). DBY had the highest strength value; 24,7 MPa and DTS4 had 18 MPa (Figure 58).

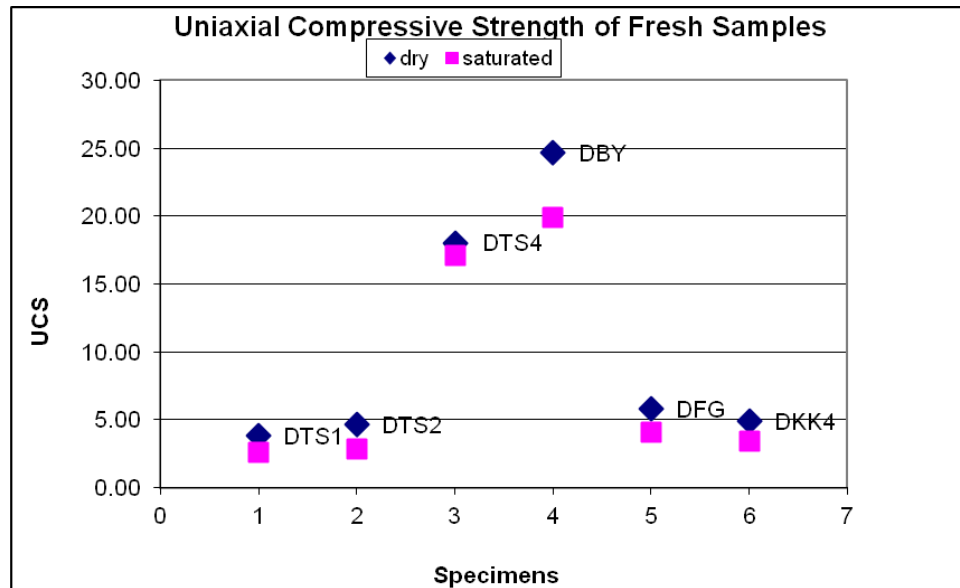


Figure 58. Uniaxial Compressive Strength graph of samples

Composition and texture of rocks and experiment conditions such as loading speed, sample preparation appropriate to the standards control the uniaxial compressive strength/ point load strength (Goodman,1989; Korkanc,2007). Low UCS values of rocks indicate being non-welded, mineralogical properties, unit weight, and resolution and porosity values. Samples having opaque mineral and finer grained crystals and matrix than phenocrysts have higher strength values.

Modulus of Elasticity versus uniaxial compressive strength trend showed that except DBY, all other rocks had low durability (Figure 59). Although samples had low durability values, DTS has been used in the temple foundation for 2000 years.

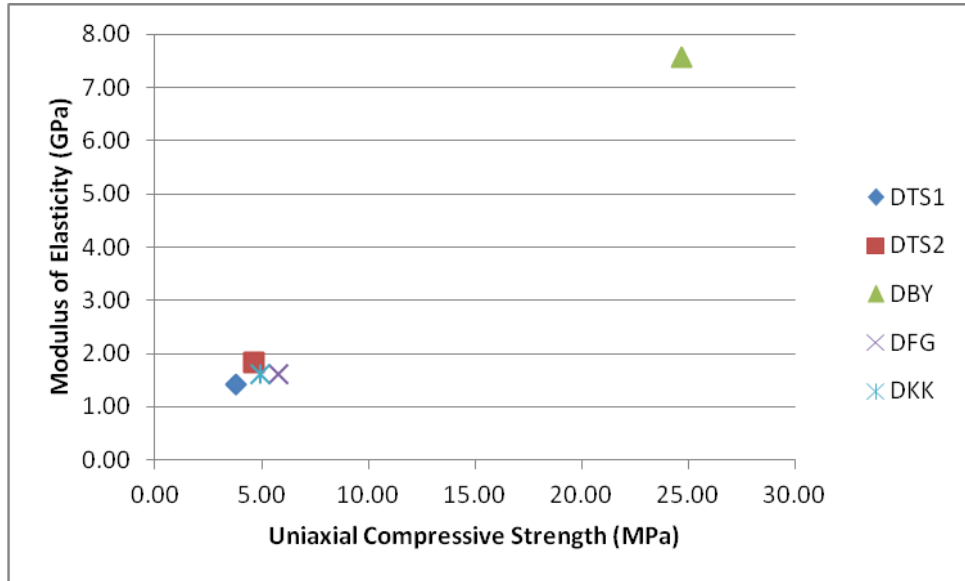


Figure 59. E_{mod} vs UCS graph of samples

According to ISRM (1981) and Deer and Miller (1966) rocks were low and very low uniaxial compressive strength values respectively.

3.1.7.2 SALT CRYSTALLIZATION TESTS

Table 16. UCS values of samples after salt crystallization cycle

	DBY	DFG	DKK
	Dry UCS (MPa)	Dry UCS (MPa)	Dry UCS (MPa)
0th cycle	24,70 ± 2,67	5,78 ± 2,17	4,94 ± 1,66
1st cycle	24,89 ± 2,17	3,94 ± 0,27	3,33 ± 0
2nd cycle	23,48 ± 3,56	3,98 ± 0,27	3,45 ± 0
3rd cycle	23,36 ± 2,67	3,68 ± 0,69	3,20 ± 0
4th cycle	22,52 ± 4,48	3,12 ± 0,15	
6th cycle	16,36 ± 0,29		

Artificial weathering by Salt crystallization cycles resulted in decrease in UCS values. All samples decreased in strength after salt crystallization cycle (Figure 60) and DBY decreased to 16.36, DFG decreased to 3.12 and DKK decreased to 3.2 MPa (Table 16). DFG and DKK were in the unsafe zone (Figure 61).

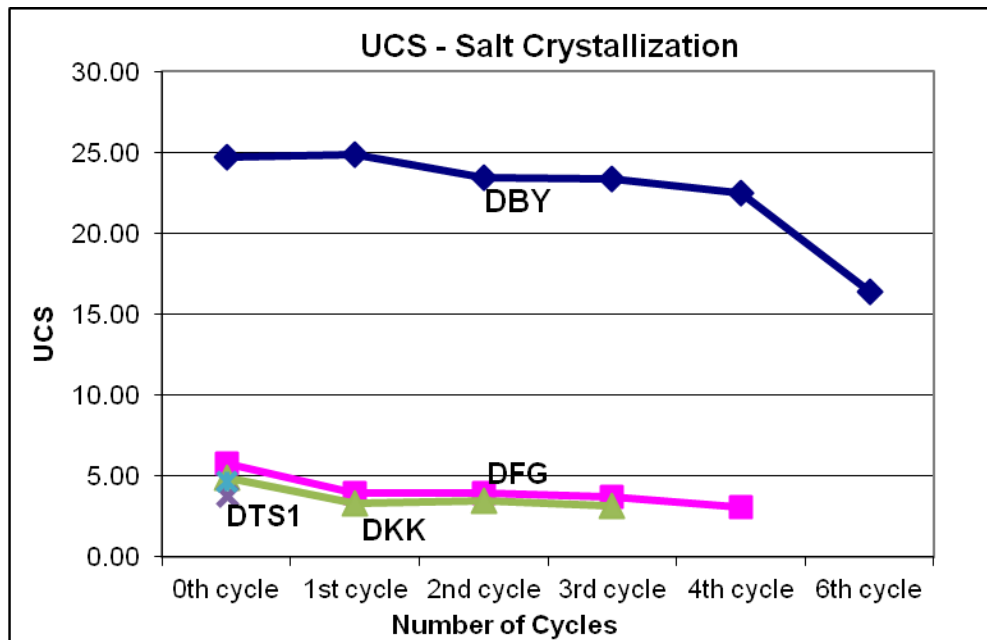


Figure 60. UCS change of samples after salt crystallization cycle

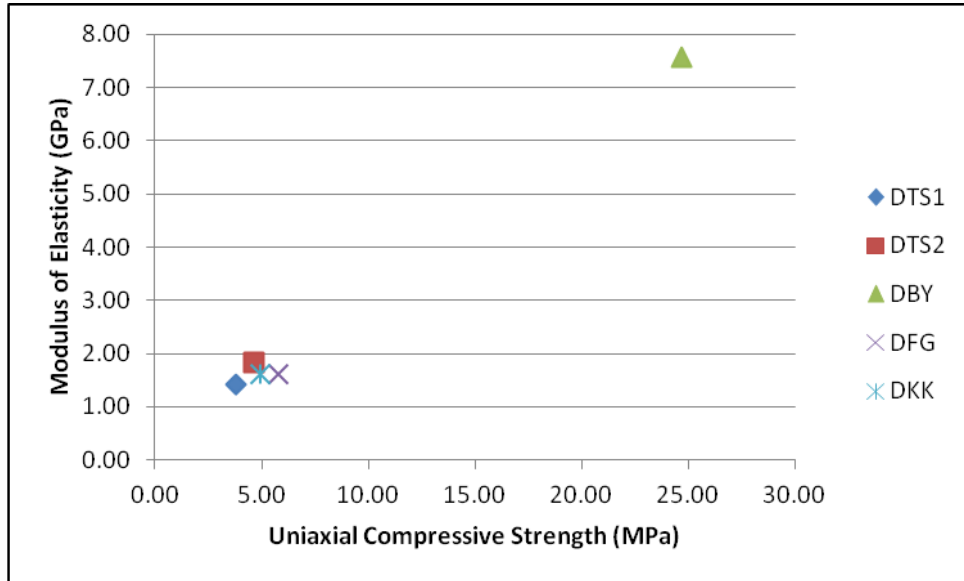


Figure 61. E_{mod} vs UCS graph of samples after salt crystallization cycle

3.1.7.3 WETTING DRYING TESTS

Table 17. UCS values of samples after wetting drying cycle

	DBY	DFG	DKK
	Dry UCS (MPa)	Dry UCS (MPa)	Dry UCS (MPa)
0th cycle	24,70 ± 2,67	5,78 ± 2,17	4,94 ± 1,66
4th cycle	19,14 ± 4,72	4,11 ± 0,55	2,89 ± 0,12
8th cycle	22,19 ± 1,65	4,60 ± 2,28	3,03 ± 0,78
12th cycle	22,98 ± 3,48	3,20 ± 0,28	
16th cycle	24,75 ± 1,69	3,50 ± 0,58	
20th cycle	21,82 ± 2,39	3,07 ± 0,17	
24th cycle	22,18 ± 3,75	3,34 ± 0,29	
28th cycle	21,64 ± 3,25	3,64 ± 0,69	

All samples decreased in strength after wetting drying cycle lesser than in salt crystallization (Figure 62) and DBY decreased to 21.64, DFG decreased to 3.64 and DKK decreased to 3.03 MPa (Table 17). Emod vs UCS graph showed that DFG and DKK were still in the non-durable side (Figure 63).

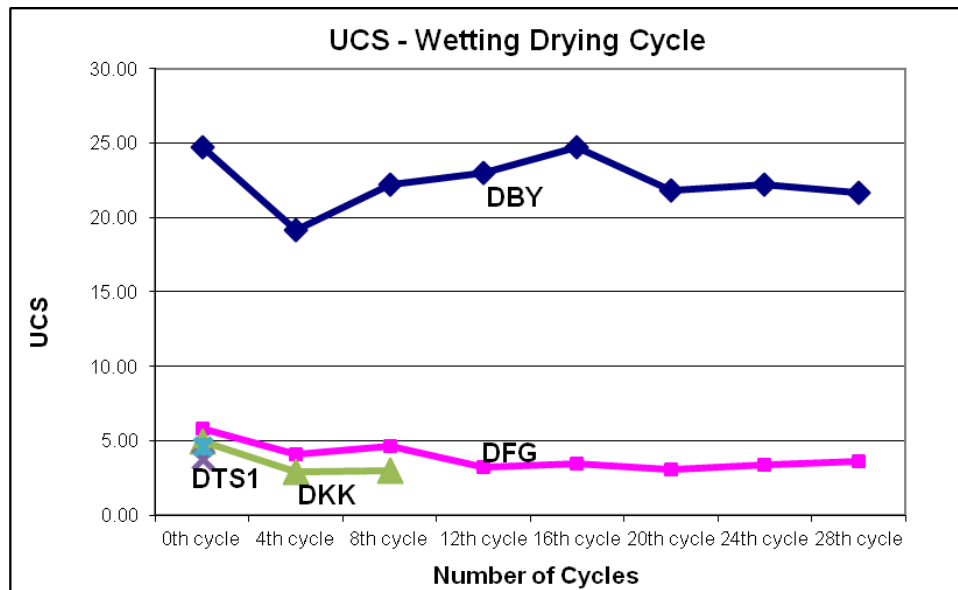


Figure 62. UCS change of samples after wetting drying cycle

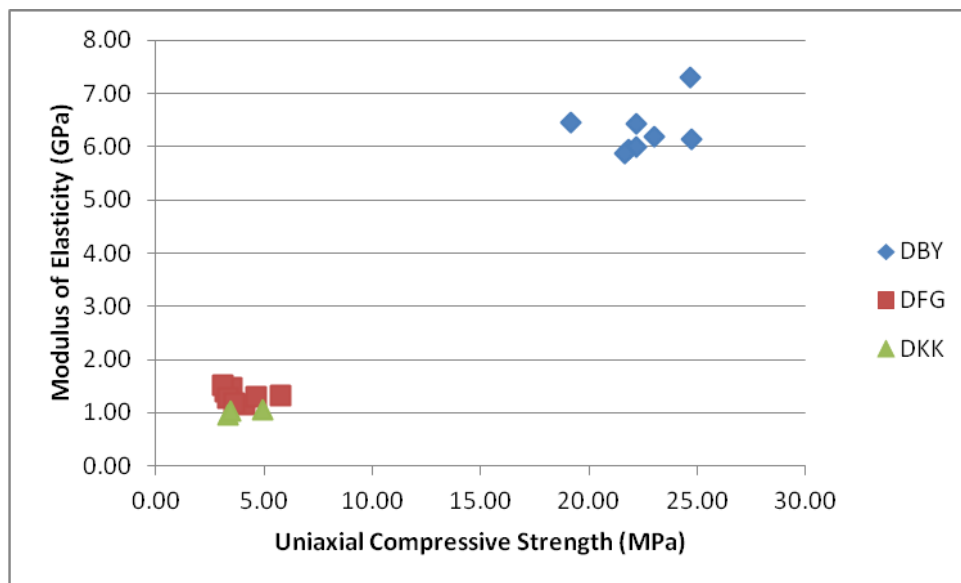


Figure 63. E_{mod} vs UCS graph of samples after wetting drying cycle

3.1.8 PORE SIZE DISTRIBUTION

Experimental results were shown according to chronological order that results of pore size distribution values of firstly fresh samples from quarries and weathered samples from temple and then of after salt crystallization cycle.

3.1.8.1 FRESH SAMPLES FROM QUARRIES AND WEATHERED SAMPLES FROM TEMPLE

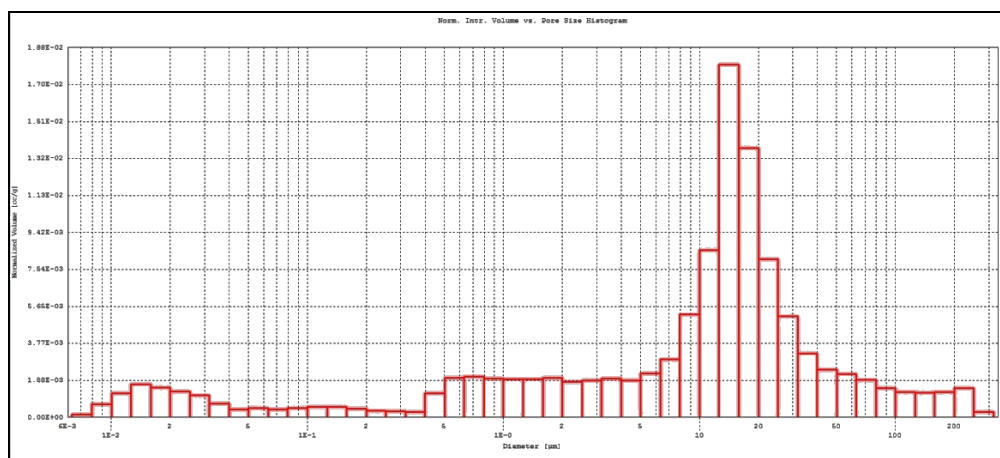


Figure 64. Pore size distribution of DTS1

The distribution showed that DTS1 had mostly 15 µm pore size and 8-50 µm was the dense size. 0,02 - 0,05 µm size pores indicated the small diameter parts (Figure 64).

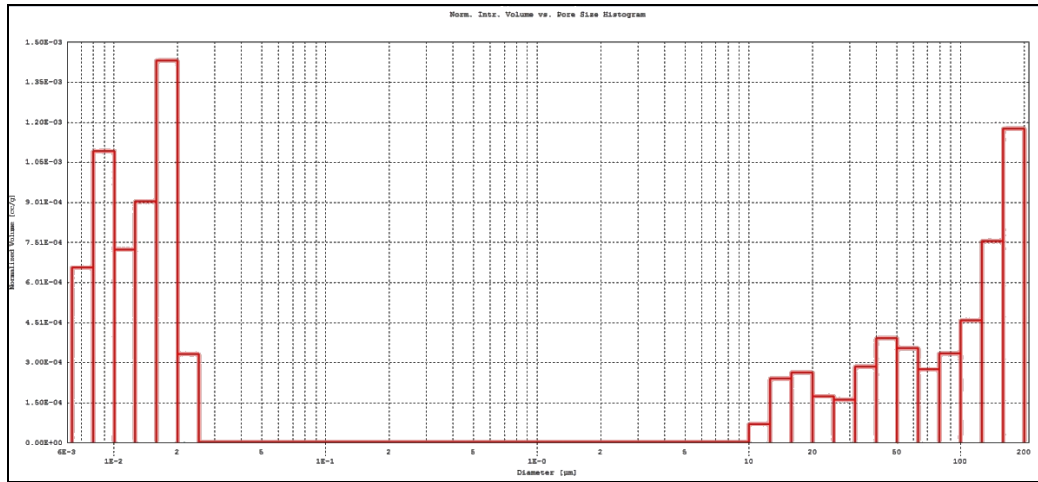


Figure 65. Pore size distribution of DTS4

DTS4 showed bimodal pore size distribution that it has no pore in between 0,03 µm and 10 µm. It had more micropores and 0,01 µm mostly. Coarser pores existed in 200 µm (Figure 65).

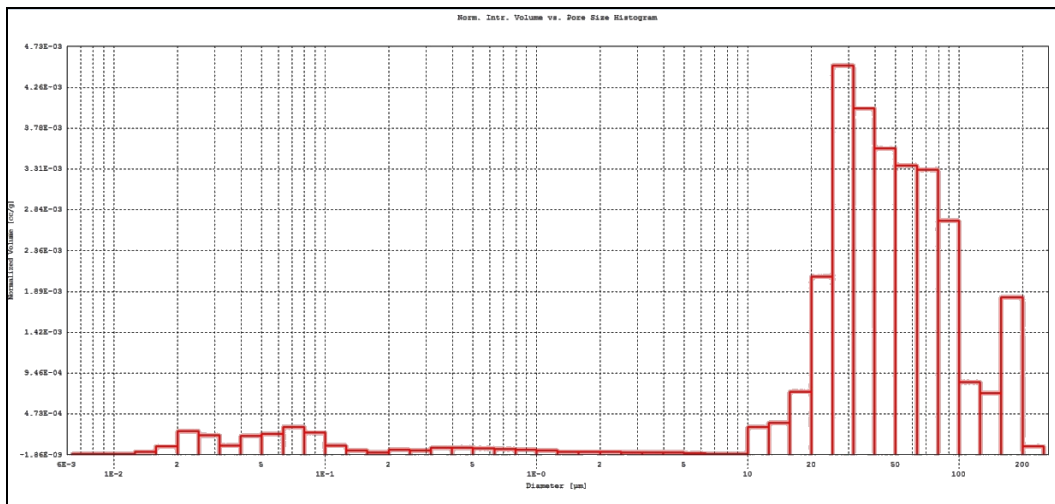


Figure 66. Pore size distribution of DBY

Unimodal pore size distribution was shown. Capillary pores are abundant. It had larger pores in between 20 and 100 µm. DBY had not so micropores. (Figure 66).

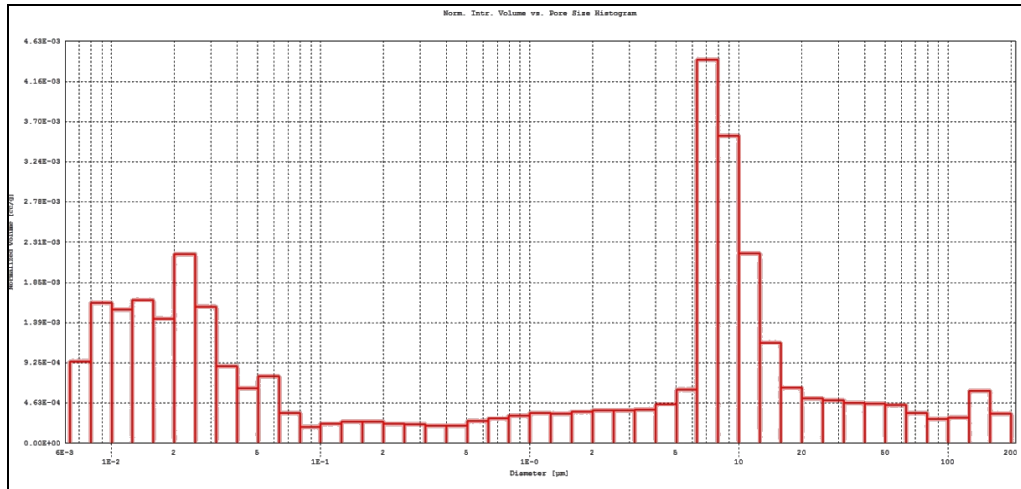


Figure 67. Pore size distribution of DFG

DFG had the highest value in around 7-15 μm . It has small size pores between 0,006 and 0,1 μm . In the bimodal pore size distribution graph other pore sizes are reliable as well. Capillary pores exist but micropores are much abundant and mesopores exist (Figure 67).

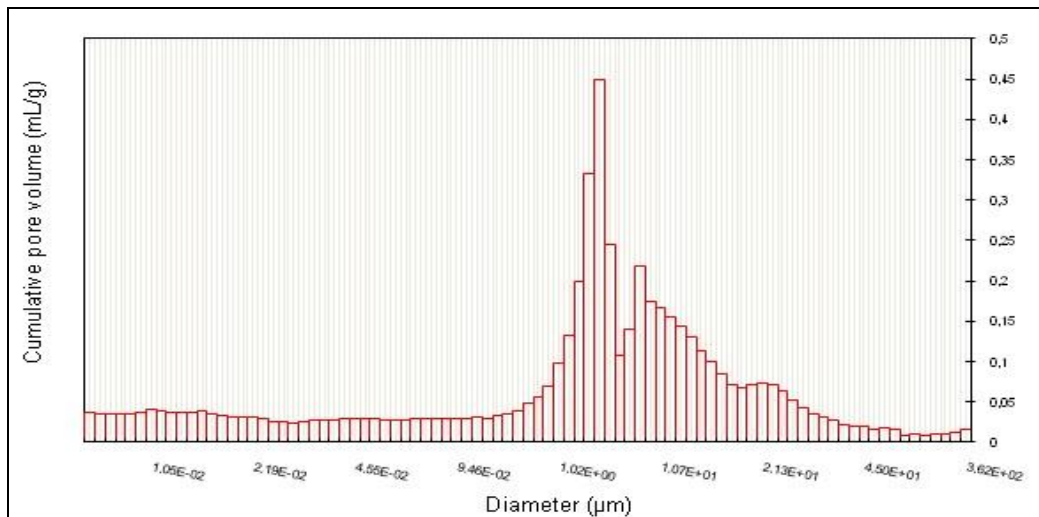


Figure 68. Pore size distribution of DKK

DKK presented unusual unimodal pore size distribution with a well defined pore threshold at 4 μ m (Figure 68). It's in fact the higher value of radius which gives access to the most quantity of mercury in the porous network. A small peak at 10A is relevant from the real size of the pore). It can be attributed to the the real macropore size.

3.1.8.2 SALT CRYSTALLIZATION TESTS

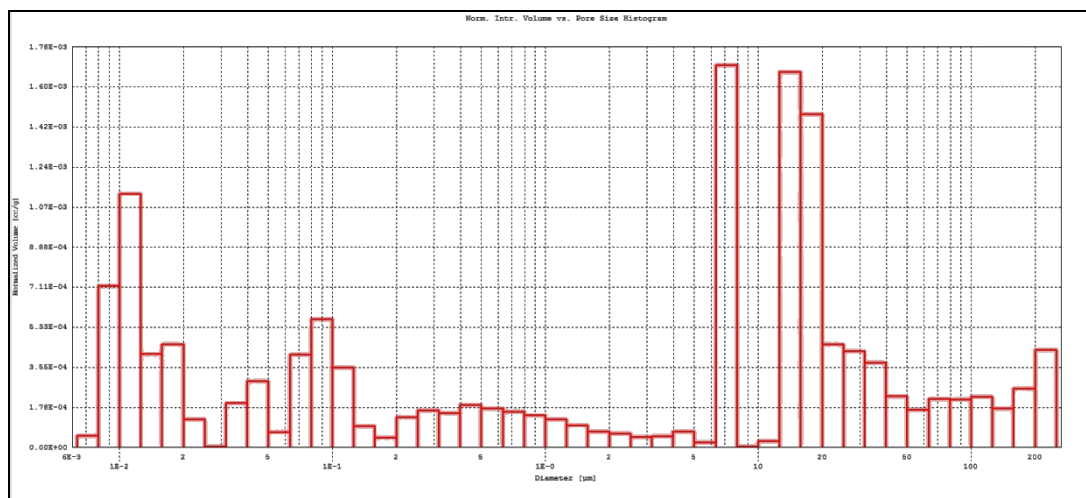


Figure 69. Pore size distribution of DBY after 3rd salt crystallization cycle

There is an increase in the distribution (Figure 69) so that micropores are supposed to be reproduced.

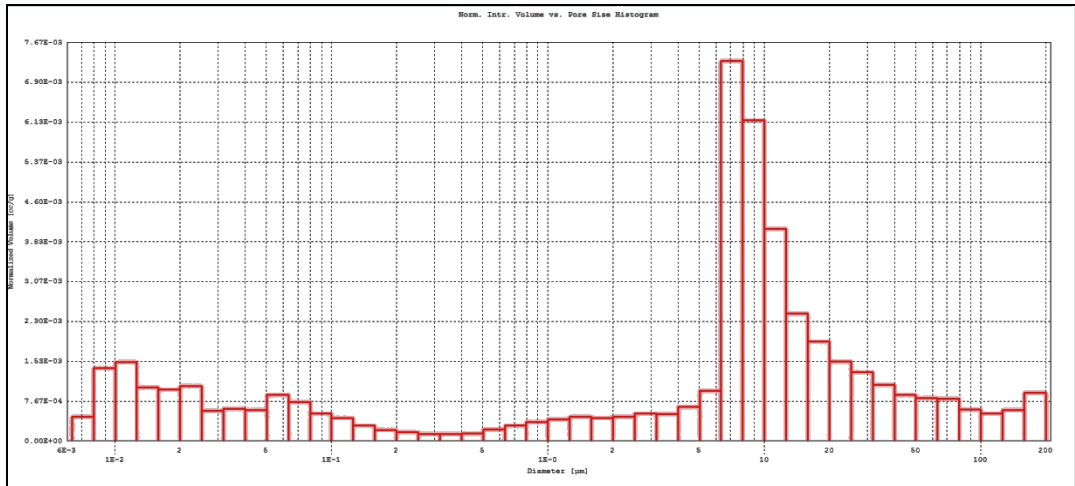


Figure 70. Pore size distribution of DFG after 3rd salt crystallization cycle

There is a slight change between the fresh sample and salt crystallized sample (Figure 70). Clay size pores decreased, pores around 10 μm increased.

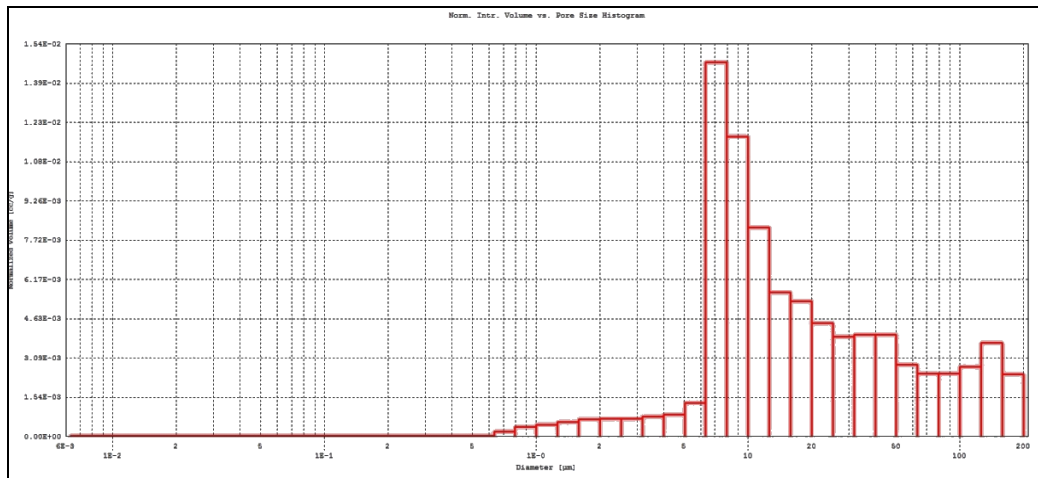


Figure 71. Pore size distribution of DKK after 3rd salt crystallization cycle

The distribution becomes unimodal after salt crystallization cycle. Clay size pores and smaller pores than 0,6 μm do not exist anymore. 6 μm – 20 μm pores increased (Figure 71).

In volcanic tuffs, amount of welding or deposition components affect the porosity that the nonwelded and bedded rocks are more porous. Crystallized rocks often have small poorly connected pores however nonwelded, vitric rocks generally have larger, better-connected pores (Flint and Selker, 2003).

3.2 MINERALOGICAL AND PETROGRAPHICAL WORKS

Microstructure of samples are determined via optical microscopy, X-ray diffraction, stereomicroscopy, scanning electron microscopy, Fourier transform infrared spectroscopy, methylene blue adsorption and X-ray fluorescence.

3.2.1 THIN SECTION ANALYSIS

In the petrographical investigations of thin sections prepared from all samples taken from the field and mineralogical composition, texture, pore-crystal size, phenocryst-matrix ratio and first-second minerals were determined.

Except the main rock DTS4 and Babakale Yolu Quarry rock DBY, all rocks showed welded tuff features.

DTS1

Hypocrystalline porphyritic textured volcanic rock fragments were embedded within volcanic glass matrix with flow pattern (Figure 72). Quartz, plagioclase, biotite, pyroxene were the amorphous and semi-amorphous crystals (Figure 73, Figure 74). Circular opaque minerals were seen. Microlithic porphyritic andesitic rock fragments in various dimensions were seen (Figure 75).

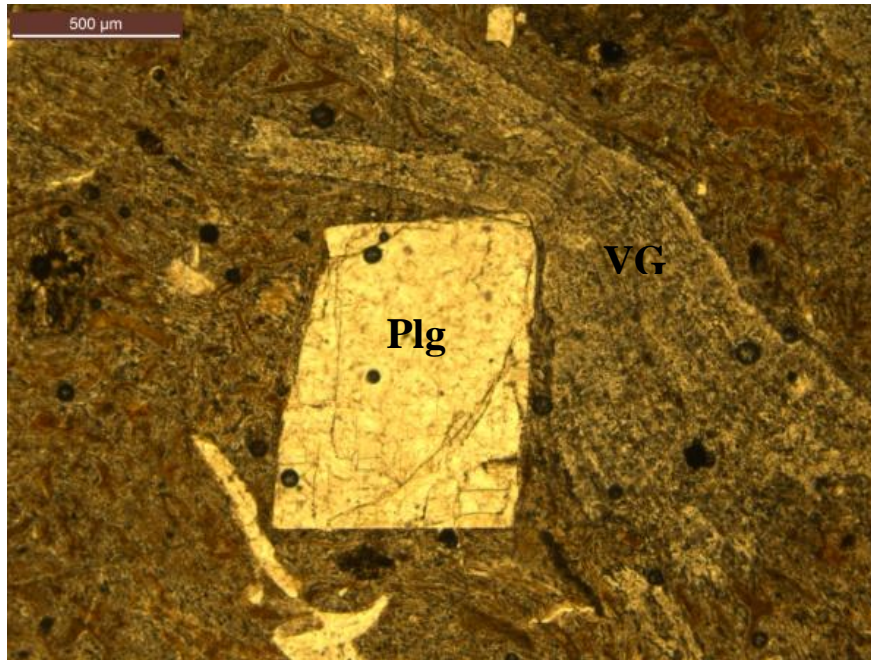


Figure 72. Photomicrograph of DTS1, single nicol, 2,5x , Plg: plagioclase, VG: Volcanic glass

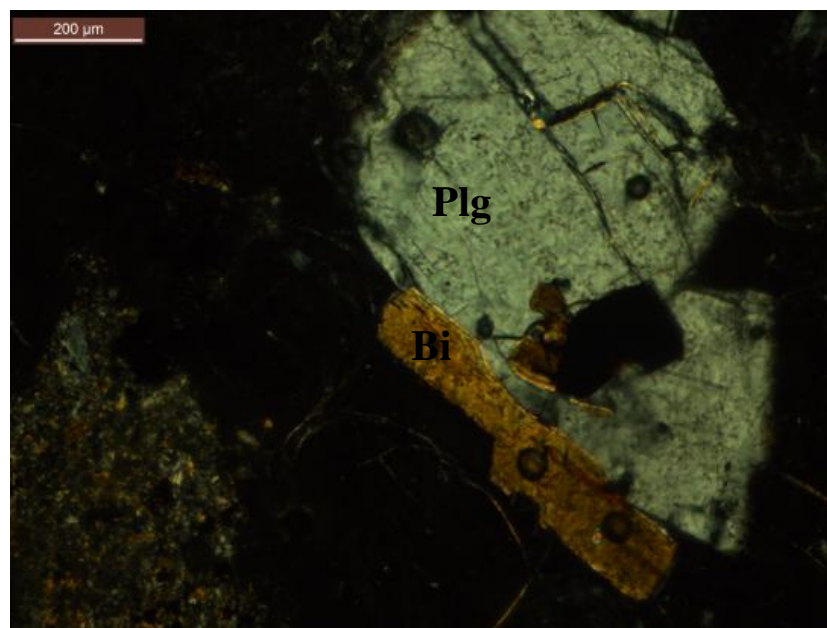


Figure 73. Photomicrograph of DTS1, cross nicol, 10x , Plg: plagioclase, Bi: Biotite

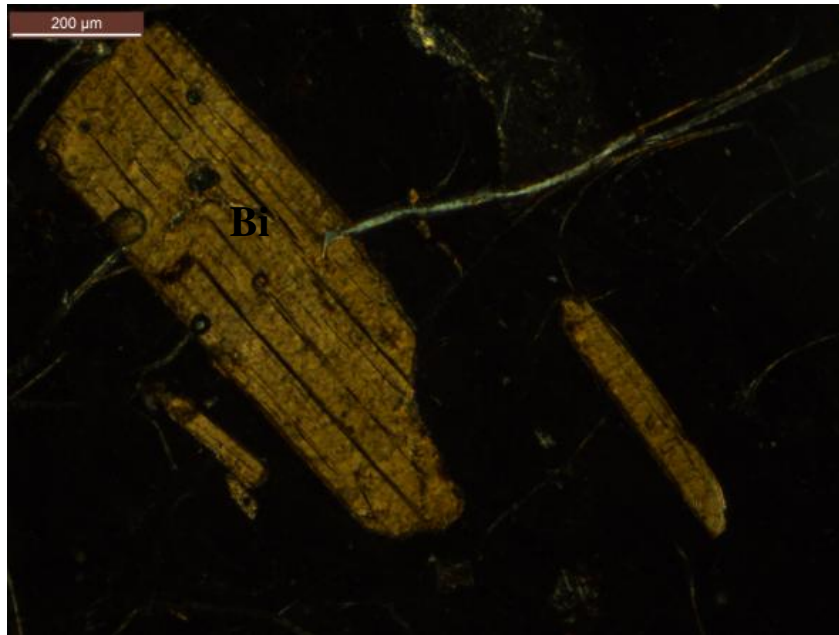


Figure 74. Photomicrograph of DTS1, cross nicol, 10x , Bi: Biotite

Various volcanic glass fragments were seen. Some of them were the forms specific for ignimbrite, some of them had flow pattern.

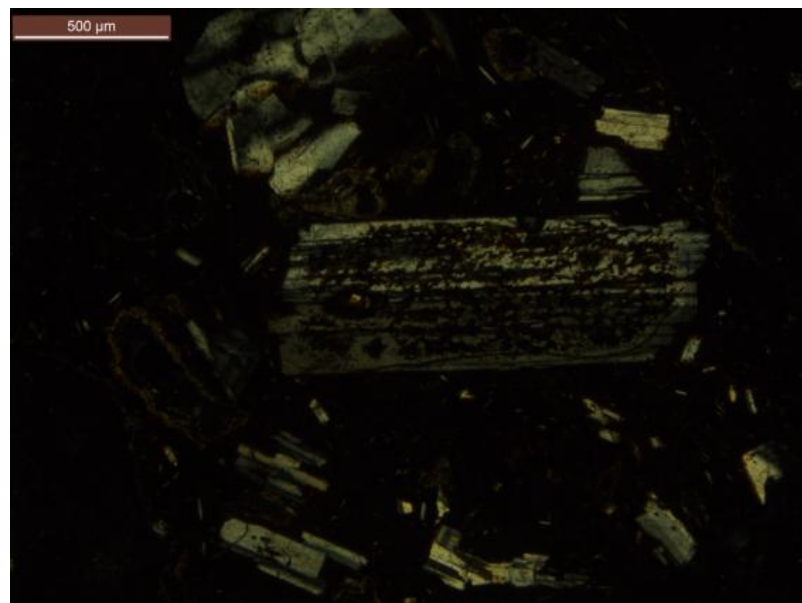


Figure 75. Photomicrograph of DTS1, cross nicol, 10x , weathered plagioclases

DTS2

Hypocrystalline porphyritic textured volcanic rock fragments were embedded within volcanic glass matrix with flow pattern. Quartz, plagioclase, biotite, and opaque minerals were the amorphous and semi-amorphous crystals (Figure 76). Microlithic porphyritic andesitic rock fragments with plagioclase pieces were seen (Figure 77).

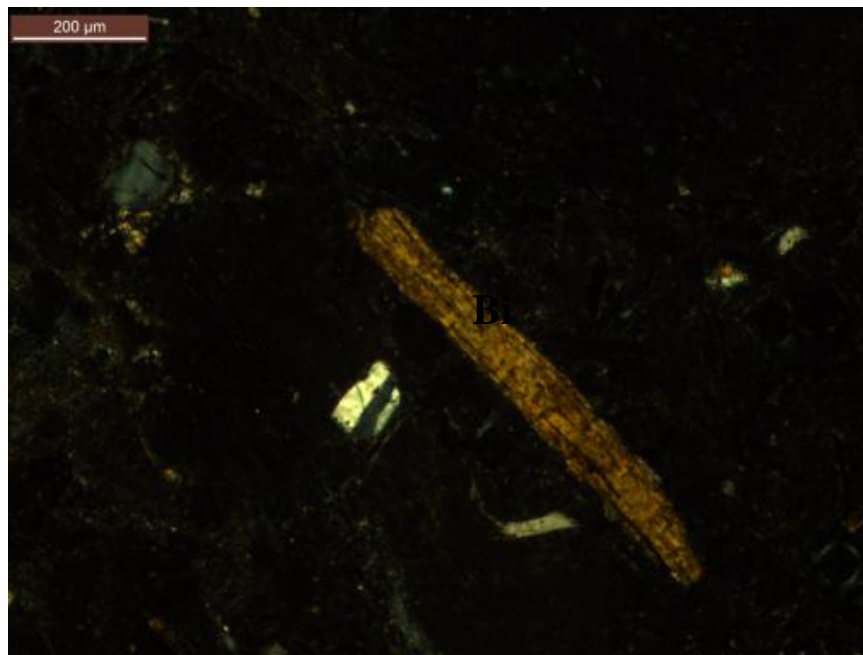


Figure 76. Photomicrograph of DTS2, cross nicol, 5x , Bi: Biotite

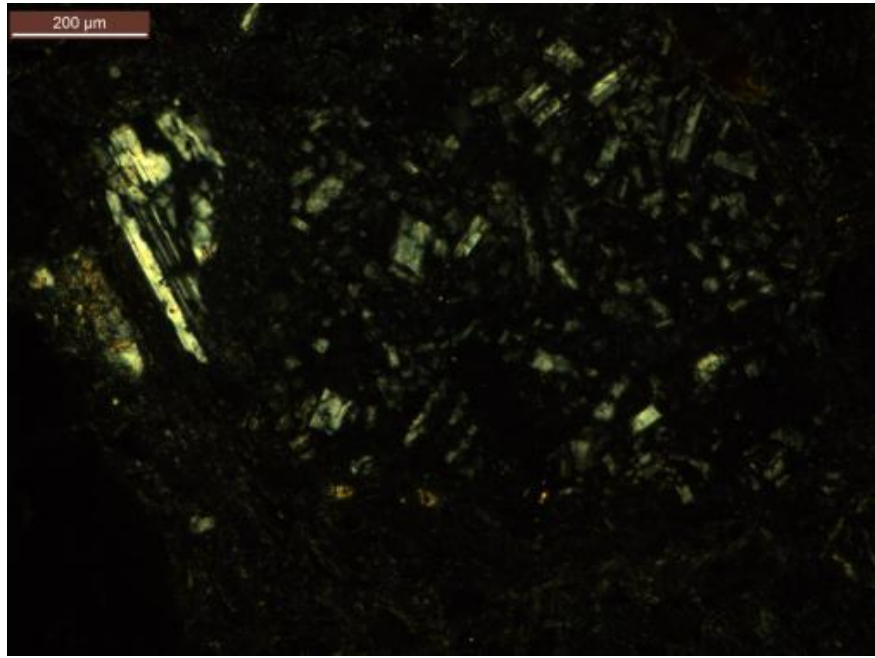


Figure 77. Photomicrograph of DTS2, cross nicol, 5x , plagioclase

DTS3

Various volcanic glass fragments were seen. Some of them were the forms specific for ignimbrite, some of them had flow pattern. There were microlithic porphyritic volcanic rock fragments. Quartz, plagioclase, biotite, and opaque minerals were embedded within tuffaceous matrix with ignimbrite features (Figure 78, Figure 79).

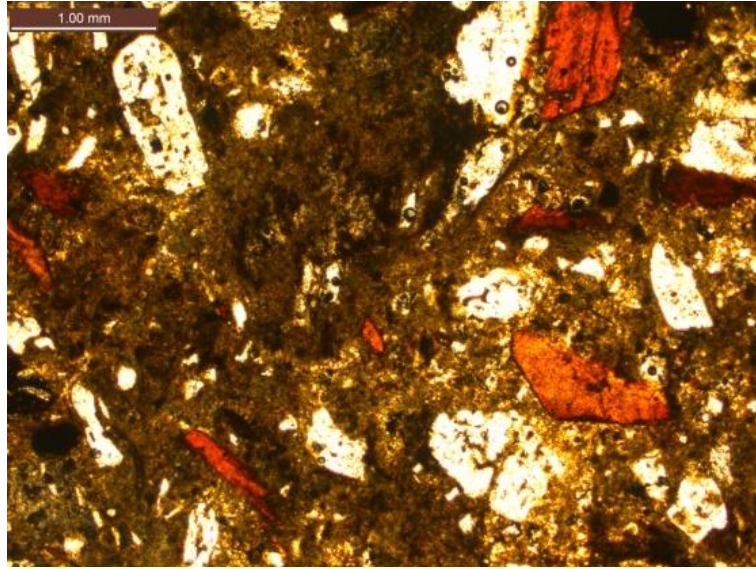


Figure 78. Photomicrograph of DTS3, single nicol, 5x , hematite coatings are seen.

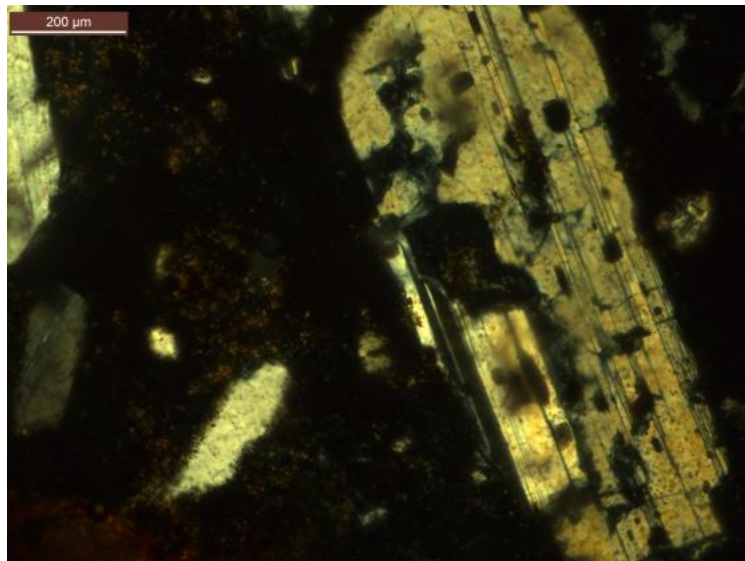


Figure 79. Photomicrograph of DTS2, cross nicol, 10x , Biotite

DTS4

Sample had a devitrified groundmass that crystallites are formed. Feldspar and opaque minerals existed in volcanic rock fragments (

Figure 80, Figure 81). Colloidal chalcedony filled in the cracks (Figure 82). Thin section image of sample resembled volcanic glass however it was detected as opal in XRD spectra. During the diagenesis it lost water, puckered up and cracks occurred (Erkan, 1994). Chalcedony filled into the cracks and openings of opal. There were a few crystal fragments such as plagioclase, quartz and biotite. There were opaque fillings in the cracks. Iron oxides and hydroxides stained some parts (Figure 82). Clay appearance existed.

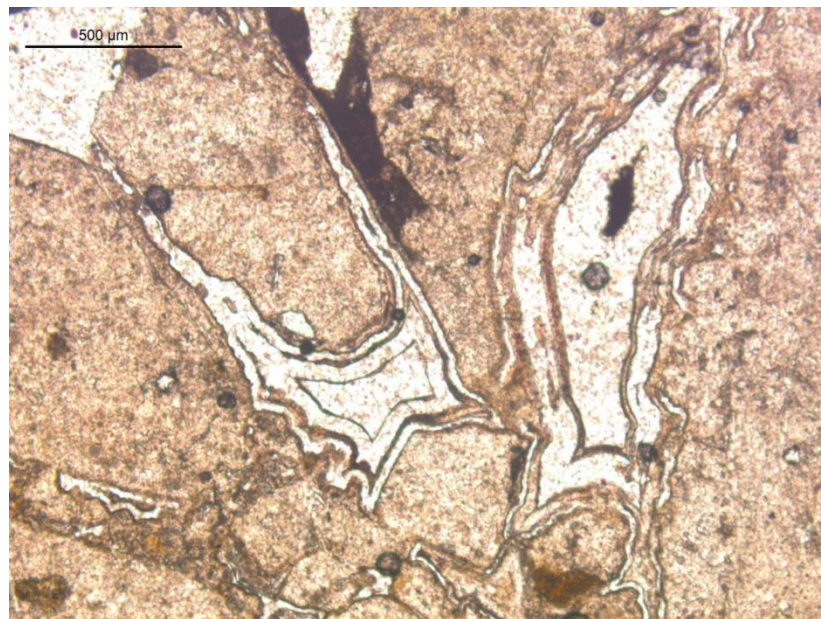


Figure 80. Photomicrograph of DTS4, single nicol, 5x

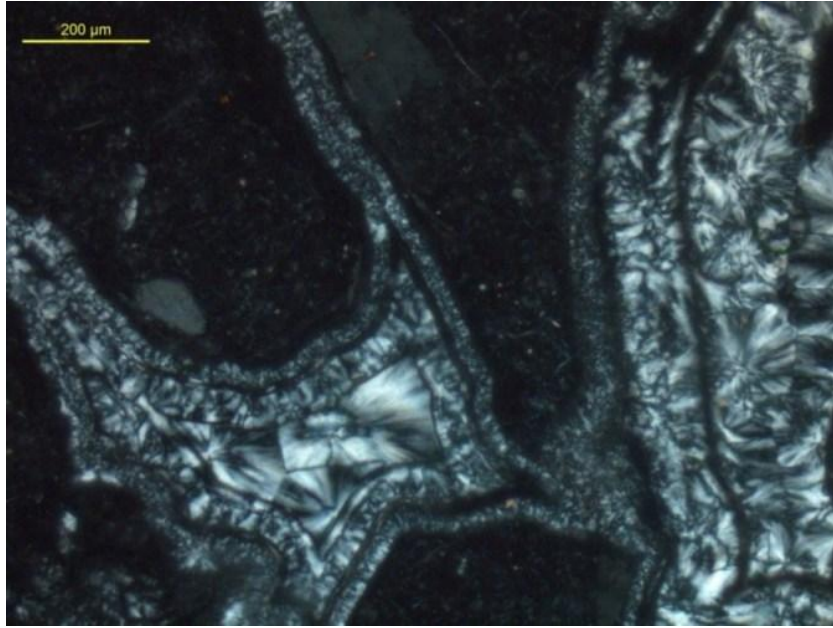


Figure 81. Photomicrograph of DTS4, cross nicol, 10x

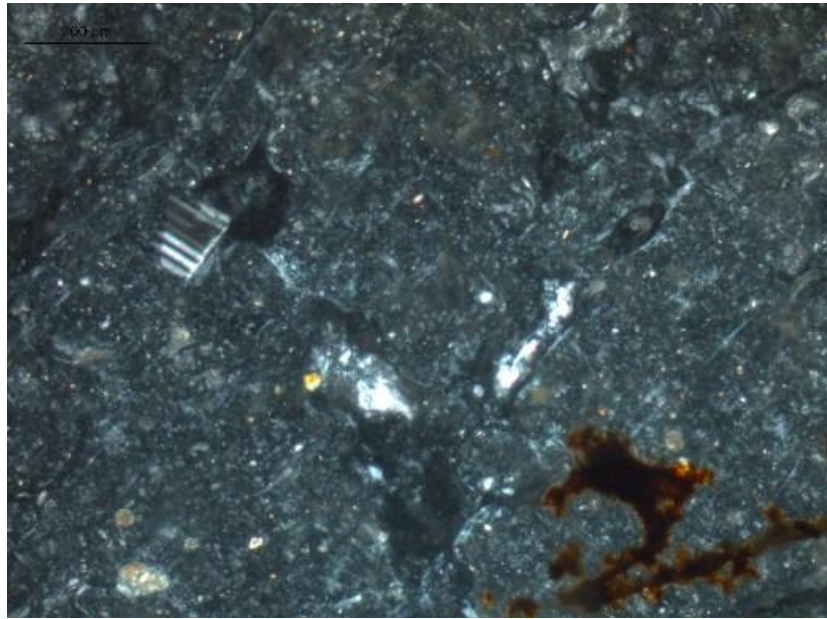


Figure 82. Photomicrograph of DTS4, cross nicol, 10x

DBY

Sample consists of crystal and rock fragments embedded within a matrix. Automorphic and semi-automorphic crystal and crystal fragments were plagioclase, sanidine, biotite and opaque minerals. One of the rock fragments observed in the thin section had porphyric spherulitic granular textured groundmass and plagioclase phenocryst (Figure 83, Figure 84). One other rock fragment was a volcanic rock fragment that has phenocrysts become plagioclase and chlorite mafic mineral (chlorite pseudomorph) and chloritic microlitic textured groundmass with ferrous cubic shaped opaque minerals. It was possibly andesite fragment (Figure 85, Figure 86). Some volcanic glass shards pertained to ignimbrite. Groundmass had ignimbritic flow patterns from place to place. Matrix/ crystal ratio is bigger than other samples.

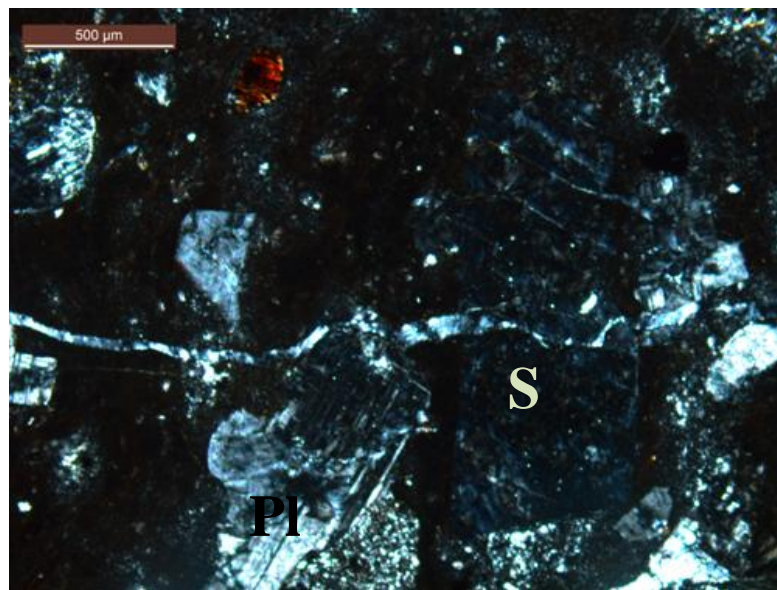


Figure 83. Photomicrograph of DBY, cross nicol, 5x, S: sanidine, Plg: plagioclase

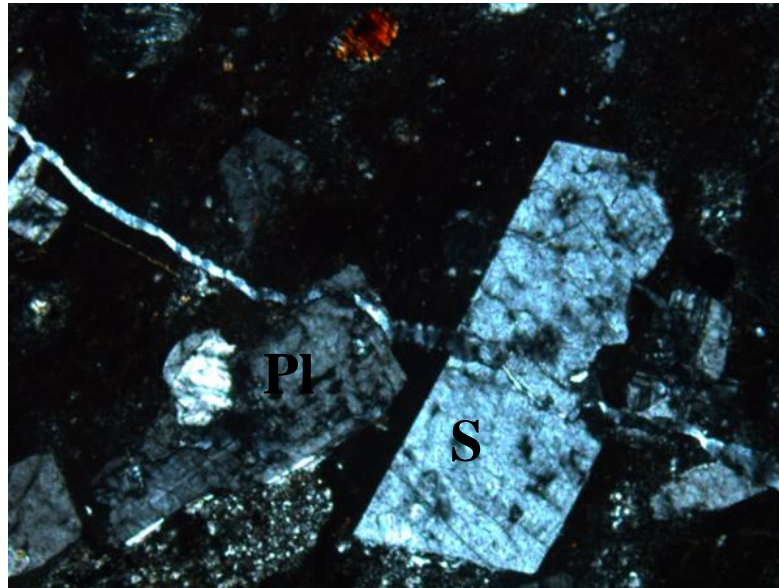


Figure 84. Photomicrograph of DBY, cross nicol, 5x, S: sanidine, Plg: plagioclase

The durability of igneous rocks under atmospheric weathering depended on their mineral constituents. Minerals that formed under high temperature, anhydrous conditions were generally not stable under atmospheric conditions.

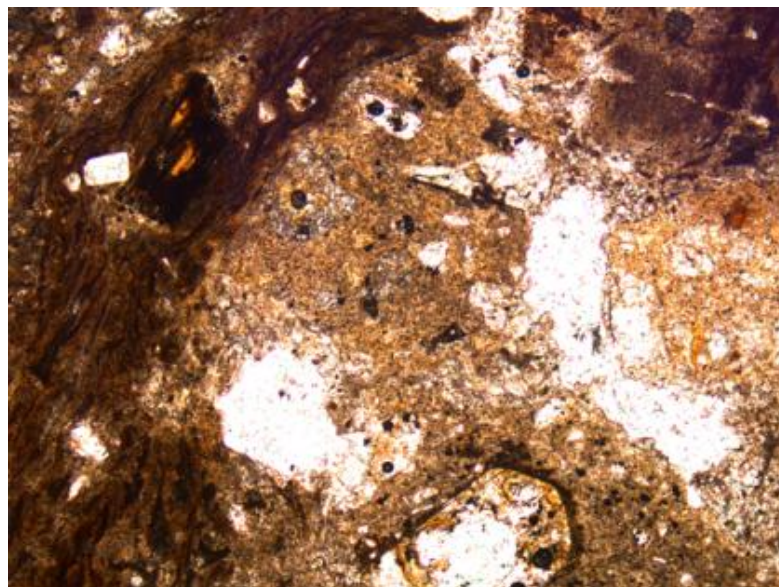


Figure 85. Photomicrograph of DBY, single nicol, 5x

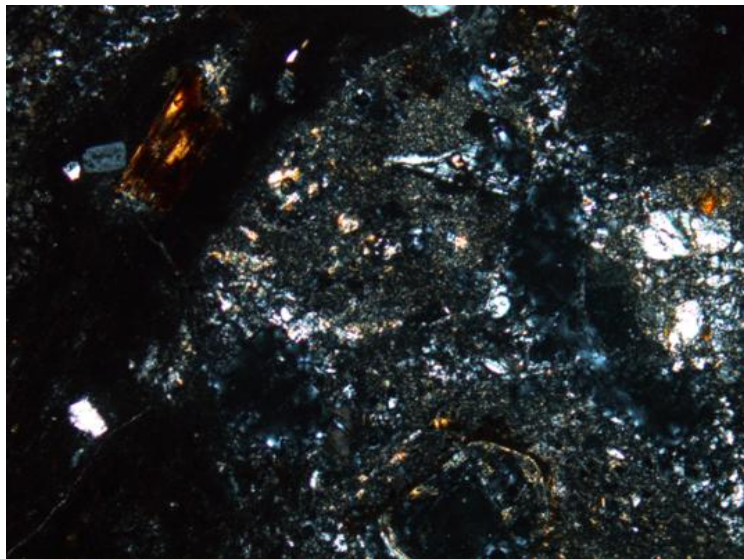


Figure 86. Photomicrograph of DBY, cross nicol, 5x

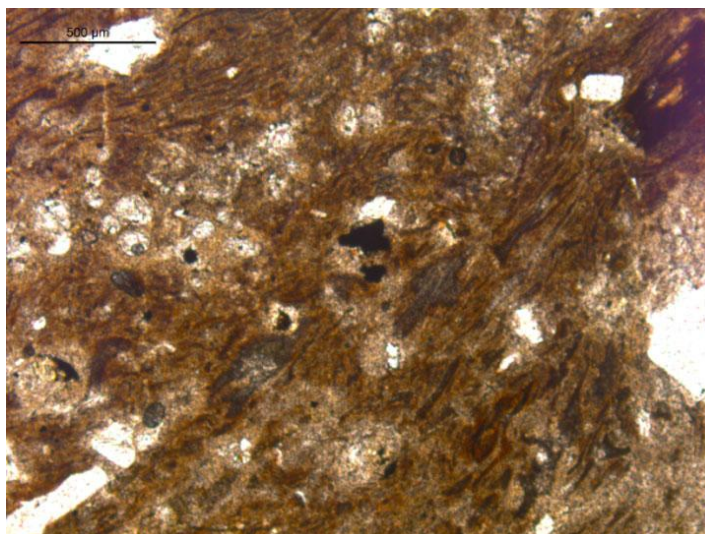


Figure 87. Photomicrograph of DBY, single nicol, 5x

DFG

Sample consisted of crystal and rock fragments embedded within tuffaceous gray matrix. Automorphic and semi-automorphic crystal and crystal fragments were quartz, plagioclase, biotite and opaque minerals (Figure 88, Figure 89). Crystals were corroded with hematite and clay minerals covered the area.

Various volcanic glass fragments existed in the section. Some of them were the forms specific for ignimbrite and had flow pattern. Microlithic porphyritic volcanic rock fragments in various dimensions were seen.

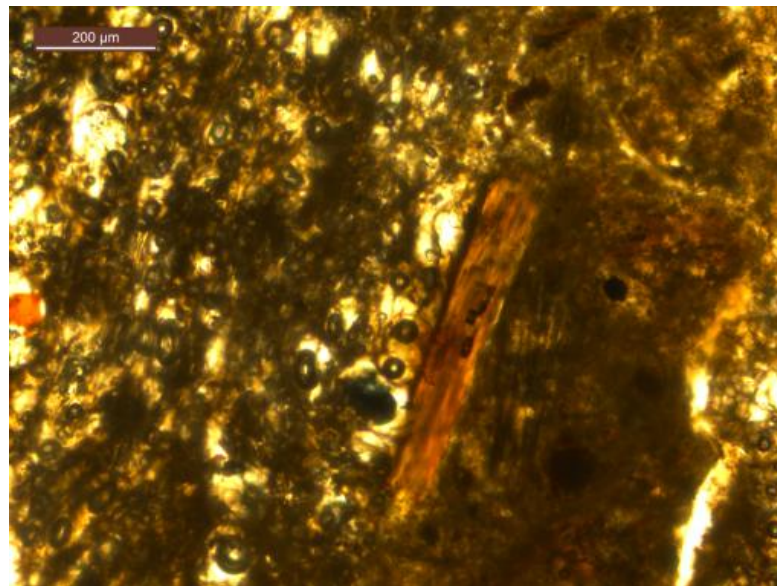


Figure 88. Photomicrograph of DFG, single nicol, 10x, biotite

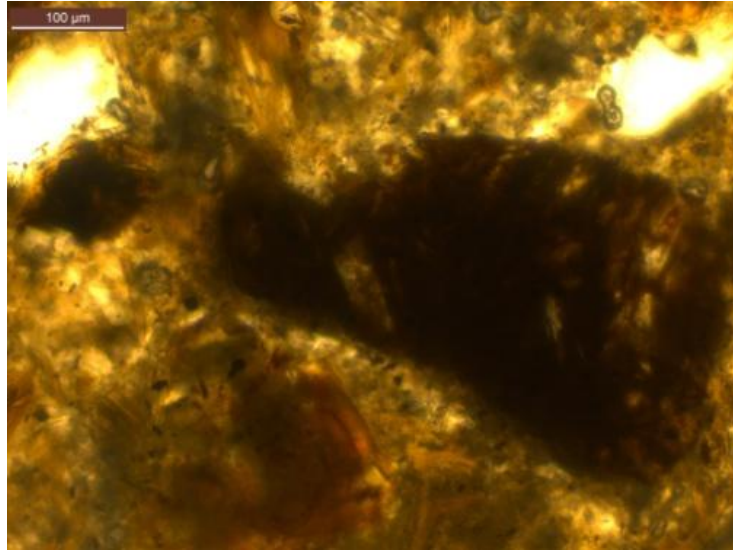


Figure 89. Photomicrograph of DFG, single nicol, 20x, hematite corrosion

DKK

Sample consisted of crystal and rock fragments embedded within a glassy matrix. Automorphic and semi-automorphic crystal and crystal fragments were plagioclase, quartz, biotite and opaque minerals. Rock fragments were seen in the thin section that has microcrystalline quartz piece embedded in volcanic glass groundmass with flow pattern (Figure 90, Figure 91). Ferrous cubic shaped opaque minerals existed. Various volcanic glass fragments also existed. Some of them were the forms specific for ignimbrite, some of them had flow pattern. Microlithic porphyritic andesitic rock fragments in various dimensions were seen (Figure 92).

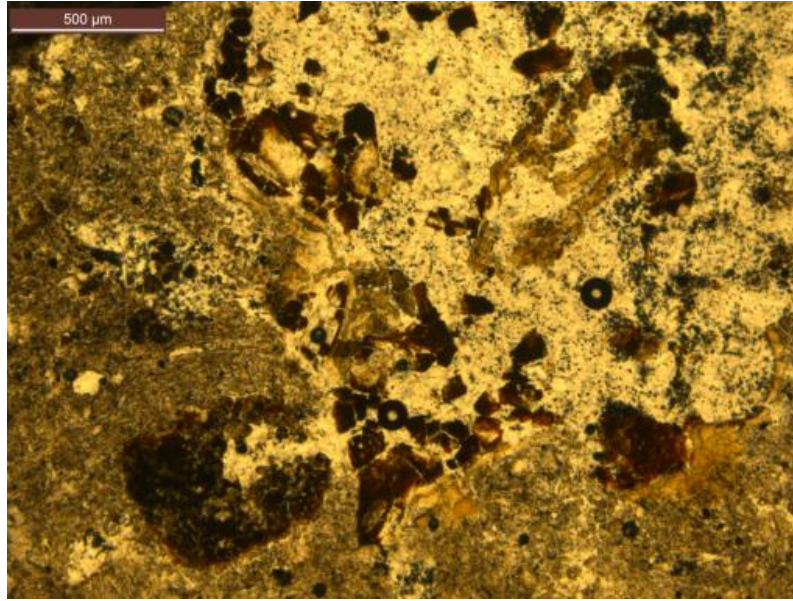


Figure 90. Thin section image of DKK, single nicol, 5x

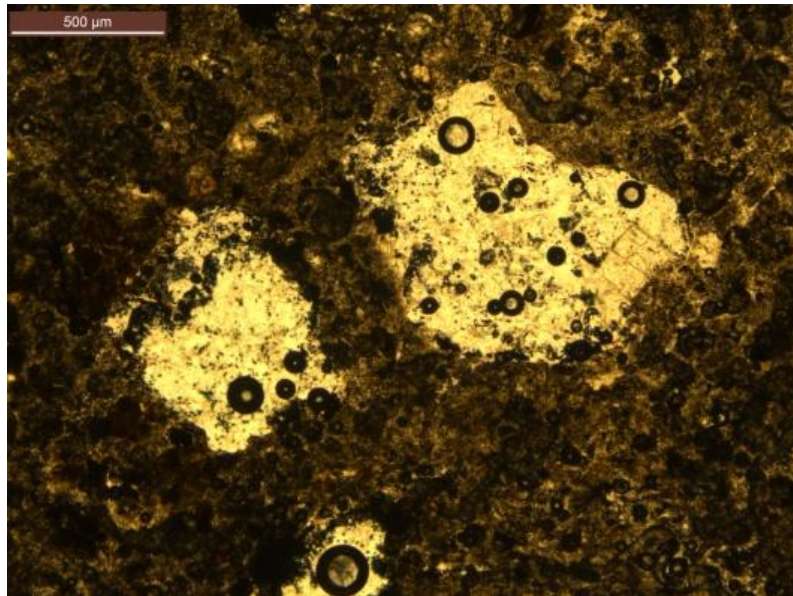


Figure 91. Thin section image of DKK, single nicol, 10x

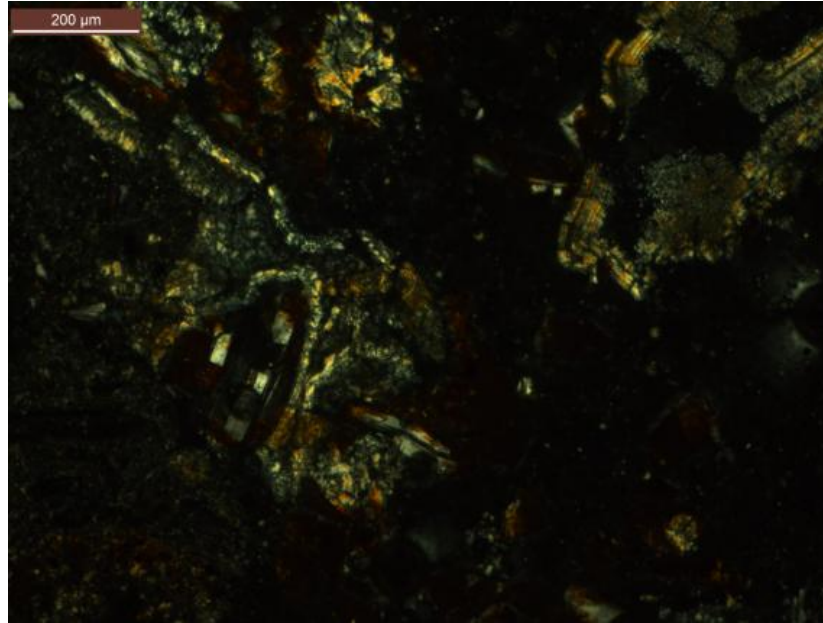


Figure 92. Thin section image of DKK, cross nicol, 10x

3.2.2 X-RAY DIFFRACTION ANALYSIS

In the X-Ray Diffraction analyses of samples;

DTS1 and DTS2 had quartz and feldspar (albite, anorthite) as main elements. Biotite and smectite peaks were observed. The trench showed amorphous phase namely volcanic glass (Figure 94).

DBY had quartz and feldspar (albite) as main minerals. Biotite was the second mineral appeared (Figure 94).

DFG had quartz and feldspar (anorthite) mainly then smectite. Volcanic glass trench was observed again (Figure 94).

DKK had quartz and feldspar (anorthite) mainly. Smectite is the secondary minerals. Volcanic glass trench was observed again (Figure 94).

The top three d-values of are given in Appendix D.

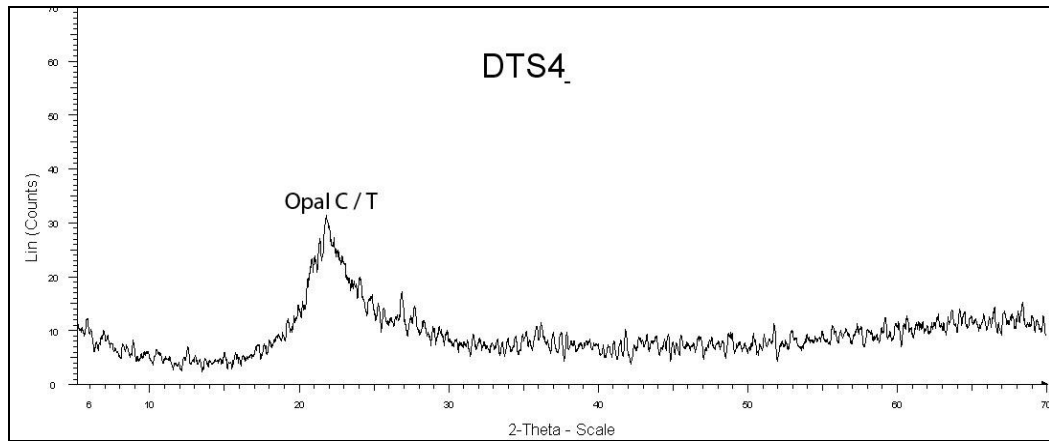


Figure 93. X-Ray Diffraction of DTS4

DTS4, the bedrock which the temple was built on, had Opal CT in its X Ray Diffraction.

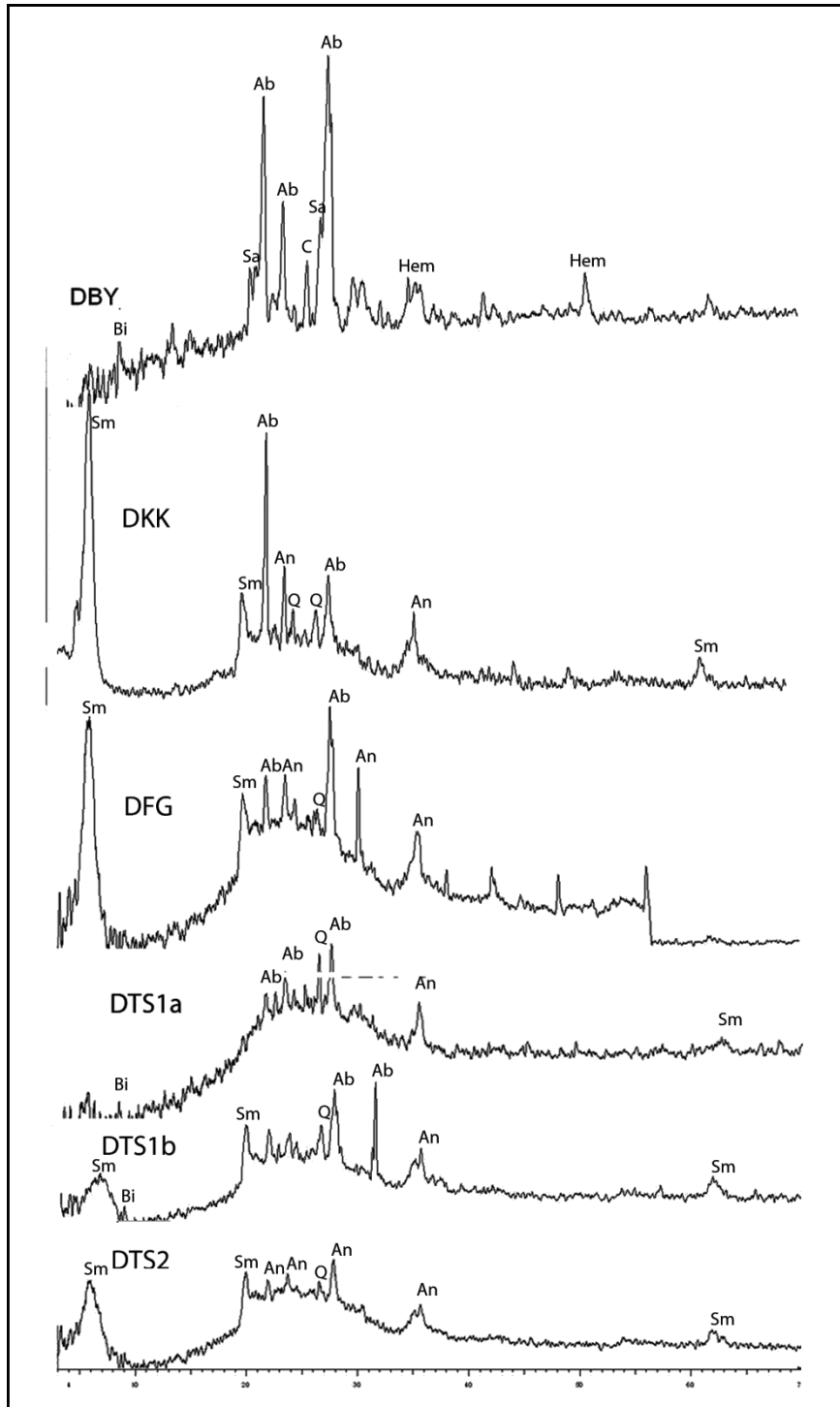


Figure 94. Unoriented X-Ray Diffraction graph of samples. Sm: smectite, Ab: albite, An: anorthite, Q: quartz, Bi: biotite, Sa: sanidine, Hem: hematite

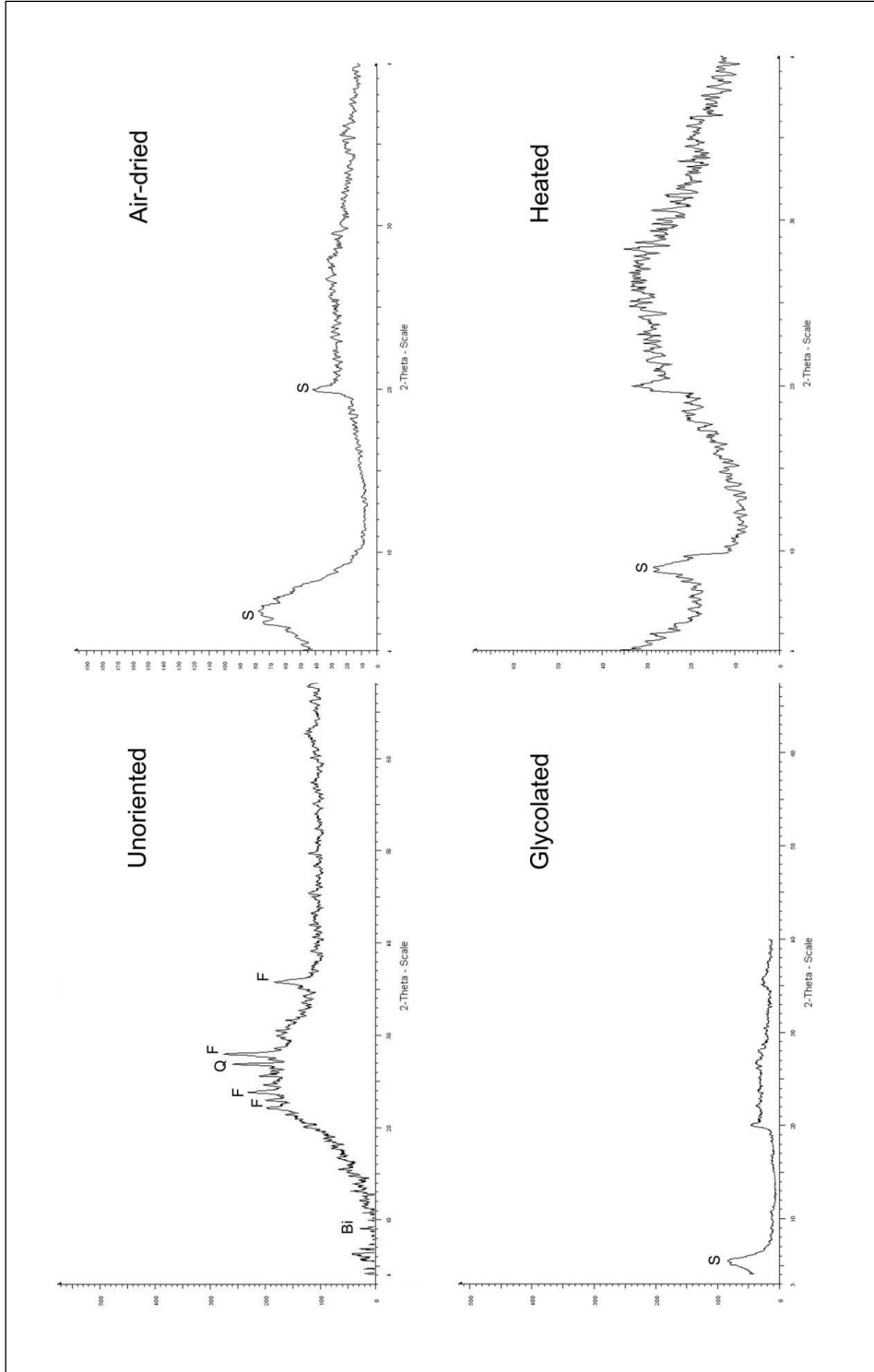


Figure 95. X-Ray Diffraction of DTS1 as unoriented, air-dried, ethylene glycolated and heated. S: smectite, F: feldspar, Q: quartz, Bi: biotite.

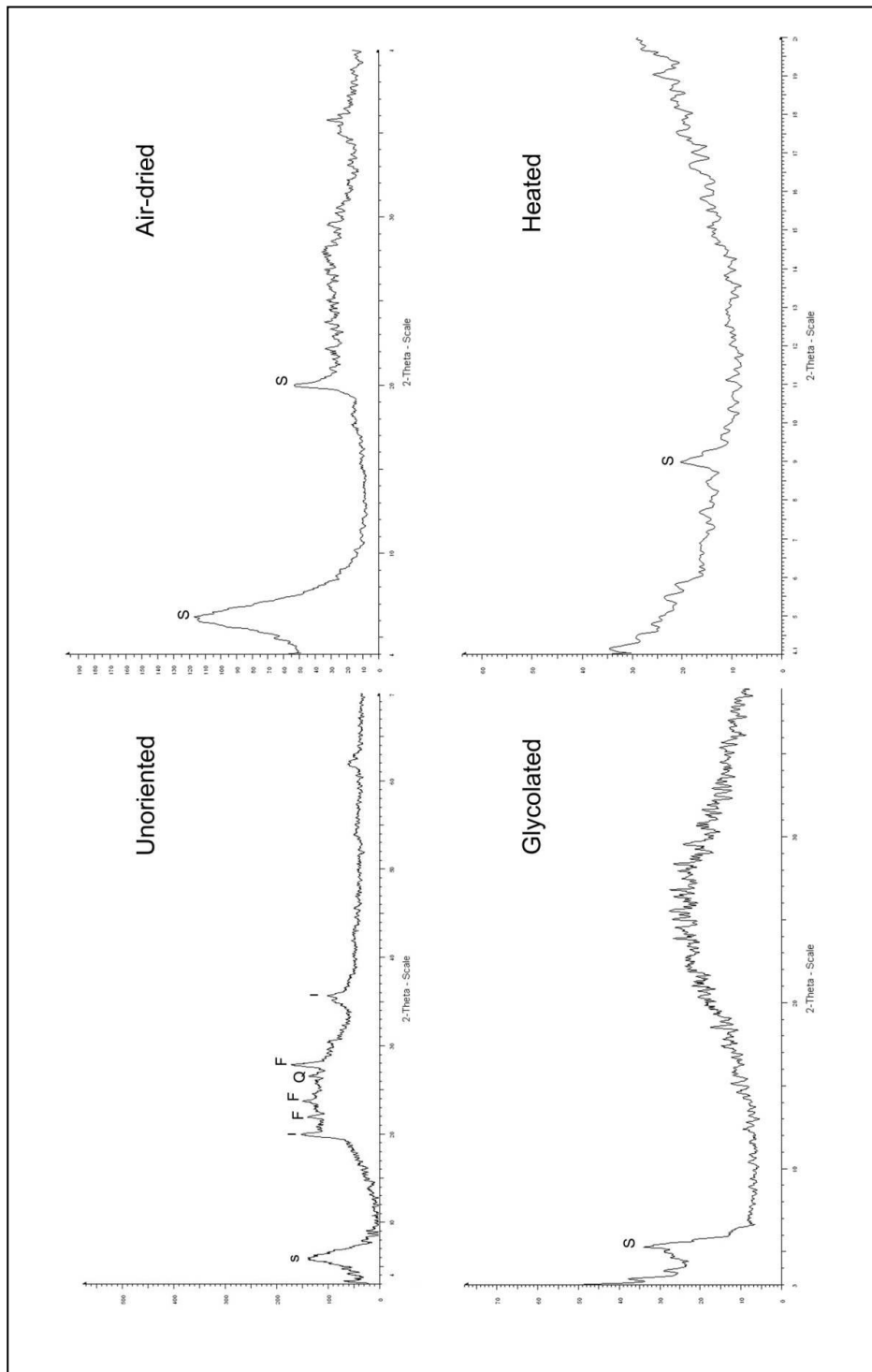


Figure 96. X-Ray Diffraction of DTS2 as unoriented, air-dried, ethylene glycolated and heated. S: smectite, F: feldspar, Q: quartz.

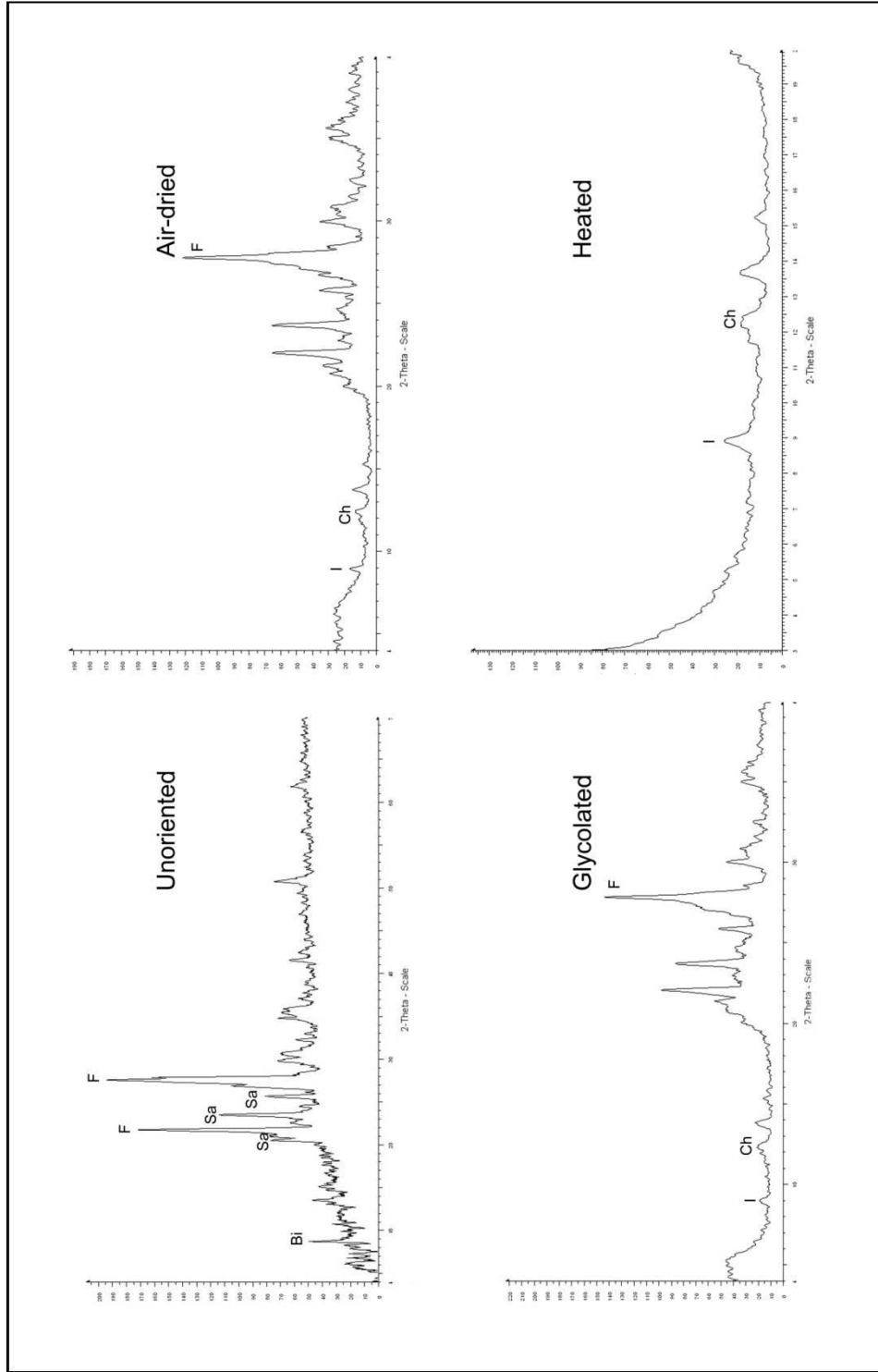


Figure 97. X-Ray Diffraction of DBY as unoriented, air-dried, ethylene glycolated and heated. S: smectite, F: feldspar. Bi: biotite. Sa: sanidine. Hem: hematite. Ch: chlorite. I: illite.

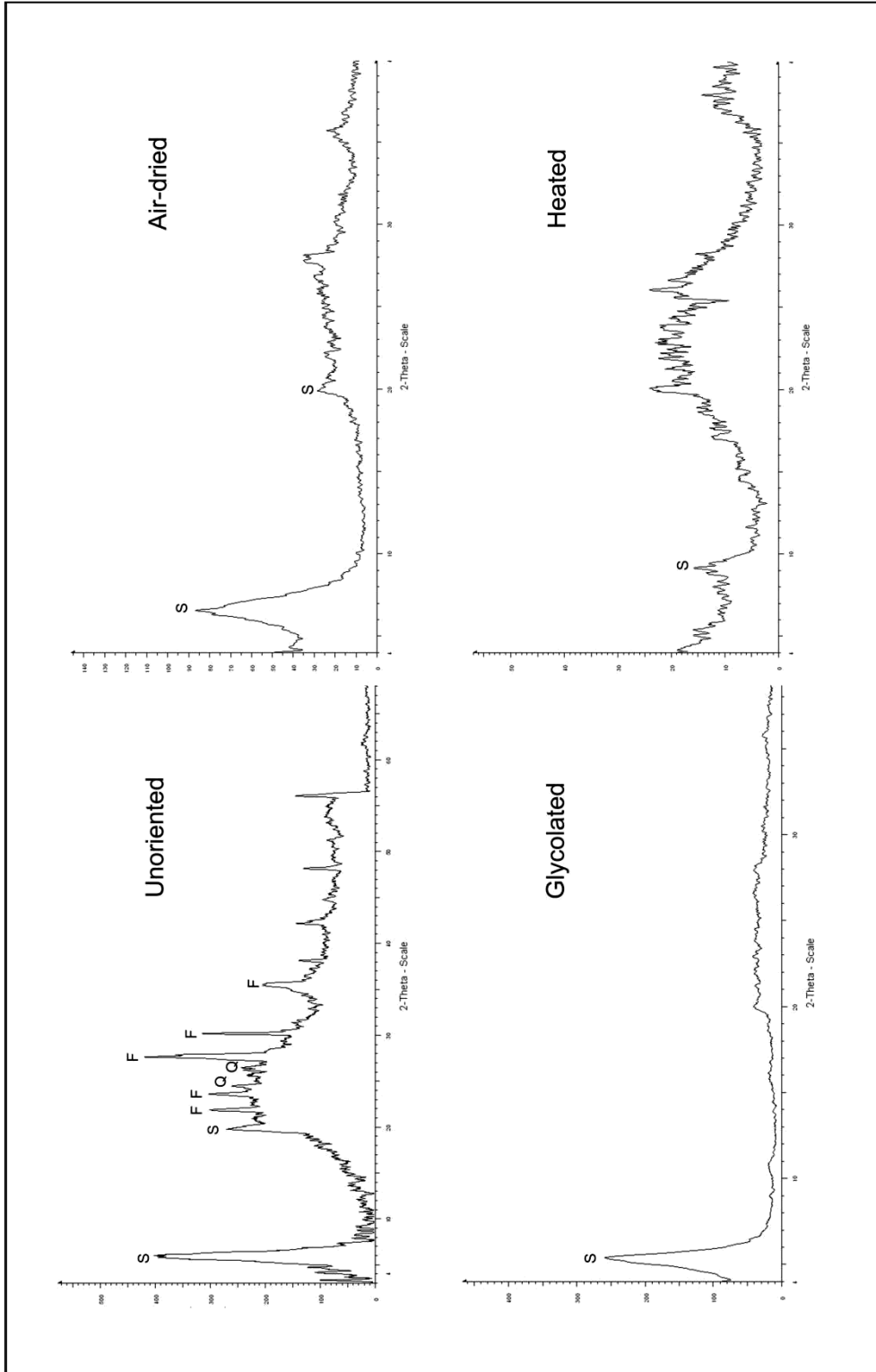


Figure 98. X-Ray Diffraction of DFG as unoriented, air-dried, ethylene glycolated and heated. S: smectite, F: feldspar, Q: quartz.

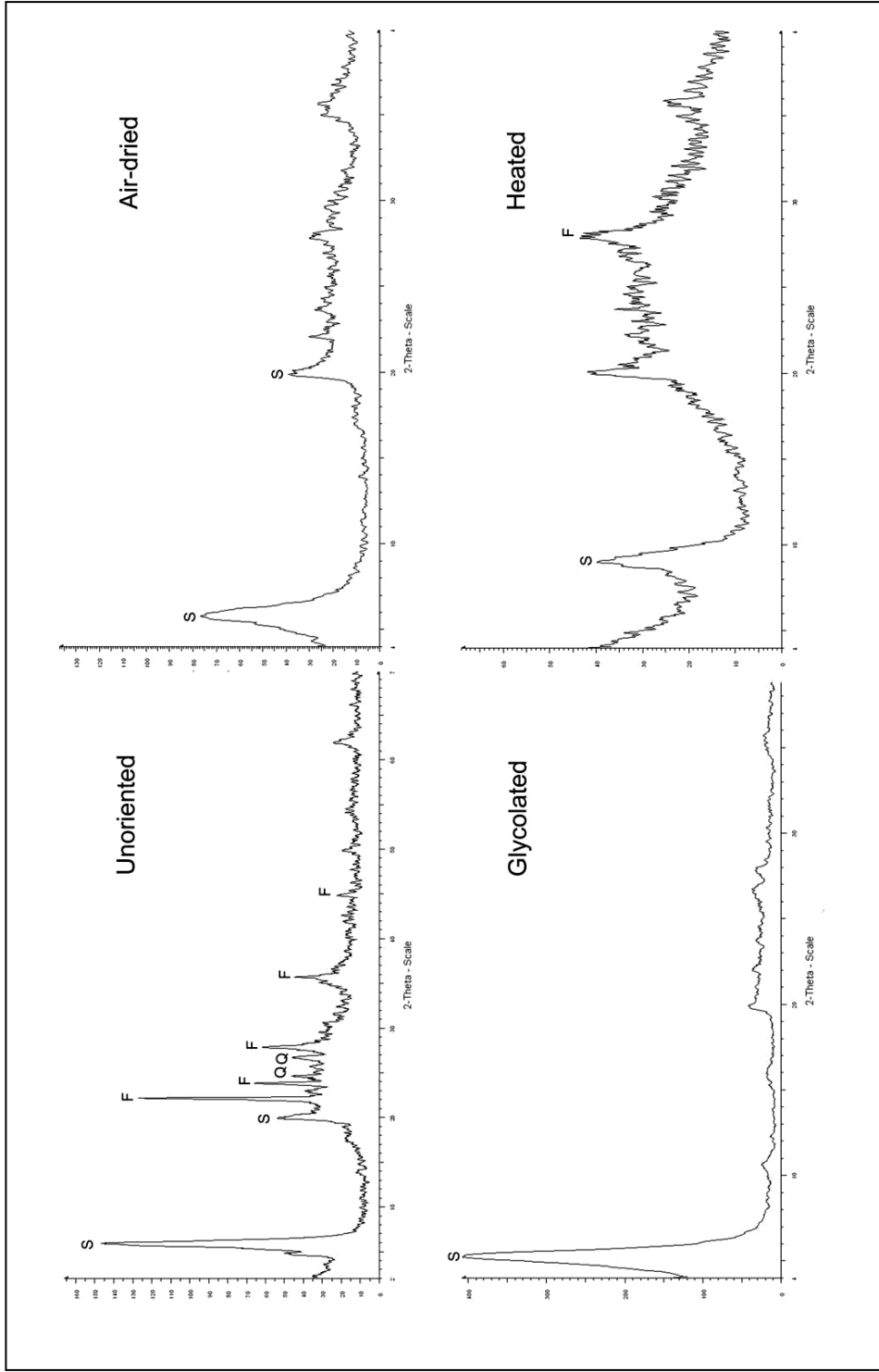


Figure 99. X-Ray Diffraction of DKK as unoriented, air-dried, ethylene glycolated and heated. S: smectite, F: feldspar, Q: quartz

In the oriented XRDs it is shown that;

In DTS1, DTS2, DFG and DKK graphs, smectite peaks were observed in air dried, ethylene glycolated and heated treatments. (Figure 95, 96, 98, 99). In air-dried samples smectite had a peak in the range 12Å to 15Å which on ethylene glycolation it expanded uniformly to 17.2Å and when heated the first diffraction peak collapsed to an illite-like 10Å.

In DBY, illite (all three situation 10Å) and chlorite (14Å and 7Å) peaks were observed in air dried, ethylene glycolated and heated treatments (Figure 97).

3.2.3 CROSS SECTION ANALYSIS

DTS1



Figure 100. Cross section image of DTS1

DTS1 is a light brownish gray, partially pale, porous, porphyritic vitric tuff with phenocrysts of quartz up to 4 cm in size. It shows ignimbritic features with several

rock fragments in it. Fragments are volcanic rock originated. Cement consists of volcanic glass and has brown color (Figure 100).

DTS2



Figure 101. Cross section image of DTS2

DTS2 has volcanic rock fragments less than DTS1 and shows welded ignimbritic features. It shows typical for volcanic rocks, which is characterized by phenocrysts enclosed in a fine-grained matrix. Cement consists of volcanic glass and has light brown-gray color (Figure 101).

DTS3



Figure 102. Cross section image of DTS3

DTS3 has small fragments and bands, hypocrySTALLINE texture and has lighter color than the others. It has isotropic and homogenous fabric (Figure 102).

DTS4

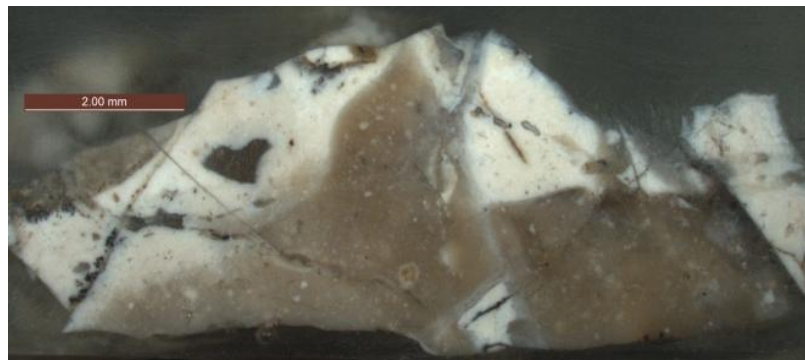


Figure 103. Cross section image of DTS4

DTS4 has white and light brown minerals. It consists of opal. Opal forms in the way: during a late stage in volcanic rocks, filling vesicles and fractures (Figure 103).

DFG

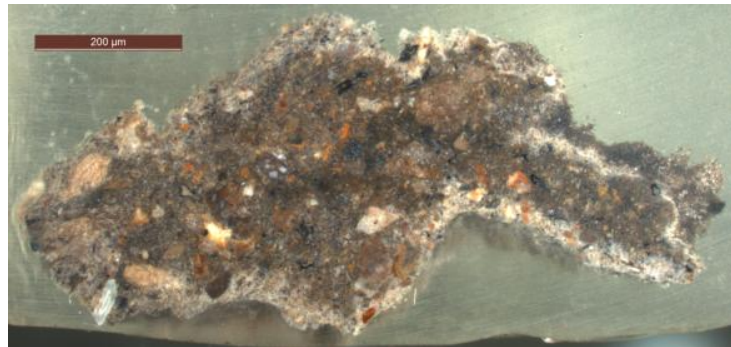


Figure 104. Cross section image of DFG

DFG has light brown-gray color and ignimbritic structure with several size volcanic rock fragments (Figure 104). The rock exhibits a hypocrystalline fabric with a weak parallel texture, where millimeter to centimeter large light color feldspar, white quartz crystals and black biotite are floating in a gray, brown groundmass. Feldspar crystals can attain sizes ranging from 0.3 mm to 1 cm. Biotites are smaller than 2 mm.

DBY



Figure 105. Cross section image of DBY

DBY has brownish color with small fragments in it. It consists mainly of feldspar, biotite and pyroxene phenocrystals in a microlitic groundmass (Figure 105).

DKK

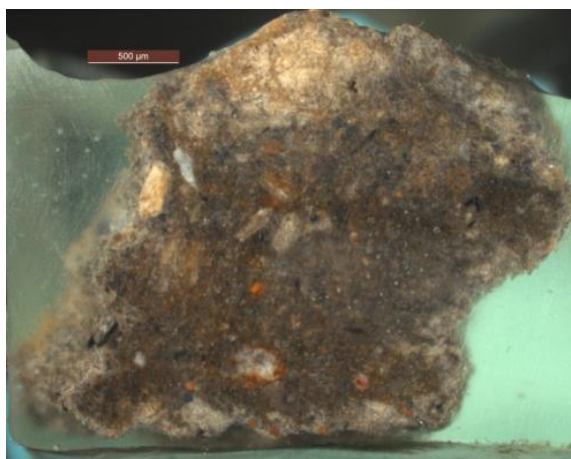


Figure 106. Cross Section of DKK

DKK has brownish-beige color with ignimbritic texture and rock fragments and volcanic glass cement. The rock exhibits a hypocrystalline fabric with a weak parallel texture, where millimeter to centimeter large light color feldspar crystals, white quartz crystals and black biotite are floating in a gray, brown groundmass. Feldspar crystals can attain sizes ranging from 0.3 mm to 2 cm. Biotites are smaller than 2 mm (Figure 106).

3.2.4 X-RAY FLOURESCENCE ANALYSIS (XRF)

In chemical analysis, elements present over 1% are considered major, from 1% to 0.01% are minor. Generally major and minor elements are reported as oxides in percentage by weight.

Table 18. Major element percentages of samples

	DTS1	DTS2	DBY	DFG	DKK
SiO ₂	64,5	63,2	66,7	65,8	65,2
TiO ₂	0,55	0,57	0,49	0,55	0,56
Al ₂ O ₃	17,8	17,3	16,8	17,8	19,3
Fe ₂ O ₃	3,29	3,69	2,91	3,29	3,38
MnO	0,07	0,11	0,12	0,1	0,07
MgO	1,77	1,78	0,5	1,74	2,42
CaO	2,78	4,37	1,88	2,28	2,31
Na ₂ O	1,63	2,34	4,11	2,05	1,46
K ₂ O	6,07	5,34	5,7	5,56	4,5
P ₂ O ₅	0,78	0,41	0,11	0,15	0,13
Total	99,94	100,53	99,99	100,03	100,43

Table 19. Minor element percentages of samples

	DTS1	DTS2	DBY	DFG	DKK
F	0,248	0,247	0,171	0,257	0,21
SO3	0,0787	0,179	0,0616	0,0438	0,0382
Cl	0,0788	0,168	0,0302	0,0695	0,0453
CuO	0,0075	0,0078	0,0051	0,0077	0,0084
ZnO	0,0109	0,009	0,0059	0,009	0,0205
Ga2O3	0,004			0,0035	
Rb2O	0,0362	0,0298	0,0245	0,032	0,0292
SrO	0,0504	0,0565	0,0585	0,0557	0,0633
Y2O3	0,0135	0,0116		0,0135	
ZrO2	0,053	0,0517	0,0495	0,0491	0,0519
BaO	0,113	0,124	0,244	0,162	0,145
PbO	0,0107	0,0257	0,0107	0,0081	0,0151
Br		0,0015			
ThO2		0,0053	0,0033	0,0054	
Nb2O5			0,0027		0,0032

Samples include 63,20- 66,70% SiO₂, 16,80- 19-30% Al₂O₃ and 0,49-0,57% TiO₂ (Table 18, Table 19).

Samples that have low SiO₂ values have low strength values as well (Figure 107, Figure 108, Figure 109, Figure 110, Figure 111, Figure 112). Besides, samples having high Fe and L.O.I values have high strength values (Korkanc, 2007).

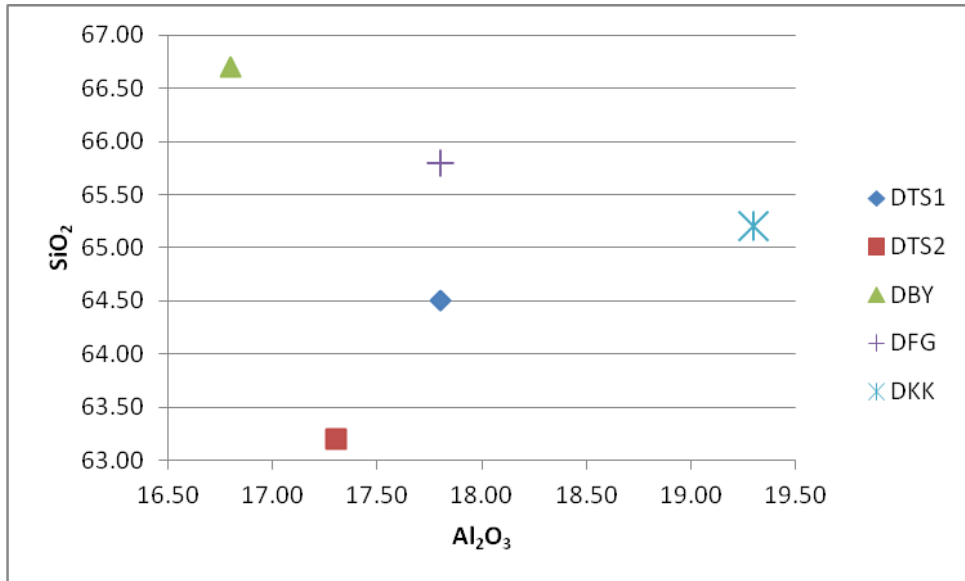


Figure 107. SiO_2 vs Al_2O_3 graph

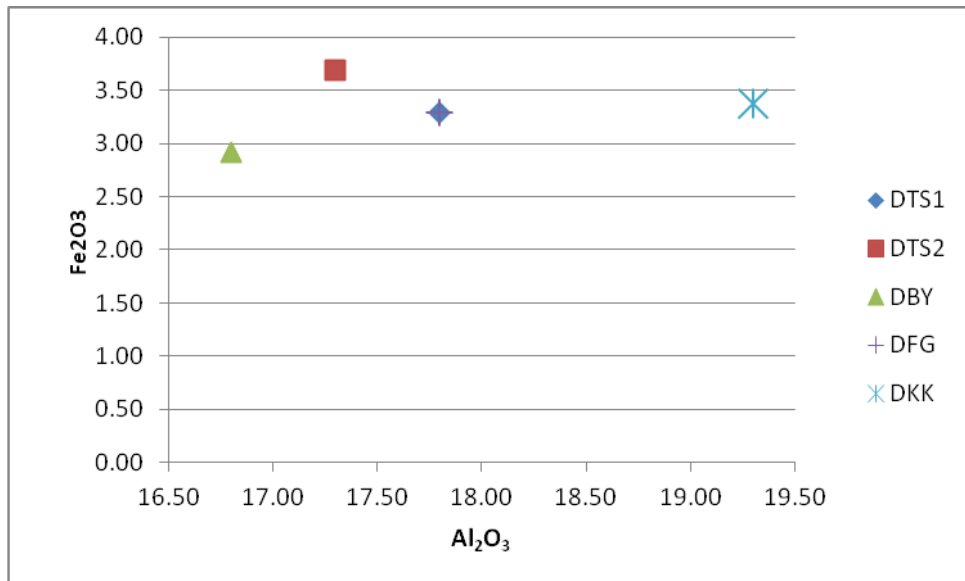


Figure 108. Fe_2O_3 vs Al_2O_3 graph

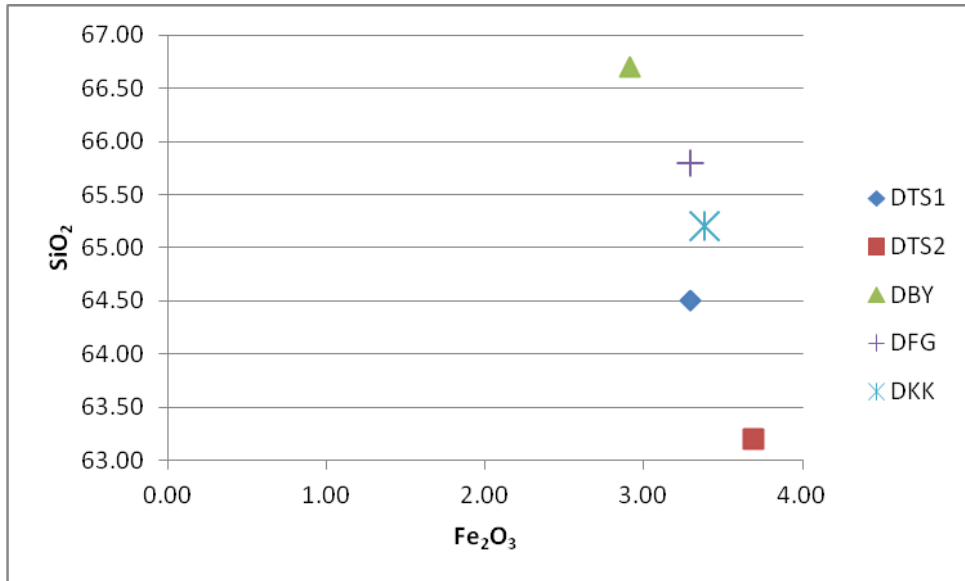


Figure 109. SiO₂ vs Fe₂O₃ graph

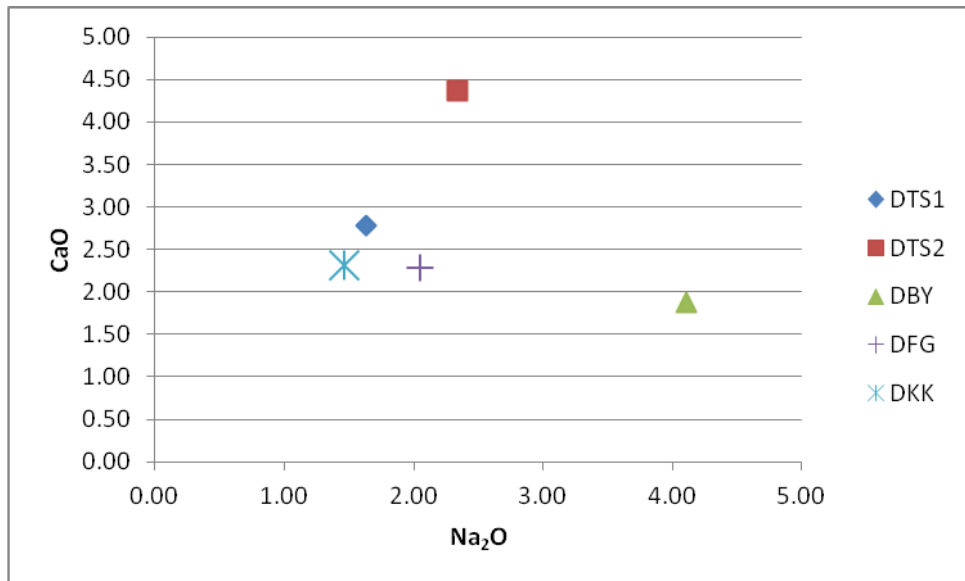


Figure 110. CaO vs Na₂O graph

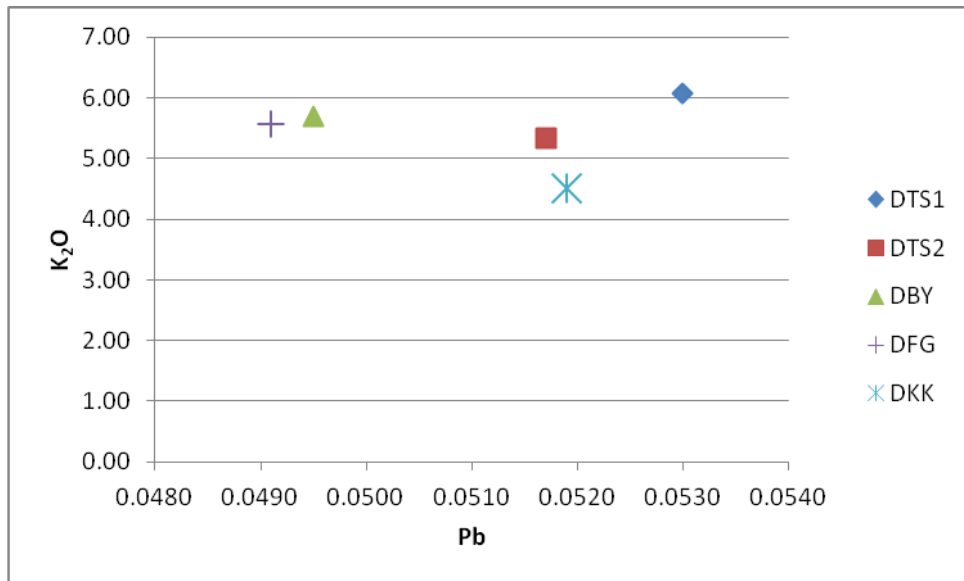


Figure 111. K₂O vs Pb graph

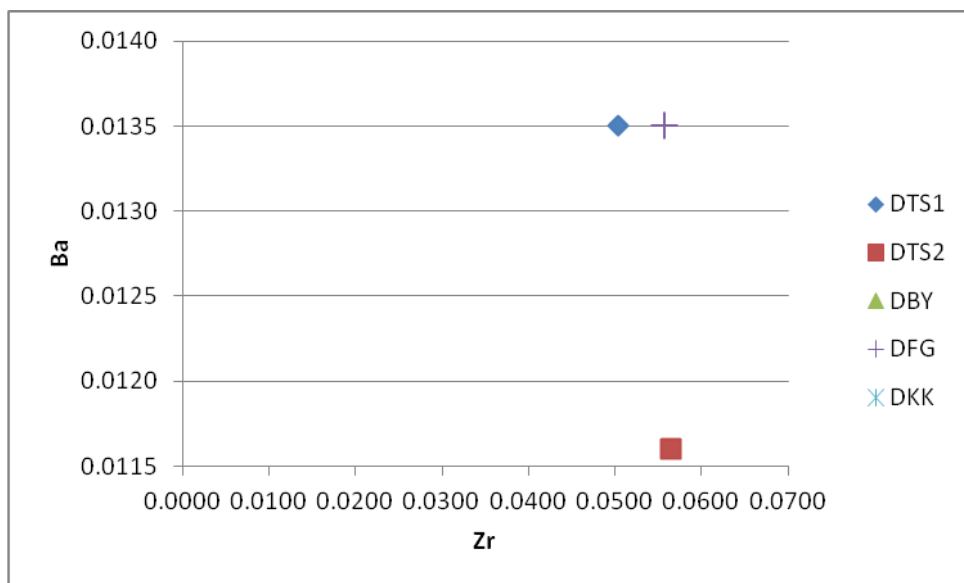


Figure 112. Ba vs Zr graph

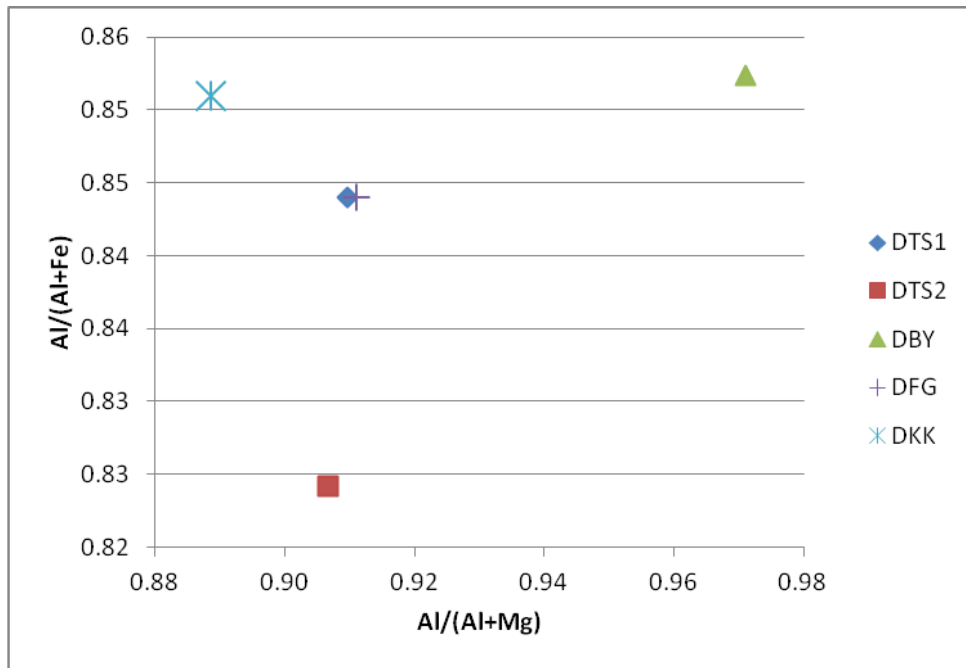


Figure 113. Al/(Al+Fe) vs Al/(Al+Mg) graph

3.2.5 SCANNING ELECTRON MICROSCOPY (SEM) – ENERGY DISPERSIVE ANALYZER (EDX)

SEM-EDX study of the samples show that it consists of equidimensional glass grains with shard morphology, particles similar to smectite in morphology, and a few particles of potassium feldspar and quartz (Figure 114, Figure 115, Figure 116). The smectite-like grains are more abundant in the material with grain size of 10-200 μm (Figure 117). Glass particles with altered surfaces contain vesicles (Figure 118).

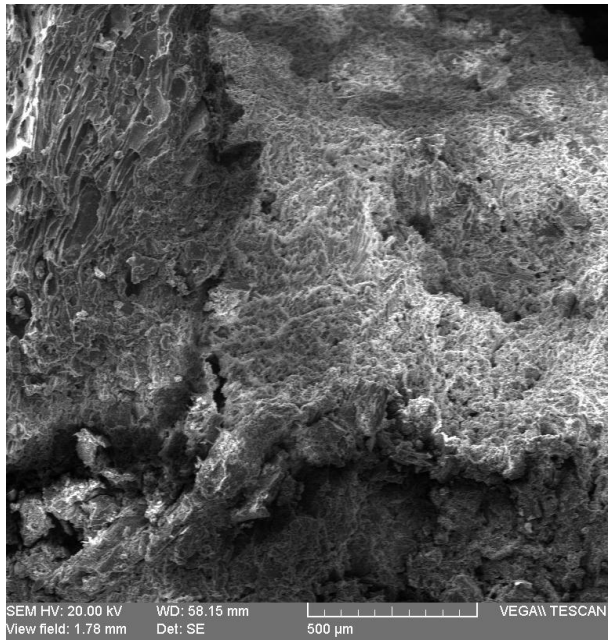


Figure 114. SEM image of DFG with honeycomb morphology of smectite

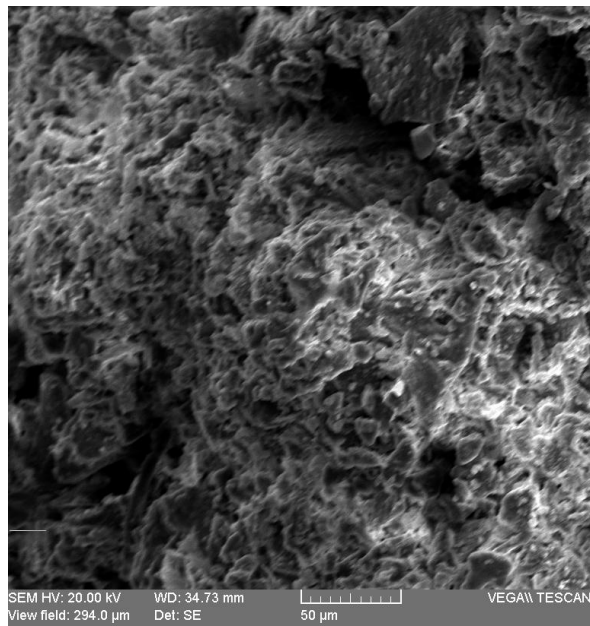


Figure 115. SEM image of DFG



Figure 116. SEM image of DKK showing quartz etch and feldspar fragments

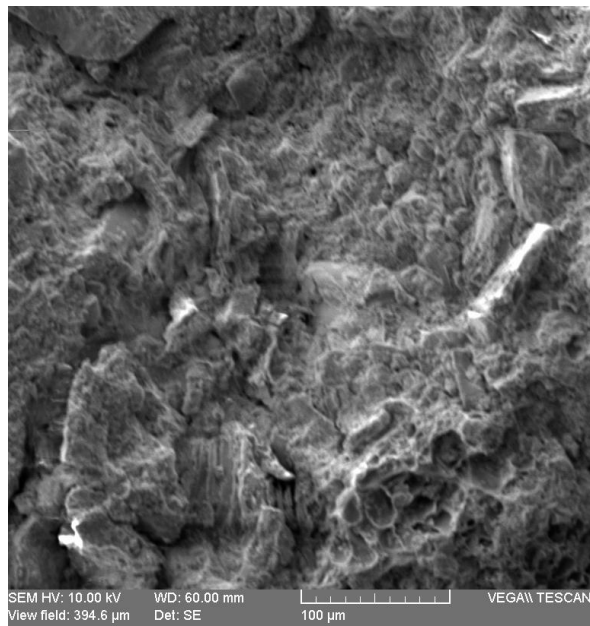


Figure 117. SEM image of DKK honeycomb type smectite in feldspar and quartz grains

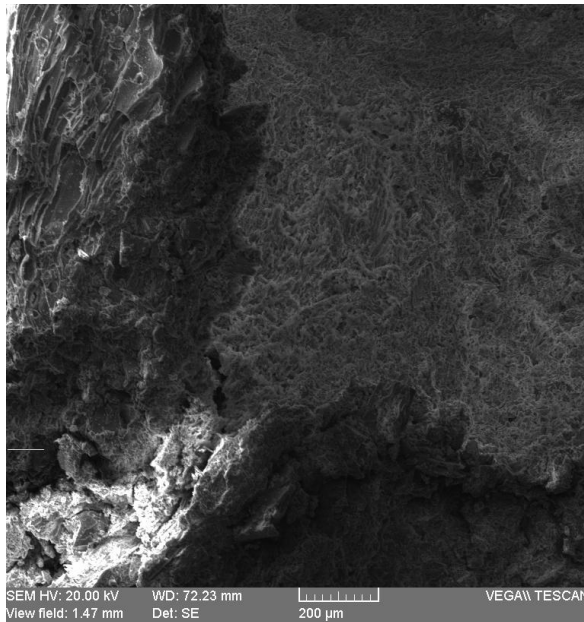


Figure 118. SEM image of DKK

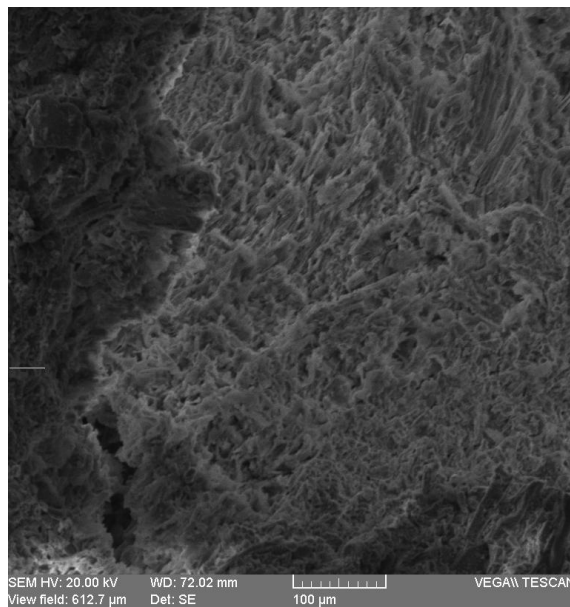


Figure 119. SEM image of DKK

SEM-EDX examination of the reaction products showed features that developed over time and reaction temperature, without apparent influence of the solution composition, in the following sequence. Glass grains with an etched surface were

seen. The chemical composition of the glass surfaces at this feature is similar to smectite. Honeycomb structures with a chemical composition consistent with smectite were present in two different arrangements. Some of them were seen in ball-shaped units and covered the inner surface of holes. Very thin flakes on surfaces were observed.

3.2.6 FOURIER TRANSFORM INFRARED SPECTROSCOPIC ANALYSIS (FTIR)

FTIR analysis of the original tuff showed that in reflectance mode, there was a band at 3650 cm^{-1} and the $3600\text{-}3000\text{ cm}^{-1}$ system of molecular water and hydroxyl groups in the glass. The OH-stretching band in 3400 and 3750 cm^{-1} region is common in silicates. The peak around 3620 cm^{-1} was in Al-rich smectite, I-S, and illite (Farmer, 1974; Russell, 1987). This band envelops a number of components corresponding to the different cation pairs linked to an OH group. The components are two Al-OH-Mg bands at 3684 and 3602 cm^{-1} , two Al-OH-Al bands at 3635 and 3618 cm^{-1} , Al-OH-Fe at 3587 cm^{-1} , Fe-OH-Mg at 3568 cm^{-1} , and two Fe-OH-Fe bands at 3554 and 3532 cm^{-1} (Madejová et al., 1994).

The most common dioctahedral smectite, are occupied mainly by Al but partly substituted with Fe and Mg. The tetrahedral contain normally Si as central atoms with some Al substitution (Madejova, 2003).

DTS1, DBY, DFG and DKK have OH band with peaks between 3618 and 3623 cm^{-1} (Figure 120, Figure 121, Figure 122, Figure 123).

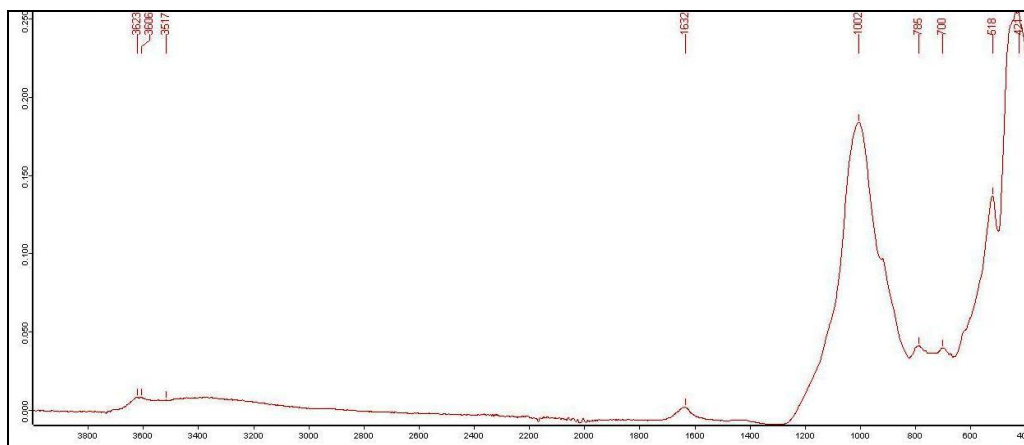


Figure 120. FTIR spectra of DTS1 peaks between 4000-3000 cm^{-1} : 3623,3606

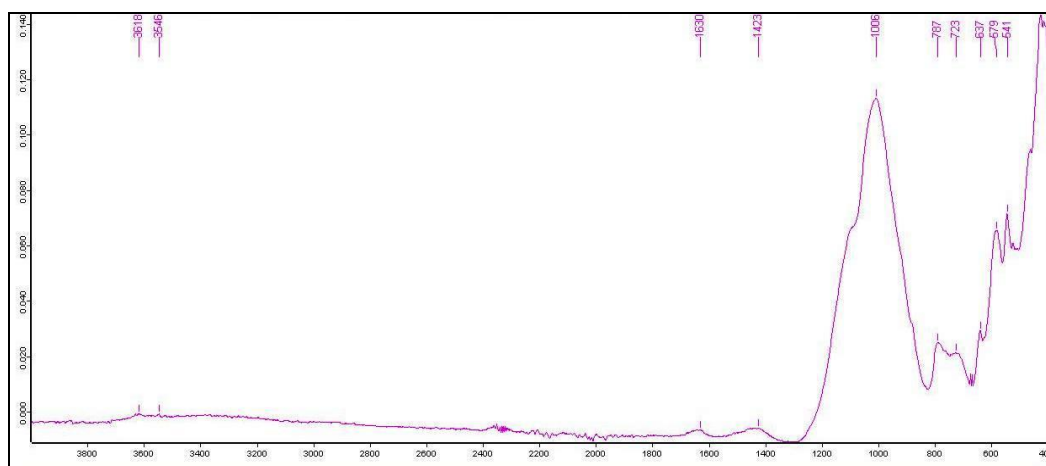


Figure 121. FTIR spectra of DBY peaks between 4000-3000 cm^{-1} : 3618,3546

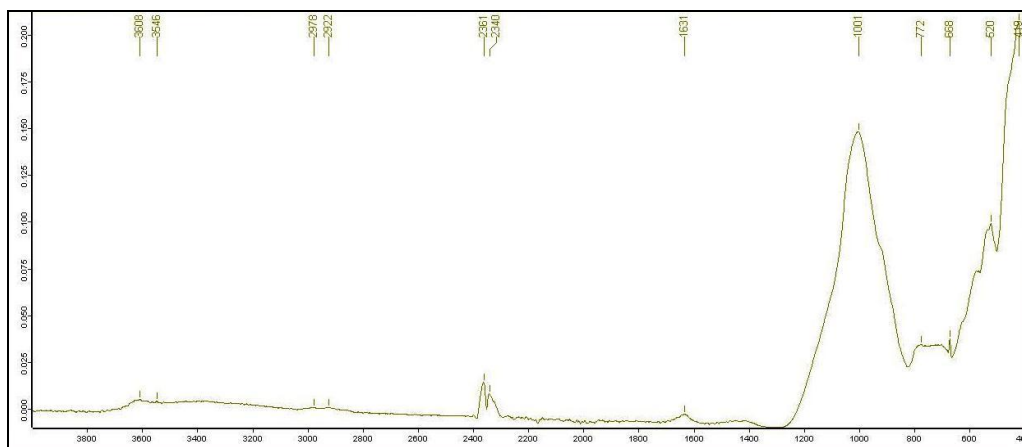


Figure 122. FTIR spectra of DFG peaks between 4000-3000 cm^{-1} : 3608, 3546

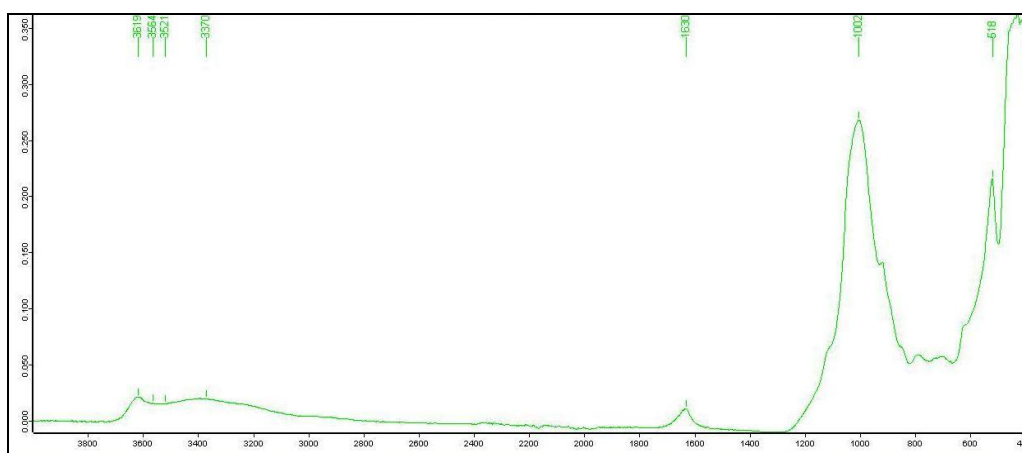


Figure 123. FTIR spectra of DKK peaks between 4000-3000 cm^{-1} : 3619, 3564

3.2.7 METHYLENE BLUE ADSORPTION TEST (MBA)

Clay mineral is the smectite which is found in samples according to XRD. Low cation exchange capacity value implies low clay content. If it is assumed that other minerals do not adsorb the methylene blue dye, C.E.C. values show that DTS1 has 5,2 - 9,8%, DFG has 6,8 - 12,7%, DKK has 11,5 - 21,5% and DBY has 1,3 - 2,4% smectite. DBY has the lowest clay content.

Table 20. MBA and CEC values of samples

Sample Code	MBA g/100g	C.E.C mEq/100g
DTS1	2,5	7,82
DFG	3,25	10,16
DKK	5,5	17,2
DBY	0,6	1,88

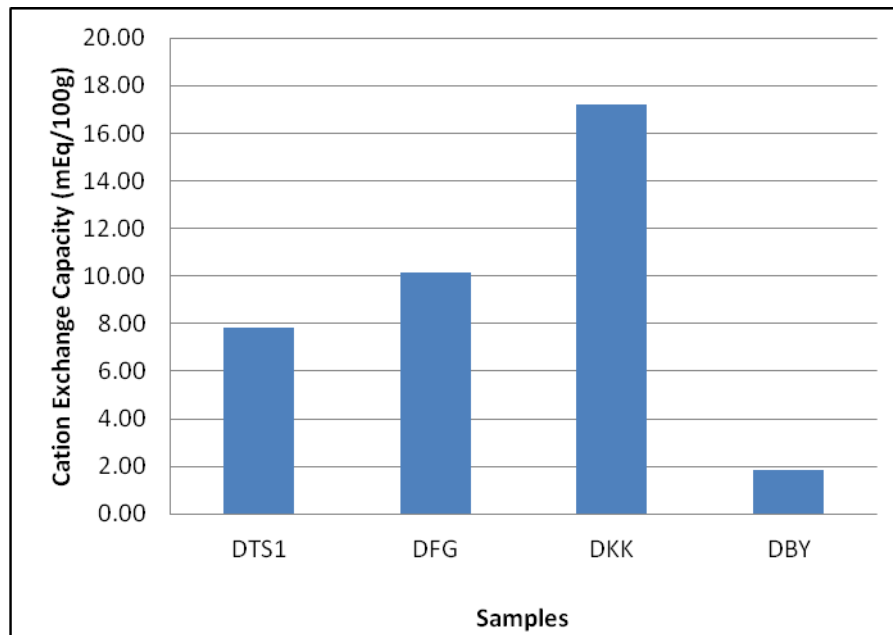


Figure 124. C.E.C. values of samples

3.3 DURABILITY ASSESSMENT OF SAMPLES

Durability assessment is done by correlation of experimental data; average pore diameter, saturation coefficient and wet to dry strength ratio are basic parameters that can be calculated from data.

3.3.1 AVERAGE PORE DIAMETER

Average pore diameter is considered to be an important parameter for the freeze-thaw and salt crystallization durability of rock. Materials having larger pores are subjected to less crystallization pressure than those with smaller pores (Scherer, 1999). The critical pore size is 5 μm below which pore water cannot be drained out of the rock. Therefore, rocks having average pore size less than 5 μm are susceptible to frost damage (Larsen and Cady, 1969). In the study, only DKK sample average pore diameter can be calculated from the intrusion data of the mercury porosimeter. The test results yield 0.34 μm , which suggests that it is susceptible to frost damage.

3.3.2 SATURATION COEFFICIENT

Saturation coefficient (S) of a stone is the ratio between the natural capacity of a stone to absorb water after complete immersion under atmospheric pressure for a definite time, and its total volume of the pores that is accessible to water (Topal, Doyuran, 1999).

$$S = (\text{water absorption} / \text{effective porosity})$$

Saturation coefficient corresponds to the rate of the pore space, which fills up with water under normal atmospheric conditions. In case that, the water saturation coefficient comes closer to 1, the proportion of pore spaces filled with water under atmospheric pressure will be higher. (Middendorf et.al., 2011)

A stone with very high saturation coefficient may be deteriorated by freeze-thaw activity (RILEM, 1980). Therefore, this value is an indicator to evaluate the durability of the stone in freeze-thaw situation. The value of saturation coefficient can mostly vary between 0.4 and 0.9. A saturation coefficient greater than 0.8, means the rock is not frost resistant (Hirschwald in Schaffer, 1972).

However, many stones have saturation coefficients within the range of 0.66 to 0.77. In this range, the saturation coefficient gives an unreliable guide (BRE, 1983).

Saturation coefficient of the DTS1, DTS2, DBY, DFG and DKK are 0.72, 0.82, 0.41, 0.81 and 0.72 respectively. Samples have normal durability values.

3.3.3 WET TO DRY STRENGTH RATIO

Wet-to-Dry Strength Ratio; swelling and non-swelling clays in a stone tend to attract water when exposed to moisture. The strength of the stone can be reduced significantly due to the presence of moisture (Topal, 1995).

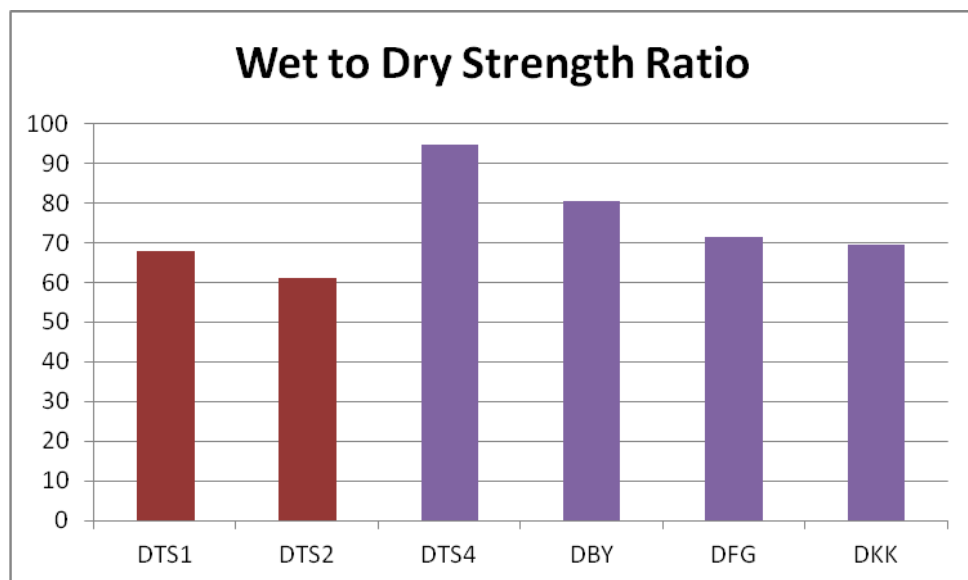


Figure 125. Wet to dry strength ratio of samples

The general stone qualities depending on the wet to dry strength ratios given by Winkler (1997) are as follows:

80-90 good and safe

70-80 further testing required

60-70 unsafe, for frost and hygric forces

< 60 very poor quality, clay present

DTS1, DTS2 and DFG, DKK have similar wet to dry strength ratios which are 61%, 61%, 71% and 69% respectively. They are all in unsafe category of Winkler. DTS4 has 95% w/d strength ratio which means it is excellent, DBY is in good and safe part with 81% wet to dry strength ratio.

CHAPTER 4

DISCUSSION

In this chapter, the field observations and laboratory test results are evaluated to better understand the proximity of ancient quarries in relation to the Apollon Smintheus Temple and the durability of those samples as building stone. Firstly Temple tuffs and then possible quarries are discussed.

Apollon Smintheus Temple Tuffs as building stone

Temple tuff is brownish gray vitric tuff. Mineralogically, it has quartz, plagioclase, biotite, pyroxene with amorphous and semi-amorphous crystals, and hypocrySTALLINE porphyritic textured volcanic rock fragments that are embedded within volcanic glass groundmass with flow pattern. The matrix includes Y shaped volcanic glass shards special for ignimbrite. It has also circular opaque minerals and microlithic porphyritic andesitic rock fragments in various dimensions.

In the XRD, it has quartz and feldspar as main elements. Biotite is the secondary mineral and amorphous phase being volcanic glass where hump is observed in basal reflections. Oriented peaks show smectite as the main clay mineral. SEM images also show smectite type with honeycomb structure.

Temple stones have high porosity and water absorption capacity, low bulk density and dry unit weight values which are 54 %, 41,15 %, 1,30 g/cm³ and 12,76 kN/m³ respectively. Their ultrasonic velocities are low because of the high porosity and

presence of cracks. Dry uniaxial compressive strength values of the temple tuffs are 3,80 MPa and 4,64 MPa. Saturated uniaxial compressive strength of them are 2,58 and 2,83 Mpa .

Temple tuffs have high porosity values by capillarity. They have high capillary coefficient; 10,50 and 12,30 $\text{kg/m}^2/\text{s}^{1/2}$, respectively. DTS1 has 2,23 and DTS2 has 1,68 $\text{kg/m}^2/\text{s}^{1/2}$ moisture absorption coefficients. DTS1 and DTS2 have similar wet to dry strength ratios that they are all in unsafe category of Winkler. DTS has 54% porosity in mesopores and a few micropores, Capillary absorption and moisture absorption coefficients are supporting the situation. The capillary coefficients of DTS, are 11.40, $\text{kg/m}^2/\text{s}^{1/2}$ that indicates mesopores. The moisture absorption coefficients of DTS, are 1.95, $\text{kg/m}^2/\text{s}^{1/2}$ indicating micropores.

Samples contain 63,20% and 64,50% SiO_2 , 17,80% and 17,30% Al_2O_3 . 3,29 % and 3,69% Fe_2O_3 values. Samples with low SiO_2 values have low strength values. Besides, samples having high Fe and L.O.I values have high strength values (Korkanc, 2007).

Cation Exchange Capacity value is 7,82 meq/100g. Clay mineral is the smectite which is found in samples using XRD. Low cation exchange capacity value implies low clay content. If it is assumed that other minerals did not adsorb the methylene blue dye, C.E.C. values showed that temple tuff has 5,2 - 9,8% smectite.

Saturation coefficients of the temple tuffs are 0,72 and 0,82. Samples have normal durability. Only DTS2 and DFG have slightly greater values than 0,8, indicating low durability “susceptible to frost activity” (Topal, 1995). However it can be regarded as durable because of that slight difference.

DTS4 of the bedrock of temple, has no pore in between 0,03 μm and 10 μm . It has more clay size pores (0,01 μm mostly). Coarser pores exist in around 200 μm . DTS4 has 18,01 MPa dry uniaxial compressive strength, and 17,08 MPa saturated uniaxial compressive strength. Thus, it has high w/d strength ratio, indicating that it has excellent durability. It is not schist that was stated before, it is a rock containing opal.

Examination of Possible quarries

Possible quarries are selected based on the regional geology and formations that have the quality of being used as building stones in around the study area. Quarry investigation studies are done in various methods besides the visual matching by color, texture, joint structure and stone extraction traces. Mineralogical and petrographical methods are supposed to compare / correlate the mineral structure of tuffs. Physical and physicommechanical experiments and artificial weathering tests are done to compare the durability properties of rocks. In this study, mineralogical, physical and physic-mechanical properties are discussed.

Microstructural properties of possible quarries and correlation between Temple stone

Fatma Gerdan Quarry (DFG) and Kızılkçeçili Quarry (DKK) samples have similar appearances with temple stone thin section images. Both of them show ignimbritic features with volcanic glass shards and matrix. Quartz and feldspar are the abundant minerals. Opaque minerals and volcanic rock fragments are also observed. Babakale Yolu (DBY) quarry sample includes sanidine phenocrysts.

Ratio of rock forming minerals and minerals in composition highly affect the unit weight. Therefore, existence and ratio of heavy minerals cause high unit weight (Erguvanli, 1975; Maharaj,2001; Korkanc,2007). Samples that have more fine grained crystal and groundmass than phenocrysts have higher unit weights. Babakale Yolu (DBY) quarry sample has higher unit weight value as it is expected.

In the cross section analyses, it is observed that; temple stones and quarry samples except Babakale Yolu (DBY) quarry sample show vitric tuff features with several rock fragments in it. Cement is consisting of volcanic glass and it has brown-gray color.

The X-Ray Diffraction (XRD) Analyses of all of the samples except Babakale Yolu (DBY) quarry sample, reveal the presence of quartz and feldspar as main minerals. DBY has sanidine as main mineral instead of quartz. Biotite is the secondary mineral and amorphous phase (volcanic glass) is observed. Temple tuff samples, DFG and DKK have all smectite peaks observed in unoriented XRD traces. Oriented XRD traces of samples show smectite as clay mineral except DBY which has illite. SEM images show smectite type honeycomb morphology in the samples, and also illite leafing may be observed.

XRF analysis was done in the Central Laboratory of METU. Samples include 63,20-66,70% SiO₂, 16,80- 19-30% Al₂O₃ and 0,49-0,57% TiO₂. Samples with low SiO₂ values have low strength values as well. Besides, samples having high Fe and L.O.I values have high strength values (Korkanc,2007). DBY has higher SiO₂ and higher strength values than the others.

Cation Exchange Capacity values are; DTS1: 7.82 mEq/100g, DBY: 10.16 mEq/100g, DFG: 17.20 mEq/100g, and DKK: 1.88 mEq/100g. If the rocks containing smectite are exposed to wetting and drying cycles, they crack in the dry period and swelling occurs in the wet period (Borchardt, 1989). Clay mineral is the smectite which is found in samples by XRD. Low cation exchange capacity value implies low clay content. If it is assumed that other minerals do not adsorb the methylene blue dye, cation exchange capacity values show that DTS1 has 5,2 - 9,8%, DFG has 6,8 - 12,7%, DKK has 11,5 - 21,5% and DBY has 1,3 - 2,4% smectite. DBY has the lowest clay content.

Mixed layering in clays is an adjustment to environment in either degradation or diagenesis. Due to the original weathering of igneous rocks; chlorite, smectite and mica interstratification is expected in humid climates (Carroll, 1970). Temple stones (DTS), Fatma Gerdan Quarry (DFG) and Kızılkeçili Quarry (DKK) had smectite as can be seen in XRD, SEM and FTIR results. Smectite includes average three Al atoms to every Fe atom (Dixon and Weed, 1989). XRF results support the assertion with one to five proportions. Babakale Yolu Quarry (DBY) has illite and chlorite according to XRD, and chlorite can be seen from the thin section as well. Illite can be seen from FTIR and SEM analyses.

Fatma Gerdan (DFG) and Kızılkeçili (DKK) quarry sample resemble temple stones in their mineralogical and petrographical properties.

Physical and physico-mechanical properties of stones from possible quarries and correlation between temple stone

In the engineering geology part of the study, effective porosity and unit weight, water absorption under atmospheric pressure, color measurements, capillary absorption, moisture absorption, qualitative analysis of the soluble salts by spot tests, uniaxial compressive strength, ultrasonic pulse velocity and pore size distribution are measured on the temple samples and quarry samples before and after salt crystallization and wetting drying cycles.

Fatma Gerdan (DFG) and Kızılkeçili (DKK) quarry samples have high porosity and water absorption capacity, low bulk density and dry unit weight values. Babakale Yolu (DBY) quarry samples have relatively low porosity and water absorption capacity, high bulk density and dry unit weight values.

The proportions of rock fragments and minerals in composition affect the unit weight of stone. Heavy minerals occurrences caused high unit weight value (Erguvanlı, 1975; Korkanç, 2007). In this study, samples that have high ratio of fine grained crystal have high unit weight values e.g DBY. The increase in the porosity caused to decrease the durability against atmospheric effects. Also the porosity increase caused lower density and lower ultrasonic velocity values. Samples that have high ratio of fine grained crystal have low porosity value.

Color measurement result of Temple samples (DTS1, DTS2) and Fatma Gerdan (DFG) and Kızılkeçili (DKK) quarries samples are similar in L, a and b values. Babakale Yolu (DBY) quarry sample has close results as well. After salt crystallization cycle, the L-a-b values slightly change; there is no significant change after wetting drying cycles.

There is not remarkable percent of salt in the stone samples according to the results of spot tests.

Uniaxial compressive strength of the Temple samples (DTS1, DTS2), Fatma Gerdan (DFG) and Kızılkeçili (DKK) quarries samples are low in comparison to Babakale Yolu (DBY) quarry samples. They have nearly the same values. The decrease in strength values after salt crystallization cycles is higher than the ones after wetting drying cycle.

Ultrasonic velocity results are similar and rather low except Babakale Yolu (DBY) quarry samples. Their low velocities are mainly because of their high porosity. After cyclic weathering tests, the values gently decrease as a result of increase in porosity.

Pore size distributions of samples show that, the pore sizes between 8 and 50 μm are in larger amounts in Temple tuff (DTS1) and it has mostly 15 μm pore size, 0,02 - 0,05 μm size pores indicating the clayey parts. Fatma Gerdan (DFG) quarry sample has mostly 7-8 μm pore sizes and it has small size pores between 0,006 and 0,1 μm . Kızılkeçili (DKK) quarry sample has pores around 4 μm diameter and very small pores also exist. DBY doesn't have finer pores. It has larger pores in between 20 and 100 μm . After 3rd salt crystallization cycle, clay size pores decrease, pores around 10 μm increases in Fatma Gerdan (DFG) quarry sample. Small pores and pores smaller than 0,6 μm doesn't exist anymore. 6 μm – 20 μm pores increases in Kızılkeçili (DKK) quarry sample. Since the Temple sample is weathered more than the quarry samples, the results of DFG and DKK after salt crystallization cycles are considered to be showing the change in the pore sizes by weathering. DTS4 has small pores mostly.

Capillary absorption and moisture capillary absorption coefficients are in agreement with the pore size distribution characteristics of stones. The capillary coefficients of DTS, DFG and DKK are 11.40, 9.12 and 11.43 $\text{kg/m}^2/\text{s}^{1/2}$, respectively. These indicate mesopores. The moisture absorption coefficients of DTS, DFG and DKK were 1.95, 2.04 and 2.32 $\text{kg/m}^2/\text{s}^{1/2}$ respectively. The moisture absorption of DBY is low indicating less finest micropores. Salt crystallization cycles give damage to samples by increasing porosity and decreasing strength and durability. On the other hand, since the material is so low in strength after salt crystallization cycles, mercury with high pressure might destroy and pore size distribution may not be followed by mercury porosimetry. Because micropore increase causes durability decrease and salt

crystallization cycle reduces the durability, increase in micropores after cycle is predicted. An actual reflection of pore size distribution may not be got by mercury porosimetry (Robertson, 1982).

Ultrasonic velocity values are close to each other except DBY which has 1813 m/s ultrasonic pulse velocity. UPV values of dry samples for DTS1, DTS2, DFG and DKK are 1011,74 m/s, 1279,34 m/s, 1102, 97 ± 226 m/s and 1021,37 ± 250 m/s, respectively. Saturated Ultrasonic Pulse Velocity values decrease a bit but with the same ratio. The values are 899,74 m/s, 1106,54 m/s, 975, 03 m/s and 914,19 m/s, respectively.

Modulus of Elasticity values are in the same trend as the ones of ultrasonic velocity. The values of samples in the same order above are ; 1,42 GPa, 1,83 GPa, 7,56 GPa, 1,41 GPa and 1,41 GPa, respectively.

Ultrasonic Pulse Velocity values of DBY, DFG and DKK decrease after salt crystallization cycles. The changes are; 1813 m/s to 1767 m/s, 1083 m/s to 988 m/s and 942 m/s to 908 m/s, respectively. DKK and DFG show the same trend. UPV values also decrease after wetting drying cycles. DBY velocity decreases from 1815 m/s to 1642 m/s. DFG decreases from 1083 m/s to 924 m/s and velocity of DKK decreases from 942 m/s to 917 m/s. Ultrasonic velocity changes from salt crystallization and wetting-drying cycle are close to each other.

Saturation coefficient of the DBY, DFG and DKK were 0.41, 0.81 and 0.72, respectively. Samples have normal durability. Although DFG have slightly greater values than 0,8 (indicating low durability), it can be accepted as durable.

Temple tuff samples, DFG, and DKK have similar wet to dry (w/d) strength ratios that they are all in unsafe category of Winkler. DTS4 has highest w/d strength ratio as excellent; DBY is in good and safe part.

Durability of samples are also tested with a geological hammer. According to scale of rock hardness (Panama Canal Company, 1959) Babakale Yolu quarry sample (DBY) is in *RH2 Medium hard* category that it could be picked with moderate blows of geology hammer and could be cut with knife. Temple Stones (DTS), Fatma

Gerdan quarry sample (DFG) and Kızılkeçili quarry sample (DKK) are in between *RHI Soft* - slightly harder than very-hard overburden, rocklike character but crumbled or broke easily by hand - and *RHI Medium soft* – could not be crumbled between fingers, but could be easily picked with light blows of the geology hammer - classes.

After Coates (1964) classification of rocks for rock mechanics; uniaxial compressive strength (UCS) values less than 5000 psi (34,5 MPa) are accepted as *weak* thus all of the samples are weak rock according to their UCS.

According to the rock classification chart (John, 1962) based on joint spacing and weathering DBY is regarded as *sound* and DTS, DFG and DKK are admitted as *weak, decomposed and weathered stones*.

Onodera (1963) presented a classification which correlated the degree of jointing and weathering with the seismic or "soundness" ratio. This procedure included both the properties of the rock material as well as the discontinuities. Descriptive geological diagnostics are also given by Onodera in which the rock is graded from excellent to bad, and assigned alphabetical symbols from A to E, respectively. Samples except DBY are in between *D* and *E*.

The durability assessments of the Apollon Smintheus tuff, Fatma Gerdan tuff and Kızılkeçili tuff using the average pore diameter, the wet-to-dry strength ratio show unsafe category. The saturation coefficient demonstrates sufficient ratio but close to frost susceptibility. Based on the field observations, the three tuffs might also be considered to be of poor durability.

Considering that the engineering properties of the discontinuities are adversely affected by the water, a stable block might become potentially unstable during winter and spring seasons since moisture reduces the shear strength parameters along the discontinuities. Water also reduces the strength of the tuff. This reduction ranges between 29% and 39%. For now, these values are not threatening but increase in strength reduction may definitely create structural problems.

The evaluation of the variations of the physical and mechanical properties of the tuff after ageing tests reveals that all are useful for the assessment of the deterioration of the tuff samples. Chiefly, uniaxial compressive strength and ultrasonic pulse velocities should be used in all studies related to tuff because the inner damage to the rock can be best determined by those values. Based on the ageing test results, salt crystallization is the most effective environmental factor producing deterioration in the tuff. The wetting-drying process is the next effective environmental factor. The adverse effect of water on the samples is obviously seen. Presence of clay minerals in the microstructure of the tuffs, their swelling and contraction during wetting-drying cycles might have caused the disintegration of tuff samples after eight and twenty eight cycles of wetting- drying. Smectite-type clay minerals which are the product of chemical weathering in the volcanic glass of the tuff, swell upon wetting and shrink upon drying. Therefore, for the conservation purpose, the direct contact of the tuff with water of any source should be avoided.

Fatma Gerdan (DFG) and Kızılköçü (DKK) quarry samples resemble the Temple stones in their engineering geological properties. Engineering properties of those two quarries and Temple stones do not show higher values, but they are appropriate as building stone under shelter.

CHAPTER 5

CONCLUSION

Apollon Smintheus Temple tuff is brownish gray vitric tuff having very high porosity and very low unit weight. Quartz, feldspar, biotite, volcanic glass and clay mineral smectite are observed in its thin sections, supported by XRD, SEM and FTIR and XRF analyses. Pore size distribution and moisture capillary absorption analyses demonstrated the micropores existence in the tuff. Durability of Apollon Smintheus Temple tuff having high capillary suction, low uniaxial compressive strength and modulus of elasticity is evaluated as *moderately weak* and *weak* in relation to rock mechanics standards.

Uniaxial compressive strength of the main rock (DTS4) has high to very high wet to dry strength ratio that shows the rock's excellent durability.

Fatma Gerdan Quarry (DFG) and Kızılkeçili Quarry (DKK) samples have similar properties with the Temple stone. They are also brownish gray vitric tuff having very high porosity and very low unit weight. Quartz, feldspar, volcanic glass and clay mineral smectite of Temple tuff are observed in their thin sections, XRD, SEM, FTIR and XRF analyses, as well. Fresh quarry samples of Fatma Gerdan and Kızılkeçili do not have high petrophysical values but especially Kızılkeçili quarry sample DKK can not resist to artificial weathering tests. Although salt crystallization is the most destructive cycle, the samples are also highly affected by wetting drying cycles. It is due to the presence of swelling clay smectite in them. Smectite which is the alteration product of volcanic glass causes disintegration of tuffs. Fatma Gerdan Quarry (DFG) and Kızılkeçili Quarry (DKK) tuffs having high capillary suction, low uniaxial compressive strength and modulus of elasticity are evaluated as *moderately*

weak and *weak* in relation to rock mechanics standards as Apollon Sminthues Temple tuffs.

Babakale Yolu (DBY) quarry tuff is gray latitic tuff having lower porosity and higher unit weight. It consists of sanidine, feldspar, biotite, chlorite and volcanic glass and clay mineral illite which can be observed in thin section, XRD, SEM, FTIR and XRF analyses. DBY having high physico-mechanical properties is resistant to salt crystallization and wetting drying cycles. It is due to the presence of non-swelling clay mineral illite and welding features of that tuff. Babakale Yolu (DBY) quarry tuff having low capillary suction, high uniaxial compressive strength and modulus of elasticity was evaluated as *medium* strength in relation to rock mechanics standards unlike the Apollon Sminthues Temple tuffs.

Considering that the engineering properties of the discontinuities are adversely affected by the water, the stable block might become potentially unstable during winter and spring seasons since moisture reduced the shear strength parameters along the discontinuities. Water also reduces the strength of the tuff. That reduction ranges between 29% and 39%. For now, these values are not threatening but increase in strength reduction may definitely create structural problems.

The evaluation of the variations of the physical and mechanical properties of the tuff after ageing tests reveal that all those physical and physico-mechanical properties of the tuff are useful for the assessment of deterioration of the tuff samples. Mainly, uniaxial compressive strength and ultrasonic pulse velocities should be used in all studies related to tuff because the inner damage to the rock can be best determined by those values. Based on the ageing test results, salt crystallization is the most effective environmental factor producing deterioration in the tuff. The wetting-drying process is the next effective environmental factor. The adverse effect of water on the samples is obviously seen. Presence of clay minerals in the microstructure of the tuffs, their swelling and contraction during wetting-drying cycles might have caused the disintegration of tuff samples after eight and twenty eight cycles of wetting- drying. Smectite-type clay minerals swell considerably upon wetting and shrink upon drying. Therefore, for the conservation purpose, the direct contact of the tuff with water of any source should be avoided.

Fatma Gerdan (DFG) and Kızılkeçili (DKK) quarry tuffs resemble Temple stones in the engineering geological properties. With regard of their engineering properties two quarries and Temple stones do not show high values, but they are appropriate as building stones to be used under shelter from rainwater.

Further investigations may focus on the field studies. The geological formation can be examined in detail for discontinuities, joints, cracks and other tuff formations as well. Future physical and physico-mechanical analyses may be done to compare the performance of stones.

.

REFERENCES

Bell, F.G., 1990, "Engineering geology and building stones of historical monuments: Construction materials; Geological origin; Quarries", Engineering geology of ancient works, monuments and historical sites, ed. Marinos & Koukis, Rotterdam, p 1867.

Bianchetti, P.L., Lombardi, G., Meucci, G., 1982, "Study of the Degradation of Tuff Blocks used in the Roman Temple of Cibele (Rome, Italy)", Fourth International Congress on Deterioration and Preservation of Stone, California, pp 29-38.

Bower, C.A., Wilcox, L.V., 1965, Soluble salts, In Black C.A. (ed). Methods of soil analysis, Part 2, Agronomy 9, Amer. Soc. of Agron., pp 933-951.

Borchardt, G., 1989, Smectites, Ch. 14, In: J. B. Dixon and S. B. Weed (ed.), Minerals in Soil Environments, 2nd Ed. SSSAJ Special Publication No: 1, p. 675-727.

BRE, 1983, The selection of natural building stone, Building Research Establishment Digest 269, Linneys of Mansfield, UK.

Broch, E., Franklin, J. A., 1972, "The Point Load Strength Test", International Journal of Rock Mechanics and Mining Science, Vol. 9, pp. 669-697.

Brandi, C., 1977, Theory of Restoration, ed. Basile, G., trans. Rockwell, C., Istituto Centrale Per Il Restauro, p51.

Capedri, S., Venturelli, G., Grandi, R., 2000, "Euganean trachytes: discrimination of quarried sites by petrographic and chemical parameters and by magnetic susceptibility and its bearing on the provenance of stones of ancient artifacts", Journal of Cultural Heritage, Vol.1, Number 4, pp, 341-364.

Calcaterra, D., Cappelletti, P., Langella, A., Morra, V., Colella, A., Gennaro, R., 2000, "The building stones of the ancient centre of Naples (Italy): Piperno from Campi Flegrei. A contribution to the knowledge of a long-time-used stone", Journal of Cultural Heritage, Vol. 1, pp. 415-427.

Caner-Saltık, E., Yaşar, T., Topal, T., Tavukçuoğlu, A., Akoğlu, G., Güney, A., 2006, "Ancient andesite quarries of Ankara", 1st Symposium on Conservation of Ancient Stone Quarry Landscapes in the Eastern Mediterranean, p 17.

Caner-Saltık, E., Yaşar, T., Topal, T., Tavukçuoğlu, A., Akoğlu, G., Güney, A., Üstünkaya, M.C., 2007, "Ancient Tuff Quarry in Aksaray", 2nd Symposium on Conservation of Ancient Stone Quarry Landscapes in the Eastern Mediterranean, Petra, JORDAN, p 20.

Caner-Saltık, E., Demirci, Ş., Türkmenoğlu, A.G., Özgenoğlu, A., Göktürk, H., Özer, A., Böke, H., İnalpulat, E., 1993, "Examination of surface deterioration of Göreme tuffs for the purpose of conservation", The Safeguard of the rock-hewn Churches of the Göreme Valley Proceedings of an International Seminar Ürgüp, Cappadocia, Turkey, pp 85-94.

Caner-Saltık, E.N., Schumann, I., Franke, L., 1998, "Stages of Damage in the Structure of Brick Due to Salt Crystallization", Conservation of Historic Brick Structures Case Studies and Reports of Research Donhead Publishing Ltd, ed. by; Baer, N.S., Fitz, S., Livingston, R.A. pp.47-58

Carroll, D., 1970, Clay Minerals: A Guide to Their X-Ray Identification, The Geological Society of America, p 37.

Church, T., 1994, Lithic Resource Studies: A Source for Archaeologists. Special Publication Number 3, Lithic Technology. Department of Anthropology, University of Tulsa, Tulsa.

Coates, D.F., 1964, "Classification of Rocks for Rock Mechanics," International Journal of Rock Mechanics and Mining Sciences, Vol. 1, No. 3, p 421.

Cook, J.M., The Troad, An Archaeological and Topographical Study, Oxford, 1973, p 227.

Çoğulu, E., 1973, Petrografi ve Petroloji, İ.T.Ü Mühendislik-Mimarlık Fakültesi Yayınları: 94, pp 191, 192.

D'Arienzo, L., Scarfato, P., Incarnato, L., 2008, "New polymeric nanocomposites for improving the protective and consolidating efficiency of tuff stone", *Journal of Cultural Heritage*, Vol. 9, pp.253-260.

Deere, D.U., Miller, R.P., 1966, *Engineering Classification and Index Properties for Intact Rock*, Technical Report No. AFWL-TR-65-116, pp 7,38,46.

Dessandier, D., Bromblet, P., Mertz, J.D., 2000, "Durability of Tuffeau Stone in Buildings: Influence of Mineralogical Composition and Microstructural Properties", 9th International Congress on Deterioration and Conservation of Stone, Venice, pp.69-79.

Dixon, J.B., Weed, S.B., 1989, *Minerals in Soil Environments* 2nd ed., Soil Science Society of America, pp 684-687.

Dönmez, M., Akçay, A.E., Genç, Ş.C., Acar, Ş., 2005, "Middle-Upper Eocene Volcanism and marine ignimbrites of Biga Peninsula", *J. Min. Res. Expl. Inst. Turk.*, vol. 131, pp 49-61.

Dreesen, R., Duser, M., 2004, "Historical building stones in the province of Limburg (NE Belgium): role of petrography in provenance and durability assessment", *Materials Characterization*, vol. 53, pp. 273– 287.

Duru, M., Pehlivan, Ş., Ilgar, A., Dönmez, M., Akçay, A.E., 2007, *Türkiye Jeoloji Haritaları, Ayvalık İ17 Paftası*, No: 98, Maden Tetkik Arama Genel Müdürlüğü, pp. 1-21.

Ferretti, M., Cesareo, R. and Marabelli, M., 1982, *Analysis of Silver Objects by Scattering and by X-ray Florescence of Monoenergetic Gamma-rays*, *Archaeometry*, Vol.24, p. 170.

Flint, L.E., Selker, J.S., 2003, "Use of porosity to estimate hydraulic properties of volcanic tuffs", *Advances in Water Resources*, vol. 26, pp. 561–571.

Fookes P.G., Dearman W.R. and Franklin J. A., 1971, "Some Engineering Aspects of Rock Weathering", *Quarterly Journal of Engineering Geology*, Vol. 4, pp. 139-185.

Franklin, J.A., Chandra, R., 1972, "The Slake Durability Test", *Int. Journal of Rock Mech. Min. Sci.*, pp. 325- 341.

Geisweid, J., Schaaff, H., 2011, "Volcanic Origin And Emplacement of The East Eifel Tuff and Its Distribution as a Building Material Since Roman Times", Geophysical Research Abstracts, Vol. 13, p 4678.

Gökçe, F., 2000, Çanakkale-Gülpınar Apollon Smintheus Tapınağı Mimarisi, Unpublished Phd Thesis, Ankara, pp. 27,36,37.

Graue, B., Siegesmund, S., Middendorf, B., 2011, "Quality assessment of replacement stones for the Cologne Cathedral: mineralogical and petrophysical requirements", Environmental Earth Sciences, vol. 63, pp 1799-1822.

Gülpınar Apollon Smintheion Excavation Report, 2007, p 35.

Hasol, D., 2005, Ansiklopedik Mimarlık Sözlüğü, 9th ed., Yapı Yayın, pp 109, 234, 379.

Heiken, G., 2006, Tuffs: their properties, uses, hydrology, and resources, The Geological Society of America, Special Paper 408, pp 1-16.

İlgar, A., Sezen Demirci, E., Dönmez, M., Akçay, A.E., Duru, M., Pehlivan, Ş., 2008, Türkiye Jeoloji Haritaları, Ayvalık İ16 ve J16 Paftaları, No: 99, Maden Tetkik Arama Genel Müdürlüğü, pp. 1-28.

ICAHM, 1990, Charter For The Protection And Management Of The Archaeological Heritage, p 3.

ICOMOS, 2005, Xi'an Declaration On The Conservation Of The Setting Of Heritage Structures, Sites And Areas, p 2.

John, K.W., 1962, "An Approach to Rock Mechanics," Journal of the Soil Mechanics and Foundations Division, Proceedings of the American Society of Civil Engineers, Vol. 88, r SM4, Part 1, p. 12.

Johnson, P.R., Pearl, F.B., Eckert, S. L., James, W.D., 2007, "INAA of pre-contact basalt quarries on the Samoan Island of Tutuila: a preliminary baseline for an artifact-centered provenance study", Journal of Archaeological Science, Vol.34, pp.1078-1086.

Kaplan, D., 2009, "Smintheion'da Kullanılan Yapı Malzemeleri-I", Unpublished article, pp 12-18.

Korkanç, M., 2007, "The effect of geomechanical properties of ignimbrites on their usage as building stone: nevsehir stone", *Jeoloji Mühendisliği Dergisi*, Vol.31, pp. 53-57.

Langella, A., Calcaterra, D., Cappelletti, P., Colella, A., Gennaro M., Gennaro, R., 2000, "Preliminary Contribution on durability of some macroporous Monumental Stones used in historical towns of Campania Region, Southern Italy", 9th International Congress on Deterioration and Conservation of Stone, Venice, pp.59-67.

Large, N.A., 1967, *Handbook of Chemistry*, McGraw Hill Book Company, p 368.

Larsen, T.D., Cady, P.D., 1969, "Identification of frost susceptible particles in concrete aggregates", National Cooperative Research Program, Rep. 66, Highway Research Board, Washington DC.

Lechevalier, J.B., 1799, *Voyage dans la Troade, ou tableau de la plaine de Troie dans son état actuel*, Paris, Laran, p 21.

Madejová, J., 2003, "FTIR techniques in clay mineral studies", *Vibrational Spectroscopy*, vol. 31, pp 1-10.

METU, 1987, "Investigation of the mechanisms of stone deterioration for the purpose of conservation of Göreme tuffs", Progress Report.

McMillan, E.E., Hofmeister, A.M., 1988, *Spectroscopic Methods in Mineralogy and Geology*, in *Infrared and Raman Spectroscopy, Reviews in Mineralogy*, vol. 18, EC. Hawthorne, ed., Mineralogical Society of America, Washington, D.C., pp. 99-159.

Newton, C.T., 1887, *Ant. of Ionia IV*, London, p 178.

Nicol, A.W., 1975, *X-Ray Diffraction*, In *Physicochemical Methods of Mineral Analysis*, New York: Plenum Press, p. 320.

Onodera, T.F., 1963, "Dynamic Investigation of Foundation Rocks In Situ," Proceedings of the Fifth Symposium on Rock Mechanics, The Macmillan Company, New York, p. 517.

Öngür, T., 1973, Çanakkale-Tuzla yöresinin volkanolojisi ve jeotermal enerji olanakları: MTA Report., Ankara, pp 15.

Özgünel, C., 2001, Smintheion- Troas'ta bir Kutsal Alan, T.C. Kültür Bakanlığı Anıtlar ve Müzeler Genel Müdürlüğü, Ankara, pp 13-269.

Panama Canal Company, 1959, Geological Logs of Drill Holes for Construction of Balboa Bridge, Substructure, Canal Zone, Balboa Heights, April.

Paterno, M.C., Charola, A.E., 2000, "Preliminary studies for the consolidation of Guadalupe tuff from the Philippines", 9th International Congress on Deterioration and Conservation of Stone, Venice, pp.155-164.

Rabinowitch, E., Epstein, L.F., 1941, "Polymerization of dye stuffs in solution-Thionine and methylene blue", Journal of American Chemical Society, p 63.

Ramasamy, V., Anandalakshmi, K., 2008, " The determination of kaolinite clay content in limestones of western Tamil nadu by methylene blue adsorption using UV-vis spectroscopy", Spectrochimica Acta Part A, Vol, 70, pp 25-29.

Ramseyer, K., Decrouez, D., Rosenthaler, L., 2006, "Provenance determination of white marble used in antiquity: from quarry to artifact", Geophysical Research Abstracts, Vol. 8.

Rapp, G.R., 2002, Archaeomineralogy, Springer-Verlag, Berlin- Heidelberg- New York, p 44.

RILEM, 1980, Recommended tests to measure the deterioration of stone and to assess the effectiveness of treatment methods, Commission 25-PEM, Mater. Struct. 13 pp 175–253.

Schaffer, R.J., 1932, The weathering of natural building stones, Department of Scientific and Industrial Research Building Research, Special report No. 18, London, p 52.

Scherer, G.W., 1999, "Crystallization in pores", *Cement and Concrete Research*, vol.29, pp.1347-1358.

Spratt, R.N., 1856, *On the Site of the Temple of Apollo Smintheus*, *Transactions of the Royal Society of Literature of the United Kingdom, Second Series* vol.5, London, p 236.

Steindlberger, E., 2004, "Volcanic tuffs from Hesse (Germany) and their weathering behavior", *Environmental Geology*, Vol.47, pp.378-390.

Šťastná, A., Přikryl, R., Jehlička, J., 2008, "Methodology of analytical study for provenance determination of calcitic, calcite-dolomitic and impure marbles from historical quarries in the Czech Republic", *Journal of Cultural Heritage*, vol.10, pp 82-93.

Timoshenko, S., 1970, *Strength of Materials*, in: Chapter II, *Analysis of Stress and Strain*, Von Nostrend Reinhold Co., Holland p.53

Topal, T., 1995, *Formation and deterioration of fairy chimneys of the Kavak tuff in Ürgüp-Göreme area*, Phd Thesis, METU, Ankara.

Topal, T., Doyuran, V., 1997, "Engineering geological properties and durability assessment of the Cappadocian tuff", *Engineering Geology*, Vol.47, pp.175-187.

Topal, T., Doyuran, V., Türkmenoğlu, A.G., 1993, "Effect of deterioration on the chemical and physical properties of Göreme tuffs", *The Safeguard of the rock-hewn Churches of the Göreme Valley Proceedings of an International Seminar Ürgüp, Cappadocia, Turkey*, pp 95-107.

Topal, T., Sözmen, B., 2003, "Deterioration mechanisms of tuffs in Midas monument", *Engineering Geology*, Vol. 68, pp. 201–223.

Topal, T., Toprak, V., Caner-Saltık, E.N., Türkmenoğlu, A.G., Tavukçuoğlu, A., Yaşar, T., Akoğlu, K. G., Güney, A., Üstünkaya, M. C., 2007, "Roman Marble Quarries of Ankara Region", *2nd Symposium on Conservation of Ancient Stone Quarry Landscapes in the Eastern Mediterranean 17-21 October 2007, Petra, JORDAN*.

Vacchiano, C.D., Incarnato, L., Scarfato, P., Acierno, D., 2008, "Conservation of tuff-stone with polymeric resins", *Construction and Building Materials*, Vol. 22 , pp 855–865.

Vacchiano, C.D., 2006, *Renovation of ancient buildings in the historic centre of Salerno: decay analysis and materials compatibility*, PhD thesis, Università Degli Studi di Salerno, Italy, pp 10-130.

Vitruvius, 2005, trans. S. Güven, *Mimarlık Üzerine On Kitap*, Şevki Vanlı Mimarlık Vakfı Mimarlığın Uluslararası Kaynakları: 14th ed., p 35

Weaver, M.E., 1993, "Reviewing Structural Conservation measures for heritage resources in rock", In: *The safeguard of the rock-hewn churches of the Göreme Valley Proceedings of an International Seminar*, ICCROM, p 152.

Weber, H., 1966, *Zum Apollon- Smintheus- Tempel in der Troas*, *IstMitt*, 16, p 100.

Williams, H., Turner, F.J., Gilbert, C.M., *Petrography An Introduction to the study of rocks in thin sections*, W. H. Freeman and Company, san Francisco, pp 146-156.

Winkler, E.M., 1997, *Stone in Architecture: properties, durability*, Berlin, New York, Springer-Verlag, p 327.

Wyszecki, G., Stiles, W.S., 1982, *Color science - concepts and methods, quantitative data and formula*, 2 ed., New York: John Wiley & Sons

Zedef, V., Kocak, K., Doyen, A., Özsen, H., Kekec, B., 2007, "Effect of salt crystallization on stones of historical buildings and monuments, Konya, Central Turkey", *Building and Environment*, Vol. 42, pp.1453-1457.

APPENDIX A

DENSITY – POROSITY- WATER ABSORPTION CAPACITY

SALT CRYSTALLIZATION CYCLE

Table 21. Physical properties of samples at the beginning

0th cycle	P(%)	D (g/cm ³)	WAC (%)	Real D	Sat. Coef	Dry unit weight	Sat. Unit weight
DBY	16±2,15	2,47±0,17	6,48±0,85	2,95±0,23	0,4±0,03	24,24±1,62	25,69±1,70
DFG	48±4,12	1,24±0,08	38,39±2,85	2,40±0,35	0,8±0,05	12,18±0,80	16,72±1,09
DKK	45±5,31	1,40±0,14	32,39±5,36	2,58±0,41	0,7±0,07	13,78±1,36	17,91±1,42

Table 22. Physical properties of samples after 2nd cycle of salt crystallization

2nd cycle	P (%)	D (g/cm ³)	WAC (%)	Real D	Sat. Coef	Dry unit weight	Sat. Unit weight
DBY	18±1,46	2,54±0,05	7,24±0,50	3,11±0,11	0,4±0,01	24,90±0,54	26,71±0,63
DFG	64±12,99	1,26±0,28	50,66±3,46	4,68±4,35	0,8±0,14	12,37±2,78	18,61±4,02
DKK	54±7,38	1,26±0,08	43,01±8,75	2,74±0,26	0,8±0,05	12,35±0,38	17,62±0,10

Table 23. Physical properties of samples after 3rd cycle of salt crystallization

3rd cycle	P (%)	D (g/cm ³)	WAC (%)	Real D	Sat. Coef	Dry unit weight	Sat. Unit weight
DBY	19±1,97	2,54±0,21	7,37±0,56	3,13±0,11	0,4±0,01	24,89±2,06	26,73±2,20
DFG	53±9,13	1,15±0,02	45,71±8,46	2,52±4,35	0,9±0,14	11,29±0,20	16,45±0,81
DKK	36±1,38	1,38±0,01	25,87±1,24	2,15±0,26	0,7±0,05	13,53±0,14	17,03±0,07

Table 24. Physical properties of samples after 4th cycle of salt crystallization

4th cycle	P (%)	D (g/cm3)	WAC (%)	Real D	Sat. Coef	Dry unit weight	Sat. Unit weight
DBY	20±1,50	2,45±0,09	8,17±0,85	3,06±0,09	0,4±0,02	24,05±0,93	26,01±0,84
DFG	51±5,21	121±0,08	42,12±5,29	2,49±40,35	0,8±0,06	11,89±0,83	16,88±0,97

Table 25. Physical properties of samples after 6th cycle of salt crystallization

6th cycle	P (%)	D (g/cm3)	WAC (%)	Real D	Sat. Coef	Dry unit weight	Sat. Unit weight
DBY	21±0,19	2,31±0,05	9,09±0,11	2,92±0,07	0,4±0,01	22,61±0,49	24,67±0,51

WETTING DRYING CYCLE

Table 26. Physical properties of samples at the beginning

0th cycle	P(%)	D (g/cm3)	WAC (%)	Real D	Sat. Coef	Dry unit weight	Sat. Unit weight
DBY	16±2,15	2,47±0,17	6,48±0,85	2,95±0,23	0,4±0,03	24,24±1,62	25,69±1,70
DFG	48±4,12	1,24±0,08	38,39±2,85	2,40±0,35	0,8±0,05	12,18±0,80	16,72±1,09
DKK	45±5,31	1,40±0,14	32,39±5,36	2,58±0,41	0,7±0,07	13,78±1,36	17,91±1,42

Table 27. Physical properties of samples after 3rd cycle of wetting drying

3rd cycle	P(%)	D (g/cm3)	WAC (%)	Real D	Sat. Coef	Dry unit weight	Sat. Unit weight
DBY	17,83±2	2,55±0,09	7,01±1	3,11±0,04	0,39±0,01	25,03±0,86	26,78±0,68
DFG	47,71±3	1,20±0,01	39,64±2,37	2,31±0,12	0,83±0	11,80±0,05	16,48±0,25
DKK	50,26±2	1,34±0,14	37,81±4,42	2,70±0,31	0,75±0,08	13,13±1,37	18,06±1,39

Table 28. Physical properties of samples after 4th cycle of wetting drying

4th cycle	P(%)	D (g/cm3)	WAC (%)	Real D	Sat. Coef	Dry unit weight	Sat. Unit weight
DBY	18,00±2	2,45±0,18	7,37±0,93	2,99±0,22	0,41±0,03	24,03±1,75	25,80±1,74
DFG	45,52±3	1,10±0,05	41,58±2,73	2,02±0,15	0,91±0,04	10,75±0,50	15,21±0,60
DKK	52,49±7	1,11±0,04	47,21±6,46	2,38±0,36	0,90±0,04	10,92±0,44	16,07±0,74

Table 29. Physical properties of samples after 6th cycle of wetting drying

6th cycle	P (%)	D (g/cm3)	WAC (%)	Real D	Sat. Coef	Dry unit weight	Sat. Unit weight
DBY	19,83±1	2,53±0,15	7,84±0,25	3,16±0,22	0,40±0,02	24,79±1,50	26,73±1,58
DFG	51,25±4	1,25±0,19	41,13±5,50	2,59±0,49	0,80±0,1	12,23±1,89	17,26±1,98
DKK	51,57±6	1,40±0,10	36,84±2,08	2,93±0,55	0,71±0,05	13,70±1,01	18,76±1,60

Table 30. Physical properties of samples after 8th cycle of wetting drying

8th cycle	P (%)	D (g/cm3)	WAC (%)	Real D	Sat. Coef	Dry unit weight	Sat. Unit weight
DBY	19,55±1	2,54±0,12	7,68±0,30	3,16±0,17	0,39±0,02	24,94±1,20	27,42±1,25
DFG	50,66±4	1,27±0,17	40,02±5,39	2,59±0,43	0,79±0,09	12,42±1,70	18,75±1,74
DKK	53,32±8	1,31±0,16	40,69±3,17	2,88±0,75	0,76±0,09	12,85±1,63	18,08±2,29

Table 31. Physical properties of samples after 10th cycle of wetting drying

10th cycle	P (%)	D (g/cm3)	WAC (%)	Real D	Sat. Coef	Dry unit weight	Sat. Unit weight
DBY	18,18±1	2,34±0,11	7,76±0,42	2,86±0,15	0,43±0,02	22,96±1,15	24,75±1,16
DFG	56,55±8	1,37±0,12	41,14±2,36	3,24±0,99	0,73±0,07	13,45±1,26	19,00±2,08

Table 32. Physical properties of samples after 12th cycle of wetting drying

12th cycle	P (%)	D (g/cm3)	WAC (%)	Real D	Sat. Coef	Dry unit weight	Sat. Unit weight
DBY	18,85±1	2,34±0,12	8,06±0,16	2,88±0,20	0,43±0,02	22,92±1,23	24,77±1,36
DFG	56,72±7	1,37±0,12	41,38±1,99	3,24±0,76	0,73±0,06	13,41±1,13	18,97±1,13

Table 33. Physical properties of samples after 14th cycle of wetting drying

14th cycle	P (%)	D (g/cm3)	WAC (%)	Real D	Sat. Coef	Dry unit weight	Sat. Unit weight
DBY	20,25±1	2,34±0,01	8,66±0,58	2,93±0,04	0,43±0	22,93±0,07	24,91±0,06
DFG	48,24±2	1,16±0,04	41,81±3,06	2,23±0,02	0,87±0,03	11,33±0,37	16,07±0,20

Table 34. Physical properties of samples after 16th cycle of wetting drying

16th cycle	P (%)	D (g/cm ³)	WAC (%)	Real D	Sat. Coef	Dry unit weight	Sat. Unit weight
DBY	19,15±1,28	2,33±0,06	8,23±0,78	2,88±0,03	0,43±0,01	22,85±0,62	24,73±0,49
DFG	48,71±2,59	1,16±0,02	42,05±3,06	2,26±0,07	0,86±0,02	11,37±0,23	16,15±0,05

Table 35. Physical properties of samples after 18th cycle of wetting drying

18th cycle	P (%)	D (g/cm ³)	WAC (%)	Real D	Sat. Coef	Dry unit weight	Sat. Unit weight
DBY	18,34±2	2,54±0,11	7,20±0,64	3,12±0,20	0,39±0,02	24,93±1,08	26,73±1,25
DFG	49,48±4	1,22±0,05	40,57±2,54	2,43±0,25	0,82±0,04	11,96±0,52	16,82±0,76

Table 36. Physical properties of samples after 20th cycle of wetting drying

20th cycle	P (%)	D (g/cm ³)	WAC (%)	Real D	Sat. Coef	Dry unit weight	Sat. Unit weight
DBY	18,22±2	2,55±0,10	7,14±0,39	3,12±0,19	0,39±0,02	24,98±0,99	26,77±1,16
DFG	50,05±3	1,23±0,04	40,74±1,57	2,47±0,23	0,81±0,03	12,04±0,39	16,95±0,67

Table 37. Physical properties of samples after 22nd cycle of wetting drying

22nd cycle	P (%)	D (g/cm ³)	WAC (%)	Real D	Sat. Coef	Dry unit weight	Sat. Unit weight
DBY	19,54±1	2,44±0,17	8,05±0,96	3,03±0,18	0,41±0,03	23,94±1,68	25,86±1,59
DFG	39,39±17	1,70±0,80	28,99±18,77	2,73±0,49	0,74±0,25	16,70±7,85	20,56±6,16

Table 38. Physical properties of samples after 24th cycle of wetting drying

24th cycle	P (%)	D (g/cm ³)	WAC (%)	Real D	Sat. Coef	Dry unit weight	Sat. Unit weight
DBY	20,73±2	2,52±0,10	8,22±0,97	3,19±0,14	0,40±0,02	24,76±0,96	26,79±0,95
DFG	55,01±8	1,32±0,16	41,70±1,33	3,05±0,99	0,76±0,09	12,91±1,53	18,30±2,34

Table 39. Physical properties of samples after 26th cycle of wetting drying

26th cycle	P (%)	D (g/cm ³)	WAC (%)	Real D	Sat. Coef	Dry unit weight	Sat. Unit weight
DBY	19,98±2	2,50±0,18	8,06±1,51	3,12±0,12	0,40±0,03	24,53±1,72	26,49±1,48
DFG	63,66±9	1,25±0,13	51,00±7,93	3,61±0,97	0,80±0,08	12,28±1,28	18,53±1,81

Table 40. Physical properties of samples after 28th cycle of wetting drying

28th cycle	P(%)	D (g/cm ³)	WAC (%)	Real D	Sat. Coef	Dry unit weight	Sat. Unit weight
DBY	21,36±3	2,48±0,17	8,69±1,93	3,15±0,09	0,41±0,03	24,34±1,69	26,43±1,37
DFG	63,11±9	1,22±0,08	52,00±7,62	3,43±0,83	0,82±0,05	11,92±0,75	18,11±1,29

APPENDIX B

ULTRASONIC PULSE VELOCITY

SALT CRYSTALLIZATION TESTS

Table 41. UPV change after salt crystallization cycle

	0 th cy		1 st cy		2 nd cy	
	UV	E _{mod}	UV	E _{mod}	UV	E _{mod}
DBY	1815,34±1,96	7,31±0,36	1811, 27±151	6,33±1,4	1824,11±165	7,71±1,3
DFG	1083,45±141,16	1,32±0,36	1090,24±164	2,29±0,6	1054,38±100,4	1,23±0,28
DKK	942,74±138,18	1,05±0,27	909,08±0,00	1,92±0,00	981,82±97,16	1,21±0,08

Table 42. UPV change after salt crystallization cycle

	3 rd cy		4 th cy	
	UV	E _{mod}	UV	E _{mod}
DBY	1811,70±186	7,70±2,04	1767,22±57,4	7,08±0,5
DFG	1074,01±176,9	1,28±0,4	988,33±320	1,22±0,6
DKK	908,20±85,09	1,07±0,15		

WETTING-DRYING TESTS

Table 43. UPV change after wetting drying cycle

	0th cy		4th cy		8th cy	
	UV	Emod	UV	Emod	UV	Emod
DBY	1815,34±1,96	7,31±0,36	1707,98±57,17	6,44±0,10	1638,66±237,48	6,43±1,99
DFG	1083,45±141,16	1,32±0,36	1079,75±4,49	1,16±0,01	988,12±234,03	1,30±0,68
DKK	942,74±138,18	1,05±0,27	979,73±121,07	0,97±0,07	917,58±166,92	1,04±0,52

Table 44. UPV change after wetting drying cycle

	12th		16th		20th	
	UV	Emod	UV	Emod	UV	Emod
DBY	1704,52±80,77	6,18±0,88	1700,66±42,40	6,14±0,64	1675,53±160,3	5,94±0,8
DFG	1045,46±221,50	1,41±0,61	1049,25±260,37	1,47±0,72	1003,39±164,4	1,32±0,5

Table 45. UPV change after wetting drying cycle

	24th		28th		32th	
	UV	Emod	UV	Emod	UV	Emod
DBY	1682,75±58,35	5,99±0,34	1652,16±183,74	5,87±1,62	1642,45±152,64	5,73±0,98
DFG	1000,83±123,63	1,28±0,39	961,27±147,29	1,17±0,32	924,38±180,39	1,08±0,33

APPENDIX C

COLOR EXPERIMENT RESULTS

SALT CRYSTALLIZATION

Table 46. L, a, b values of DBY after salt crystallization cycle

DBY	L	a	b
1	59,39±0,92	3,53±0,19	4,38±0,34
2	61,78±2,73	3,19±0,20	5,18±0,61
3	60,20±1,17	3,57±0,24	5,31±0,61
4	59,91±1,09	3,96±0,09	5,49±0,72

Table 47. L, a, b values of DFG after salt crystallization cycle

DFG	L	a	b
1	50,05±1,16	3,92±0,27	8,71±0,61
2	53,49±3,45	3,61±0,42	7,99±0,73
3	48,81±2,48	3,59±0,17	8,28±0,54
4	49,50±2,37	3,38±0,31	7,94±0,36

Table 48. L, a, b values of DKK after salt crystallization cycle

DKK	L	a	b
1	51,89±0,00	3,09±0,00	5,74±0,00
2	53,42±3,41	3,55±0,29	7,46±1,15
3	57,18±7,16	3,23±0,67	4,48±0,71

WETTING DRYING CYCLE

Table 49. L, a, b values of DBY after wetting drying cycle

DBY	L	a	b
4	30,93±0,70	2,26±0,13	2,73±0,05
8	53,45±5,61	3,59±0,21	5,26±0,63
16	53,01±0,04	3,22±0,01	4,13±0,00
24	59,74±0,05	3,54±0,01	4,28±0,00
32	56,72±1,86	3,94±0,07	5,31±0,09

Table 50. L, a, b values of DFG after wetting drying cycle

DFG	L	a	b
4	34,94±0,38	2,92±0,05	6,98±0,09
8	49,00±3,04	3,21±0,40	7,82±0,75
16	49,58±0,02	3,69±0,00	9,00±0,00
24	49,58±0,34	3,76±0,02	8,91±0,01

Table 51. L, a, b values of DKK after wetting drying cycle

DKK	L	a	b
4	44,85±0,70	2,79±0,23	5,49±0,02
8	44,37±0,35	2,85±0,02	4,59±0,02

APPENDIX D

ORIENTED AND UNORIENTED X RAY DIFFRACTION

Table 52. “d values” of samples in XRD spectras

Unoriented First three d values (Å)			
Quartz	3.34	4.25	1.81
Albite	3.19 (4.03)	3.78 (3.22)	3.68 (3.66)
Anorthite	3.18 (3.20)	3.75 (3.18)	3.21 (4.04)
Sanidine	3.33	3.28	4.24
Biotite	10.2	3.38	2.62
Hematite	2.7	2.51	1.69
Opal C-T	4.08	2.51	2.86
Oriented d values (Å)			
	Air-dried	Glycolated	Heated
Smectite	12-15	16-17	10
Illite	10	10	10

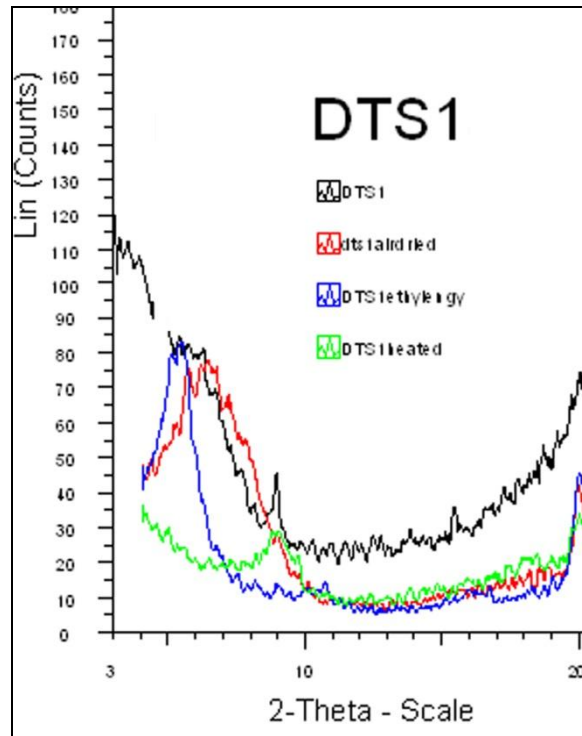


Figure 126. Oriented and unoriented smectite peaks of DTS1 (red; air dried 12, 13, 15 Å, blue; glycolated 16, 17Å, green; heated 9,10 Å)

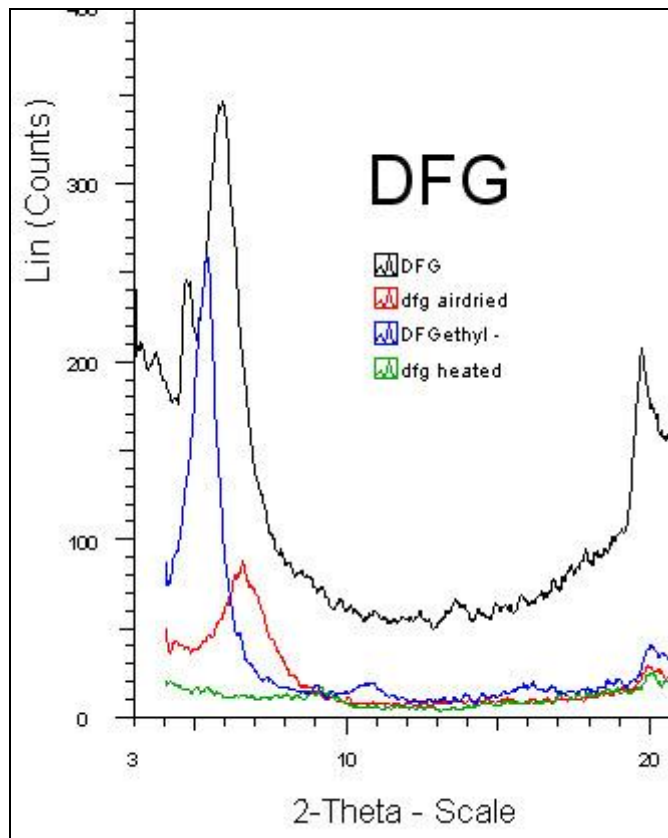


Figure 127. Oriented and unoriented smectite peaks of DFG (red; air dried 13 Å, blue; glycolated 16 Å, green; heated 10 Å)

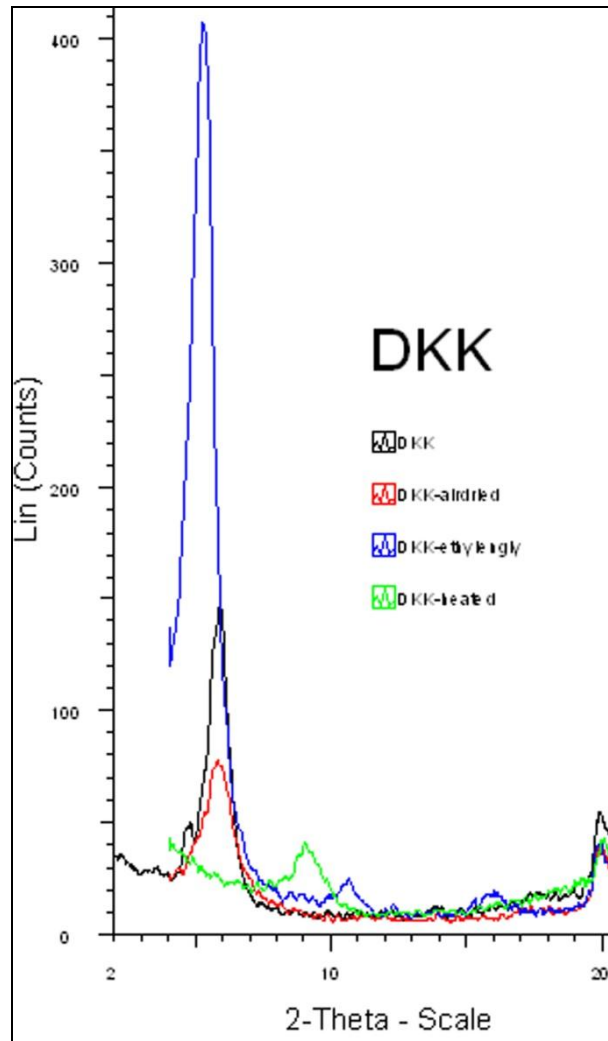


Figure 128. Oriented and unoriented smectite peaks of DKK (red; air dried 15 Å, blue; glycolated 17 Å, green; heated 10 Å)

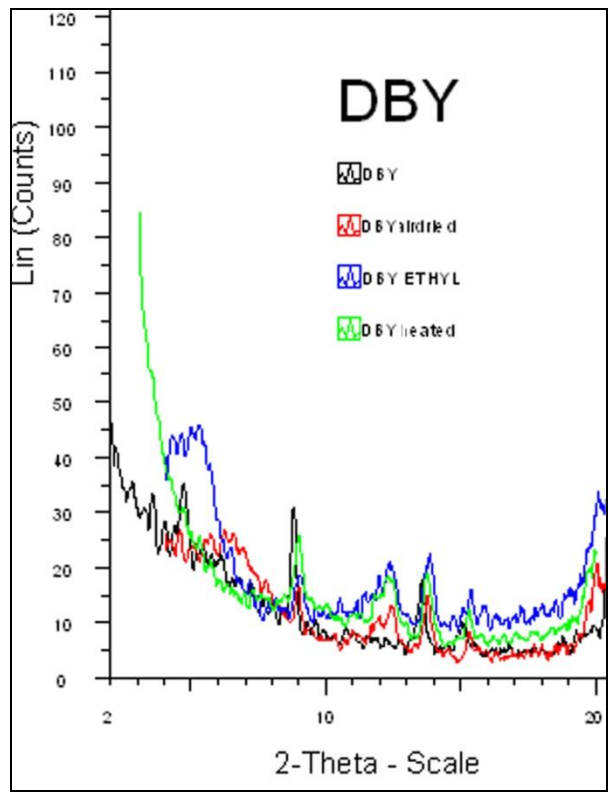


Figure 129. Oriented and unoriented illite peaks of DBY (red; air dried 10 Å, blue; glycolated 10 Å, green; heated 10 Å)

APPENDIX E

PLAN OF APOLLON SMINTHEUS TEMPLE

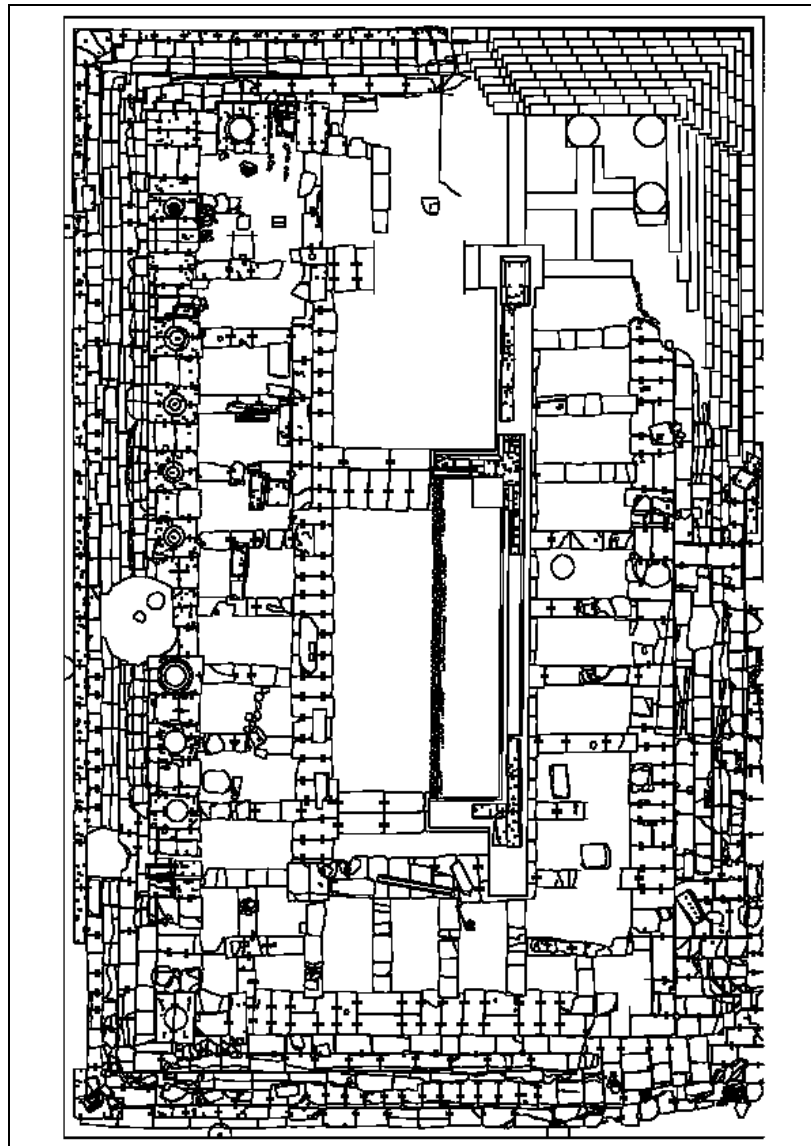


Figure 130. Plan of Apollon Smintheus Temple

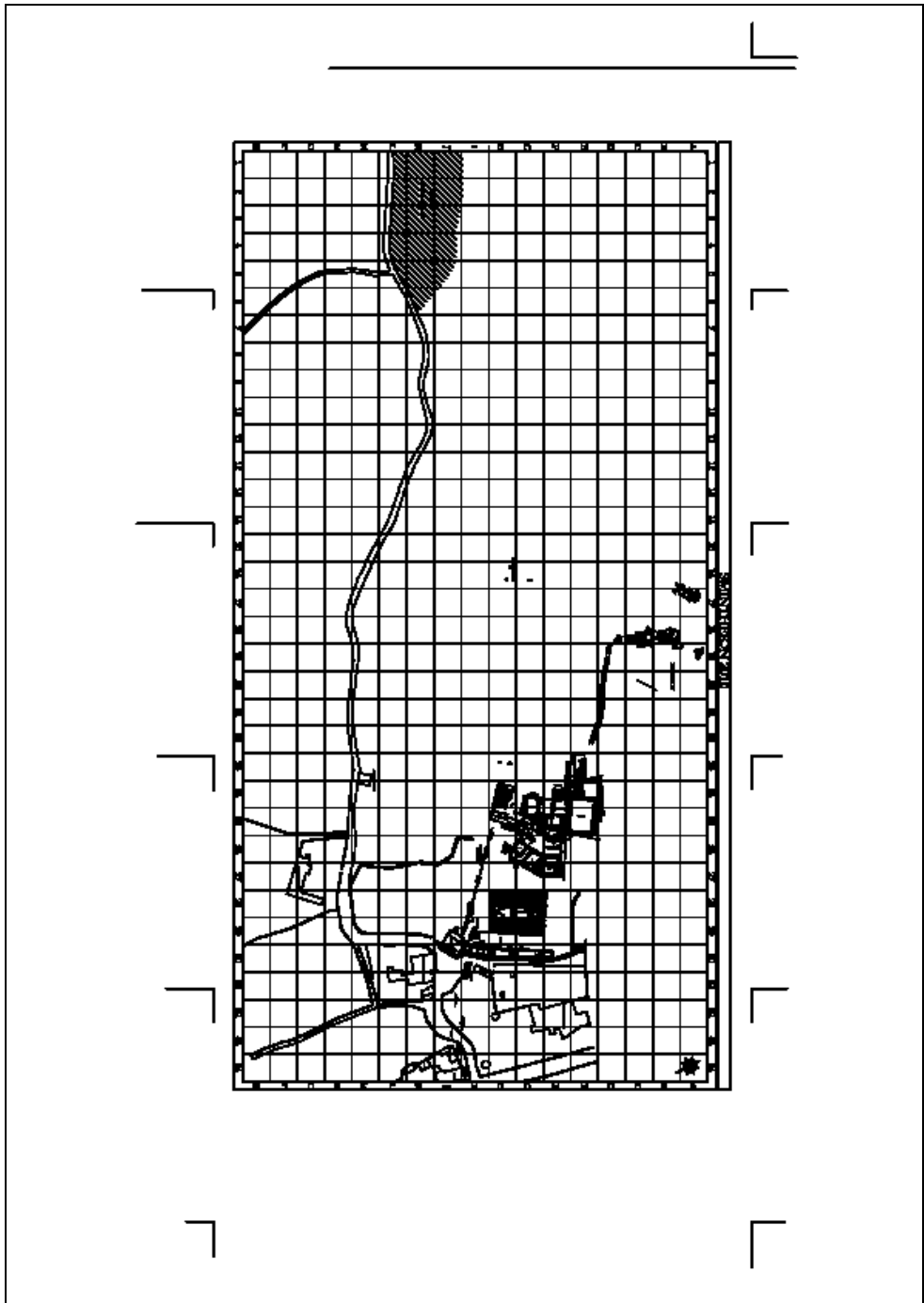


Figure 131. General plan of Smintheion